University of
Southern
Queensland

INVESTIGATION OF FIBRE REINFORCED SHAPE MEMORY POLYMER COMPOSITES FOR STRUCTURAL COMPONENTS

A Thesis submitted by

Chris Emmanuel Kotikawattege Don

BSc Eng (Hons)

For the award of

Doctor of Philosophy

2023

ABSTRACT

Shape memory polymers (SMPs), comprising a distinctive shape memorizing capability, is a significant and evolving branch of smart polymers. Shape memory polymer composites (SMPCs) were developed by reinforcing the SMP matrix to improve the inherently weak mechanical properties and durability of SMPs. General polymer composites have become a successful substitute construction material. Similarly, with both the structural performance and shape memory effect (SME), SMPCs will be ideal candidates to remedy the challenges of futuristic construction techniques. Specifically, SMPCs can be used effectively in prefabricated modular constructions, curved beams and other civil infrastructures to overcome drawbacks associated with the high requirements of labour, time and cost. This research aimed to develop circular and square hollow sectioned (CHS and SHS) structural SMPC components for the construction industry. E-glass, carbon and natural basalt fibres were integrated as reinforcements. The thermomechanical, mechanical, shape memory and programming damage characteristics were evaluated to analyse material performance. The SMPC structural sections were fabricated with a specially designed mould and the SME, damage predictions, structural performance and proof of concept were analysed. The durability of SMPCs was also investigated; mainly in terms of behaviour under fire, smoke generation, thermal decomposition, volatile gas characterisation, fatigue, moisture and elevated temperatures. Importantly, this thesis presents a firsthand, in-depth programming damage analysis framework to fill knowledge gaps in the SMPC research field by linking experimental outcomes with viscoelastic FEA studies. Overall, this study established a comprehensive and well-rounded SMPC design outline to develop SMPC structural sections for civil constructions for the first time. The outcomes of this thesis will guide engineers to revolutionize well established construction methods and technologies, and provide innovative solutions to make civil constructions smarter, faster and cheaper.

CERTIFICATION OF THESIS

This Thesis is entirely the work of Chris Emmanuel Kotikawattege Don except where otherwise acknowledged. The thesis contains no material that has been submitted previously, in whole or in part, for the award of any other academic degree or diploma.

Date: 03/02/2023

Endorsed by:

Associate Professor Jayantha Ananda Epaarachchi

Principal Supervisor

Professor Thiru Aravinthan

Associate Supervisor

Student and supervisor's signatures of endorsement are held at the University.

ACKNOWLEDGEMENTS

TABLE OF CONTENTS

LIST OF TABLES

LIST OF FIGURES

ABBREVIATIONS

A_D	Damaged area
A_T	Total deformed area
A	Fatigue constant
ADP %	Areal damage percentage
ASTM	American society for testing and materials
CB	Carbon black
CFT	Composite fibre technologies
CHS	Circular hollow section
CNT	Carbon nanotubes
CSM	Critical stress margin
D	Mid span displacement
D_F	Function of fatigue parameters
D_S	Specific optical density
D(T)	Optical density
DGEBA	Bisphenol A diglycidyl ether
DMA	Dynamic mechanical analysis/analyser
DSC	Differential scanning calorimetry
d_o	Outer diameter
E	Elastic modulus
EMI	Electromagnetic interference
f	Frequency
f_y	Yield strength
F	External force
FEA	Finite element analysis
Fe_3O_4	Ferrous oxide
FRP	Fibre reinforced plastic/polymer
FTIR	Fourier-transform infrared spectroscopy
GFRP	Glass fibre reinforced polymer/plastic
GO	Graphene oxide

gsm	Grams per squre meter (g/m^2)
HGM	Hollow glass microspheres
HTSMP	High temperature shape memory polymer
IR	Infrared
ISO	International organization for standardization
k_f	Form factor
L	Load levels
L_M	Load mean
L_A	Load amplitude
M_S	Nominal section capacity for bending
MWCNT	Multi-walled carbon nanotubes
m_2	Fatigue material constant
N	Fatigue cycles
N_S	Nominal section capacity for axial compression
NIR	Near infrared radiation
PDA	Polydopamine
PTFE	Polytetrafluoroethylene
PU	Polyurethane
R	Stress ratio
R(t)	Relaxation modulus
RH	Relative humidity
R_f	Fixity ratio
R_r	Recovery ratio
r	Bend radius
r_c	Critical bend radius
S_{11}	S_{XX}, normal stress in x direction
S_{22}	S_{YY}, normal stress in y direction
S	Support span
S_c	Critical span
SEM	Scanning electron microscope

SHS	Square hollow section
SiC	Silicon carbide
SiO_2	Silicon dioxide
S/N	Signal to noise ratio
SME	Shape memory effect
SMP	Shape memory polymer
SMPC	Shape memory polymer composites
SP-x	Specimen number "x", x ϵ (1, 2,… 9)
T	Light transmittance
T_g	Glass transition temperature
T_s	Storage onset temperature
T_δ	Temperature at Tan δ peak
TETA	Triethylenetetramine
TGA	Thermogravimetric analysis
TiO_2	Titanium dioxide
TRGO-GF	Thermally reduced graphene oxide coated glass fabric
TTS	Time temperature superposition
t	Time
UTS	Ultimate strength
UV	Ultraviolet
UV-VIS	Ultraviolet–visible spectroscopy
V	Visibility
Vf	Final volume
Vi	Initial volume
v/v %	Volume fraction
w/w %	Mass fraction
Z_e	Effective section modulus
σ_C	Compressive strength
E_C	Compressive modulus
σ_T	Tensile strength

E_T	Tensile modulus
λ	Wavelength
γ	Gamma
σ	Stress
σ_o	Damage onset stress
ε	Strain
ε_{UL}	Ultimate deformation strain
η	Viscosity coefficient
τ	Relaxation time
α, β	Material specific fatigue parameters

CHAPTER 1: INTRODUCTION

1.1 Background

Shape memory polymers (SMPs) belong to a rapidly growing branch of smart materials discovered in 1980s [1]. As an innovative material, SMPs have the potential to revolutionize Materials Science due to their distinctive capabilities. They have emerged as promising materials in recent years with a unique ability to undergo significant deformation under external load and recover their original shape under the application of an external stimulus [1-3]. Recently developed SMPs are responsive to different stimuli such as heat [4], electricity [5, 6], light [7-9], magnetic fields [10], microwaves [11] and moisture [12]. Of these stimuli, heat activation can be considered as the most abundantly researched stimulating method in the field of SMP [13]. SMPs provide significant advantages compared to traditional materials such as shape deformability, recoverability, ease of manufacturability and the ability to tailor their thermomechanical properties [14]. Figure 1.1 presents an overview of the shape memory effect (SME) of a shape memory material activated by heat [15].
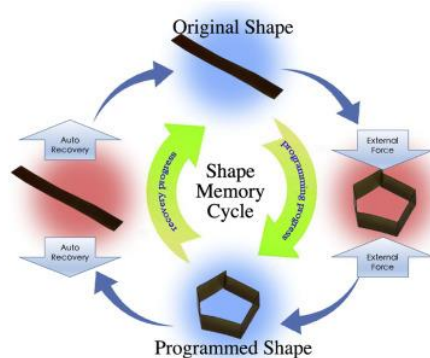
Figure 1.1: The shape memory
cycle of SMPs and SMPCs [15]

Even though SMPs have remarkable properties compared to common materials, inherent poor mechanical properties are their major drawbacks [16]. It has been found that the poor structural properties of neat SMPs

lead to significant difficulty in integrating SMPs in structural applications. As a consequence, different types of fillers and fibre reinforcements have been integrated with the SMP matrix to enhance mechanical properties [7, 17, 18]. The matrix binds these fillers and fibre reinforcements together and distributes induced stresses through the whole shape memory polymer composite (SMPC). Particulate nano-scale fillers such as graphene oxide (GO) [19], multi walled carbon nanotubes (MWCNT) [20], carbon black (CB) [5] and rare earth organic fillers [21] produce thermal [19], electrical [5, 20] and photothermal [21] property enhancements, and fibre reinforcements improve structural properties such as resistance to cyclic loading [22], modulus, stiffness and strength [17].

Currently, the SMPCs are mainly used in space applications as conventional materials are heavy, high volume consumed in the space craft and high deployable shock effects which weaken the effectiveness of space missions. SMPC hinges [20], truss booms [23], solar arrays [20], reflector antennas [2, 24], morphing structures [24, 25], morphing skins [26] and mandrels [27] are a few of the renowned applications proposed for SMPCs. However, recent studies have shown that SMPCs pose comparable structural properties to common fibre reinforced plastics (FRP) used for constructions [28, 29]. Additionally, the unique shape deforming capability of SMPCs, which promotes shape recovery, could be efficiently used to reduce construction costs through easier handling and manufacturing in challenging building technologies.

Prefabricated modular construction is an emerging modern construction technology developed by researchers and engineers to offer faster and efficient building constructions. This new trend in construction has become a game changer for extremely challenging constructions in overly congested cities where space is limited and time is critical. Compared to traditional construction methods, prefabricated modular construction offers safer manufacturing, faster construction speeds, better quality

control, fewer workers on site, less resource wastage and a smaller environmental impact [30]. Importantly, in prefabricated constructions, different modules of a building are manufactured in a factory and transported to the construction site. These prefabricated modules are then stacked on top of each other to construct a building using cranes. An overview of this modern construction technique is given in Figure 1.2 [31]. Despite their exciting benefits, difficulties with the transportation and handling of heavy, large modules is a major drawback in modular construction [32]. Furthermore, researchers have demonstrated the ability of polymer composite materials to mitigate the heaviness of steel prefabricated modules [30].

Figure 1.2: The process of prefabricated modular constructions [31]

Excitingly, SMPCs have the potential to replace general polymer composites due to their intrinsic properties similar to common FRPs and the additional temporary shape changing and recovering ability. Thus, light weight modules prefabricated with SMPCs can be heated and deformed to a compact shape in factory for easy transportation. SMPC modules can then be heated on-site to recover the initial shape and construct the building. Hence, the integration of SMPCs into structural components, panels, etc. promotes easy transportation and handling, thus mitigating the current drawbacks of prefabricated modular constructions. Further, these compactable SMPC integrated components can be used for emerging concepts such as deployable structures for space habitats which can be used for space exploration [33]. In addition, the fabrication of steel curved

structures and arches has also been a highly expensive and energy demanding process, even with current technological advancements. In order to transform the manufacturing of curvy structural components into a commercially viable, user friendly and quick process, SMPCs would be the best alternative to heavy steel.

Having sufficient mechanical properties such as tensile and compressive strengths is mandatory for SMPC components. Increasing the fibre content in the composite improves its mechanical properties and, as a consequence, the thickness of the composite is increased. However, the increase in thickness and fibre content causes local damage, fibre buckling and delamination during shape programming procedures, and need to be studied.

The durability of construction materials is a vital factor that needs to be investigated when evaluating the performance of alternative materials suitable for constructions. Factors such as UV absorption properties, behaviour under fire and thermal decomposition, fatigue characteristics, and moisture and elevated temperature effects are some of the prominent concerns [34-36]. As these structures are exposed to long term sunlight, there can be adverse effects on the polymer matrix. Long term UV exposure can degrade the polymeric structure, eventually hindering the structural performance of the SMPC. Also, it is important to point out the importance of studying the effects of moisture and increased temperature on a construction material [37, 38]. In practise, the materials are frequently exposed to natural phenomena such as rain, humidity and environmental temperature fluctuations which may result in the degradation of strength, stiffness, etc. Moreover, fire safety is another prominent factor relevant to the construction field [39]. Building codes and housing standards highly stress the aspects of fire safety as fire can be catastrophic and put the lives of people in danger. Importantly, factors such as heat release, flammability, fire initiation time, fire spread rate, smoke emission and toxicity are closely

related to broad fire safety characteristics [40]. Apart from the abovementioned phenomena, cyclic loading patterns on civil components due to natural causes and in service forces can cause the premature failure of infrastructure. However, fatigue behaviour analysis is typically undermined by its complexity and unpredictability. To ensure that civil infrastructure is safe and its lifetime maximised under service conditions, a material's characteristics such as endurance limit, failure mode, etc should be studied thoroughly.

According to the author's knowledge, there has not been any research work carried out on the use of fibre reinforced SMPs for the construction of civil infrastructure. This research study contributes SME and structurally comparable novel composite materials to overcome the significant difficulties encountered in prefabricated modular constructions, curved structures and other similar applications. The unique properties of SMPCs will provide greater flexibility to the design, manufacture, construction and assembly of structural components. Furthermore, they will save significant amounts of assembly and commissioning costs in modular constructions and other civil engineering applications.

1.2 Research problems

I. The inclusion of fibre reinforcements enhances the structural properties of the weak SMP matrix and can be tailored as per the requirements of applications. As a consequence, SMPCs have been considered to be promising structural materials. However, research to integrate SMPCs into structural components has not been undertaken in the recent past. To date, the developments of SMPs and SMPCs have focused exclusively on biomedical and space applications. The implementation of the SME in structural components can be advantageous in many space cramped and time critical construction applications. Therefore, the investigation into how the

smart SMPCs can be incorporated into common structural members such as circular hollow sections (CHS) and square hollow sections (SHS), is timely. Further, to make such components and structures commercially viable, the possibility of using natural and cost-effective fibre reinforcements such as basalt should be investigated.

II. To be used effectively in hollow structural sections, SMPCs should possess better mechanical properties. The fibre fraction of the SMPC is directly proportional to the structural performance of the material and makes the SMPC thicker. As a consequence, the ability of the SMPC to deform into compact shapes can be difficult and can cause material damage during shape training or programming. Such material defects can significantly reduce structural performance. The fibre volume fraction should be optimized to have a balanced configuration of structural performance and retain the SME of the composite. However, the current understanding of the undesirable effects of SMPC thickness and fibre content are not adequate. Therefore, understanding the programming defects, their root causes, impact on structural performance and ways to mitigate such setbacks should be studied.

III. Constitutive models and computer aided simulation techniques have been developed to illustrate the SME of SMPCs in terms of shape deformability, fixity and recoverability. However, the coupling of SMPC relaxation properties and mechanical properties at the programming temperature which allows the study of stress build up and damage onset predictions, has not been well explained numerically or analytically. The ability to simulate the shape training stage of SMPC components numerically and identify programming parameters to prevent damage are essential to enhancing their performance and building large scale civil engineering applications. Therefore, a user-friendly finite element analysis (FEA) based

simulation technique needs to be developed and validated to ensure that deformed SMPCs are damage free and retain their maximum structural potential.

IV. Construction materials are frequently exposed to a wide variety of environmental and loading conditions. To ensure the safety of people, strict construction standards demand that a building material's performance be investigated in terms of ultraviolet (UV) absorption, moisture and elevated temperature effects. Also, emergency situations such as fire, exposure to high temperature that can cause thermal decomposition, hazards of evolving gases and fatigue characteristics need to be investigated. In the recent past, the thermomechanical and mechanical performances of SMPCs have been well investigated, but SMPC behaviour of other application specific conditions stated above have not been well researched. Therefore, to be successfully integrated into real life civil infrastructure, the overall performance of the SMPC should be well investigated and understood.

1.3 Research aim and objectives

The aim of this research is to investigate the use of the SME in structural components such as CHS and SHS that can be used in the civil construction field. This broadens the current application fields of SMPCs and creates the possibility of remedying unsolved challenges in the construction of prefabricated modular buildings, curved structures, foot bridges and deployable structures on earth as well as in outer space. Furthermore, this study aims to characterise SMPC's properties in a wide range of application related conditions and demonstrate the applicability of SMPC structural members in constructions. To achieve the research outcomes, the following specific objectives have been identified:

1) Review and understand the types of SMPs, reinforcement types, current limitations and applications of the SMPCs.

2) Develop and optimize a suitable SMP matrix and reinforced SMPCs, and understand their behaviour as constructions materials.

3) Study the performance of SMPC hollow section profiles, and further understand SMPC characteristics through numerical analysis.

4) Investigate the durability of SMPCs under various operational conditions including UV absorption, behaviour under fire and thermal decomposition, evolving gas characterization, tension-tension fatigue behaviour, long term moisture exposure and elevated temperature effects.

1.4 Research methodology

To achieve the above mentioned research objectives, the following systematic methods were defined at the start of the study. Initially, a suitable SMP base matrix was selected along with hardeners that create the SME. Then, the SMP matrix was synthesised to ensure the material characteristics are favourable for civil engineering applications. To further enhance structural performance, fibre reinforcements were integrated to the SMP. The SMPC material parameters were optimized via a Taguchi study and further refinements were suggested to prevent damage and strength deterioration, due to shape programming. A viscoelastic FEA study was developed through ABAQUS software to identify the damage onset stress during programming and further analyse the SMPC performance during programming. Then, CHS and SHS profiles were fabricated with the identified SMP composition and SMPC parameters. The SME of these profiles were evaluated and used to further validate the developed numerical technique. In addition, the established FEA technique was utilized to demonstrate the applicability of SME of SMPCs in large scale applications. Finally, the durability of the developed SMPC was evaluated experimentally, to understand the behaviour as a construction material.

1.5 Significance of the research

The author of this thesis believes that the outcomes of this research will be highly beneficial to mankind by providing new knowledge to the construction industry and materials, making future constructions cost effective, user friendly, quicker, safe and durable even in unexpected conditions. Being able to provide every person with their own affordable home with the implementation of these advancements and findings in civil engineering would be remarkable. Importantly, the outcomes of this research can be utilized to broaden the application spectrum and current limitations of these outstanding SMPC materials, and will generate novel technological trends in future constructions and space explorations.

1.6 Structure of the thesis

This thesis is composed of six chapters. A brief description of each chapter is given below:

- Chapter 1: The first chapter introduces the research study. The scope, research problem, objectives and significance are also described

- Chapter 2: The second chapter includes a critical review of the literature to identify the research gap that justifies the study. It provides a comprehensive study on recent advances of SMP types, SMPCs, natural basalt fibre, numerical modelling, current durability studies, GFRP applications and modular constructions. In addition, this chapter comprises a broad review of the developed applications and SMPC trends

- Chapter 3: The third chapter includes my research work mainly related to material development and characterisation. It describes the synthesisation of the SMP and the optimization of the SMPC parameters considering programming defects caused by high thickness and fibre content.

- Chapter 4: The fourth chapter details the experimental and simulation methods, results and discussion on the application of SME in real scaled CHS and SHS structural components. Furthermore, it provides a numerical approach to predict damage during programming and demonstrates how SME can be implemented in the proposed applications. Importantly, it includes the proof of concept for the application of SMPCs in structural components and a simplified structure.

- Chapter 5: The fifth chapter consists of the durability studies of the developed SMPCs. As per the proposed applications in civil infrastructure, the experimental methods, results and discussion on UV absorption, fire and thermal decomposition, fatigue, moisture and high temperature effects of the SMPCs are included.

- Chapter 6: The final chapter presents the conclusion that summarizes the main findings of the study and suggests recommendations for future work.

1.7 List of publications

> *Q1 Journal Articles:*

J1 - K. D. C. Emmanuel, H. M. C. M. Herath, L. H. J. Jeewantha, J. A. Epaarachchi, and T. Aravinthan, "Thermomechanical and fire performance of DGEBA based shape memory polymer composites for constructions," Construction and Building Materials, vol. 303, 2021, doi: 10.1016/j.conbuildmat.2021.124442
(In Appendix A)

J2 - K. D. C. Emmanuel, L. H. J. Jeewantha, H. M. C. M. Herath, J. A. Epaarachchi, and T. Aravinthan, "Damage onset analysis of optimized shape memory polymer composites during programming into curved shapes," Materialia, vol. 26, 2022, doi: 10.1016/j.mtla.2022.101599 *(In Appendix B)*

J3 - Emmanuel, K., Jeewantha, L., Herath, H., Epaarachchi, J., and Aravinthan, T., 2023, "Shape memory polymer composite circular and square hollow members for deployable structures," Composites Part A: Applied Science and Manufacturing, 171, p. 107559 *(In Appendix C)*

➢ ***Conference Proceedings:***

C1 - K. D. C. Emmanuel, J. Jeewantha, H. M. C. M. Herath, J. A. Epaarachchi, T. Aravinthan, "Fire properties of glass, carbon and basalt fibre reinforced shape memory polymer composites", Twenty-Third International Conference on Composite Materials (ICCM23), Belfast, England *(Accepted)*

C2 - K. D. C. Emmanuel, J. Jeewantha, H. M. C. M. Herath, J. A. Epaarachchi, T. Aravinthan, "Effect of thickness on the shape memory properties of Bisphenol A epoxy based shape memory polymer composites", SMASIS, 2021, vol. 85499: American Society of Mechanical Engineers, p. V001T02A002

CHAPTER 2: LITERATURE REVIEW

2.1 Introduction

SMPs are rapidly evolving and represent an expanding branch of smart materials research. With the application of an external stimulus, SMPs exhibit an interesting ability to revert shape deformations and return to their original shapes. The SMPCs developed by the inclusion of fibre reinforcements and particles, outperform neat SMPs in terms of structural performance and durability. As a consequence, the improved structural performance amplified the application spectrum of SMPCs in a wide variety of structural applications.

Nowadays, civil engineers seek for opportunities to improve effective building methods and incorporate innovative materials, to speed up building rate, reduce costs, minimize losses, enhance safety and improve the durability of infrastructure. Interestingly, the SME of SMPCs can be effectively used in developing constructions methods, similar to glass fibre reinforced polymers (GFRPs) which has become a successful substitute construction material.

In this chapter, recent research in relation to the state-of-the-art SMPs and their composites is presented. Moreover, current research findings on the SMPC programming damage mechanisms and numerical modelling techniques, are also described. This chapter further presents the advantages of natural fibre reinforcements, current civil engineering related GFRP applications and insight into the developing prefabricated modular constructions. Above all, future research prospects and directions are also highlighted. This establishes the context and provides a broad foundation for the current study.

2.2 Shape memory polymers

SMPs are a distinct class of smart materials with an intrinsic programmable property that gives them an advantage over other types of smart material families. That is due to their ability to "memorise" one or more temporary shapes and, moreover, the capability to recover their initial shape upon exposure to an appropriate stimulus [41-43]. Stimuli types such as; light, magnetism, moisture, electricity and heat were researched in the recent past [44]. The thermo-responsive SMPs are the most prevalent of these SMPs [26, 45, 46].

2.2.1 Mechanism of SME

Thermally responsive SMPs show shape memory behaviour as the polymer chains have tendency to make network structures. The molecular mechanism of thermally activated SMPs during shape recovery is shown in Figure 2.1 [26]. Cross links/fixed phase and switching segments/reversible phase are the two main components that result in the SME in SMP. The cross links or net points define the permanent shape of SMP, while switching segments absorb the external stress and upholds the temporary shape. The net points may be either chemical (covalent bonds) or physical. The molecular switches are capable of fixing the deformed shape temporarily under environmental conditions by making additional reversible cross links. These additional temporary cross links can be formed by physical interactions or by chemical bonds which avoid the jump back of the deformed chains. After reheating, the glassy domains will become soft, releasing entropic energy by recoiling the chains that drive the material to return to its original shape [26, 47].
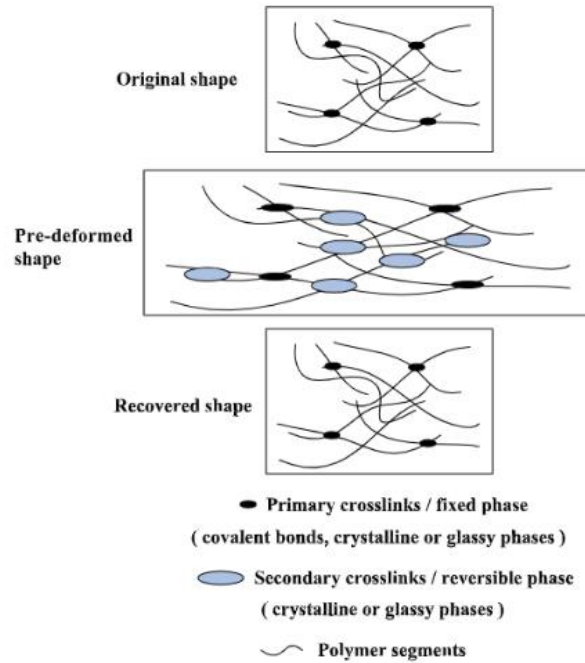
Figure 2.1: Representation of polymer
networks during shape recovery [26]

2.2.2 Thermomechanical behaviour of SMPs

When a SMP is manufactured, the initial shape will be memorized by the material. At a temperature higher than its glass transition temperature (T_g), the material can be easily deformed into a temporary shape with an external force. This process is known as 'programming/packing/training'. As the material is heated up, it will change the physical state from glassy to rubbery, making it soft and deformable. Then, the molecular structure will hold the temporarily deformed shape while it is cooled back to a low temperature freezing the polymer structure. The extent to which the material is able to fix the deformed shape is known as 'shape fixity' [48]. Due to relatively higher stiffness of the glassy phase compared to the rubbery phase, the strain decreases slightly and material will attain the fixed shape. This is termed as the 'spring back effect'. Subsequently, by increasing the temperature over T_g, the shape recovery process initiate as the strain relaxes recovering the shape of the material [49]. This cycle is called a 'stress free strain (ε) recovery' in SMP as illustrated in Figure 2.2

[50]. The above described process is schematically represented in the Figure 2.3 [26].
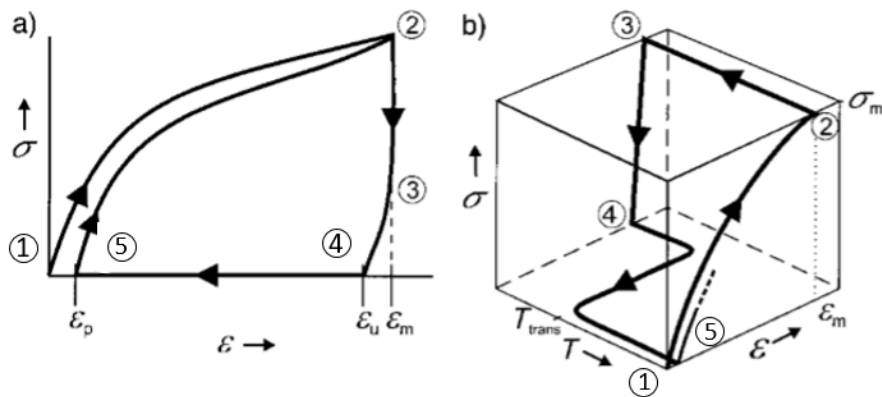
Figure 2.2: Stress free strain recovery thermo-mechanical cycle; (a) σ-ε curve (b) σ-ε-T curve [50]

- ***Point 1:***

Initial shape with the material heated above T_g. $\varepsilon = 0$ %

- ***Process 1-2:***

Deforming the material with an external force (F) and ε increases

- ***Process 2-3:***

Material is cooled at a constant strain until it becomes glassy. F is unchanged

- ***Process 3-4:***

F is removed. There will be a slight change is ε due to spring back effect

- ***Point 4:***

Deformed shape

- ***Process 4-5:***

Material is heated back (above T_g) initiating shape recovery

- ***Point 5:***

Recovered shape
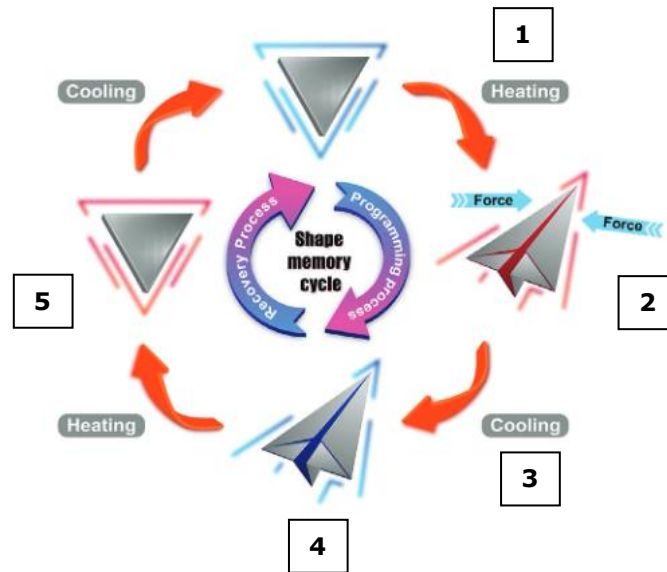
Figure 2.3: The shape memory cycle [26]

2.2.3 SMP types

A number of functional SMPs with remarkable SME have been developed so far. SMPs based on cyanate, styrene, polyurethane (PU), and epoxy are a few examples of such smart materials [28, 51, 52]. The evaluated values of T_g, elastic modulus at room temperature, and elongation at break (at T_g) for the above mentioned SMPs can be summarized as; cynate based: 160–260 ℃, 2.5–3.5 GPa, 20–30%, styrene based: 50–85 ℃, 2–3 GPa, 100–120%, and epoxy based:100–180 ℃, 3–4 GPa, 40–60%.

Cyanate resin is a thermosetting plastic with higher T_g values. Furthermore, cyanate resin has low dielectric loss and strong heat stability [53]. Cyanate ester is a good material for electronic circuit boards, dielectric coatings, high strength adhesives, aerospace composites, and wave transmitting materials because of these qualities [54]. Recent research studies on cyanate based SMPs have shown stable morphology and chemical composition after high-low vacuum thermal cycling, demonstrating their suitability in space environments [55, 56]. However, due to their high thermal stability and high T_g, cyanate based SMPs require a considerable amount of thermal energy for their activation [57].

It is clear that styrene based SMP has a relatively low T_g while exhibiting a relatively high value of elongation at break, making it appropriate for use in active large deformation structures at low actuation temperatures [52, 58]. Interestingly, styrene based SMPs can be modified through molecular cross linking or structural physical designing, to facilitate two-way shape memory behaviours [59]. Moreover, these SMPs are highly suitable for soft robotic actuators [60, 61].

The PU based SMPs poses a narrow range of T_g around the room temperature and can undergo large changes in elastic modulus above and below T_g [62]. Additionally, the PU based SMP materials were found to be biocompatible, non-toxic and non-mutagenic. Hence, PU based SMPs are highly focused for biomedical and clinical devices that can restore or self-deploy with the body temperature [63-65].

The epoxy based resins are of interest due to their wide use as structural components [66]. High strength, as well as outstanding thermal and chemical stability, are among their key properties [67]. Consequently, epoxy based thermosets were pursed for structurally demanding smart applications due to their excellent shape memory properties such as shape fixity and recovery [68-71].

2.2.4 Applications of SMPs

The PU SMPs are well known for their property of biocompatibility as it demonstrates excellent compatibility with the living tissue [24]. This interesting phenomenon of PU SMPs have been analysed by Cabanlit et al (2007) which significantly improved the interest of incorporating SMPs in biomedical applications. The ability of the SMPs to alter its activation temperature by means of chemical composition was highly advantages such that, the material can be activated with human body temperature. Blood clot removal devices, vascular stent, surgical suture, drug release devices [72] and orthodontic appliances are few of the improved biomedical SMP

devices [3, 47, 73, 74]. Figure 2.4 (a) illustrates how the device pierce the blood clot. Then it is activated due to exposure of the body temperature making a coil shape shown in Figure 2.4 (b). Finally, the device is pulled out through the blood vessel along with the clot as in Figure 2.4 (c). Interestingly, Lendlein et al (2002) [75], developed a biodegradable surgery SMP prototype that can be thermally induced to shrink and tighten the wound after suturing, as given in Figure 2.5 [75]. Further, a 4D printed biomedical occlusion device was developed with SMPs for the treatment of atrial septal defect, shown in Figure 2.6 [76]. The recovery of the occlusion device was subjected to an in vivo feasibility assessment in the presence of a magnetic field [76].

(a)	(b)	(c)
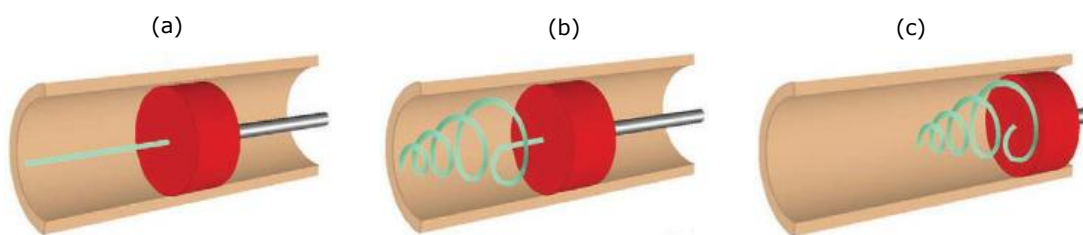
Figure 2.4: Removal of a blood clot [75]
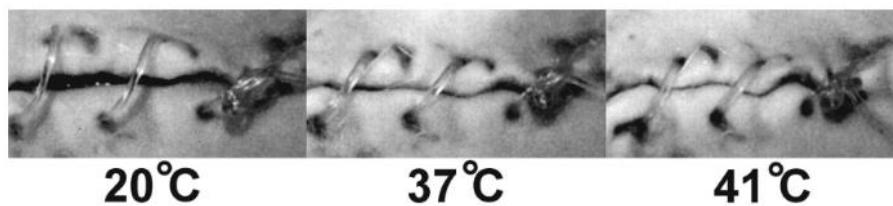
Figure 2.5: Degradable SMP suture for wound closure [75]
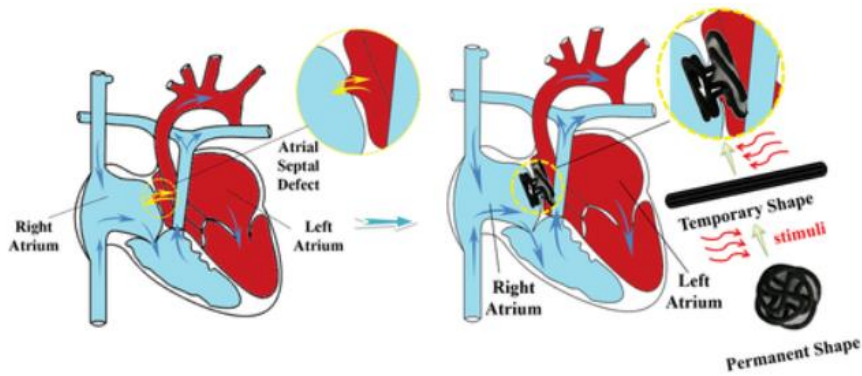
Figure 2.6: Representation of the SMP medical device before
and after interventional therapy with an occluder [76]

2.3 Reinforced SMPCs

Despite of the outstanding characteristics of SMPs, poor intrinsic mechanical properties is one of their major drawbacks. Consequently, these difficulties have severely limited the applications of SMPs [77]. However, through physical blending, in-situ polymerization and chemical crosslinking, reinforcements such as fibres and fillers can enhance the mechanical performance of SMPs [78-80]. Hence, the effects and improvements of integrating particulate nanoparticles [81, 82], chopped strand fibres [83], unidirectional fibres [84] and woven fibre mats [85] with the SMP were highly researched.

Addition of functional nano fillers such as; carbon nano tubes (CNT) [11], CB [86], ferrous oxide (Fe_3O_4) [87], silicon carbide (SiC) [88], nickel nanorods [77], gold particles [89], graphene oxide (GO) [90], etc, develop some of the intrinsic material properties such as; thermal conductivity, electrical conductivity, magnetic response and facilitate alteration of the SMP's responsiveness to different stimulus types [27, 81, 91-93]. A summary of the particulate fillers and their respective influence on the SMPC activation method, is illustrated in Figure 2.7 [81].
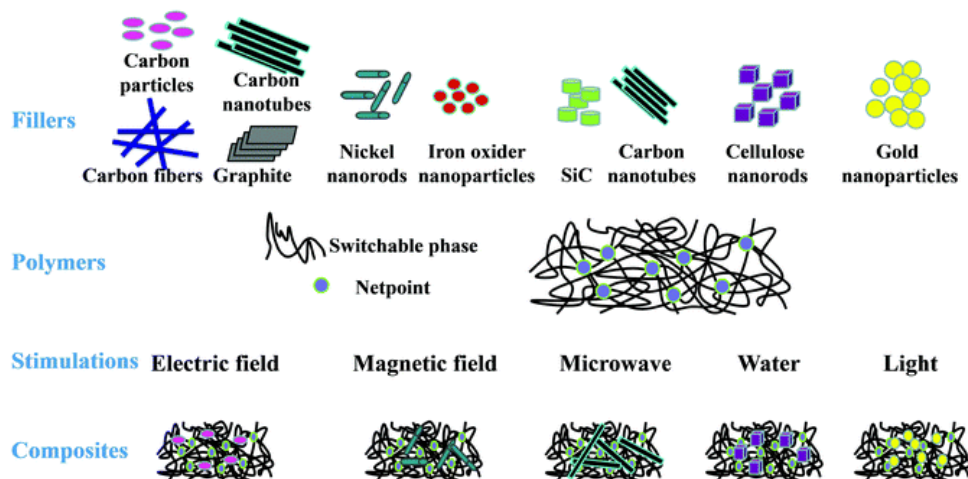
Figure 2.7: Different SMP activation methods and related filler types [81]

2.3.1 Properties of SMPCs

The cyclic behaviour, mechanical properties and SMEs of glass fibre reinforced shape memory PUs with variable fibre contents were investigated by Ohki et al (2004) [22]. The study showed that, the Tensile strength at a certain temperature has enhanced as a result of glass fibre reinforcing. Surprisingly, the reinforced SMPC samples performed better in terms of crack propagation and cyclic loading. Moreover, Ohki et al. demonstrated that an optimal fibre weight ratio between 10% and 20% exists for extremely low residual strain under cyclic loading. Figure 2.8 depicts how the Young's modulus of PU SMPs increased with fibre weight ratios but decreased with temperature [22].
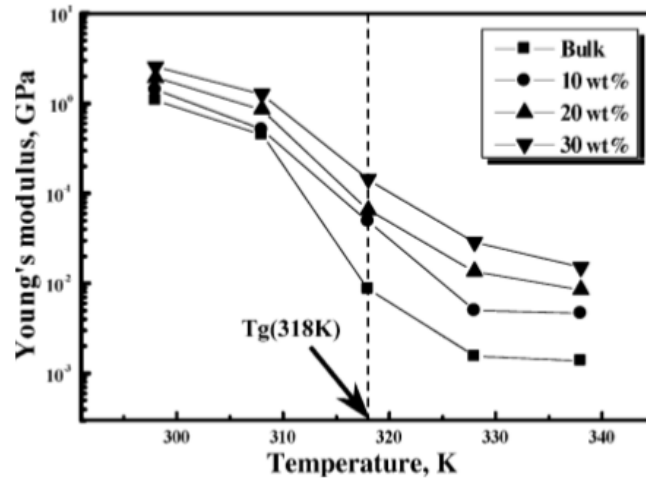
Figure 2.8: Effect of temperature on the young's modulus
of reinforced PUs with different fibre fractions [22]

Fejos et al. (2012) investigated the shape memory characteristics of a Glycerol based SMP reinforced with 38 v/v% woven glass fibre fabric, in a dynamic mechanical analysis (DMA) utilising the 3-point bending mode [94]. The results demonstrated that the recovery stress has increased by two folds compared to the neat SMP. Surprisingly, the introduction of glass fibre reduced shape fixity and recovery rate while having no effect on shape recovery [94].

Azzawi et al. (2017) also investigated the impact of fibre reinforcement on the mechanical properties and geometrical shape stability of a styrene based SMPC [95]. Their findings demonstrated that the addition of glass fibre improved the mechanical properties of the SMP below T_g. The storage modulus of SMPCs with 20% and 25% fibre content was respectively, 1.75 and 2.35 times greater than that of the neat SMP. However, the inclusion of the reinforcing fibres reduced the dimensional stability of the SMPC samples during heating. As proposed, the application of a constant tensile load reduced the undesired thermal deformations of SMPCs during heating. Furthermore, it was revealed that the T_g of the SMPC increases with increasing fibre content. That is due to the low thermal conductivity of glass fibre resulting a delay in the commencement of heating and softening of the polymer matrix [95].

Xu et al. (2022) investigated properties of SMPCs reinforced by GO/SiO$_2$ modified carbon fibre. The GO/SiO$_2$ fillers were deposited on the surface of carbon fibre and added them into the polymer matrix to prepare the composite samples with different GO/SiO$_2$ self-assembly layers. Decomposition of nanoparticles GO/SiO$_2$ on carbon fibre reinforcement significantly improved thermal conductivity. The SMPC with four self-assembled layers showed maximum fracture stress and elastic modulus, and corresponding fracture strain decreased as the number of layers increased [96].

Asar et al. (2022) studied the effects of thermally reduced graphene oxide coated glass fabric (TRGO-GF) as a sensing element and reinforcement to fabricate thermos-responsive PU based self-sensing SMPC. Interestingly, addition of TRGO-GF resulted improvements in storage modulus (4 folds), T$_g$ (by 2 ^{o}C), flexural strength (2 folds), tensile strength (3 folds) and elastic modulus (2.5 folds), compared to the plain SMP [97].

Overall, further studies of chopped, unidirectional and woven reinforcement effects of glass, carbon, and Kevlar fibres have shown significant improvements in material strength, stiffness and shape memory performance compared to their pristine SMPs based on PU, epoxy and styrene [13, 98-101].

2.3.2 Durability of SMPCs

- **Outer space related conditions**

Several important factors must be considered when selecting materials for applications in space environment, which is extremely harsh. Few of such conditions are high vacuum, ultra-high or low temperature cycle effect, UV and gamma (γ) radiation [2]. Leng et al (2013) studied the impact of γ radiation (1×10^5 Gy and 1×10^6 Gy) on epoxy based SMP, to simulate radiation exposure of 140 days. Results have shown a slight decrease of T$_g$ (~10%) and tensile strength but have maintain sufficient strength required

for space applications. Further, the shape recovery rate was increased due to 1×10^5 Gy radiation exposure [102].

The effects of UV radiation on the thermomechanical characteristics and SME of a styrene based SMP and its glass fibre reinforced (GFR) SMPC was examined by Azzawi el al (2018). It was revealed that the mechanical properties, shape recovery rate, recovery stresses and T_g have declined, while no impact on the fixity ratio and relaxation modulus was observed [103].

The UV degradation effects on the discoloration, UV absorbability, surface hardness, thermomechanical properties and SMEs, of styrene and epoxy based SMPs filled with varying percentages of nano-zinc oxide (ZnO) particles was studied by Wong et al (2015) [104]. The specimens were aged with UV intensity and temperature, eleven and three times, respectively, higher than typical ambient conditions. Interestingly, the selected UV intensity level of the accelerated test correspond to 22 days of sunlight. It was revealed that all styrene based specimens were hardened after accelerated UV ageing, whereas epoxy based samples were softened [104].

- **Water/moisture effects**

Xu et al (2011) studied the combined UV radiation and water immersion (rain water and saturated salt water) effects on a close celled syntactic foam based SMP which was developed as a sealant in expansion joints. The combined effects of UV and water resulted in a greater reduction in strength and ductility than UV alone. Further, the property decline for foams immersed in saltwater was less than that in rainwater. The T_g of the SMP foam was also reduced due to water immersion [105].

A series of experimental studies on the effects of moisture on the T_g and thermomechanical properties of an ether based PU SMP was performed by Yang et al (2006) [106]. The study showed that the T_g of the SMP decreases with the increase of immersion time in room temperature water and the

change is thermally reversible. Water absorbed in the SMP weakens the hydrogen bonding between N−H and C=O groups (Figure 2.9), which causes a significant decrease in T_g. Water absorbed by the SMP can be divided into two categories; free water and bound water. The cyclic differential scanning calorimetry (DSC) test can determine their amounts in the SMP. It has also been discovered that free water can be completely eliminated by evaporation at roughly 120 °C. Interestingly, the study concluded that only bound water significantly influence the T_g and uniaxial tensile behaviour [106].
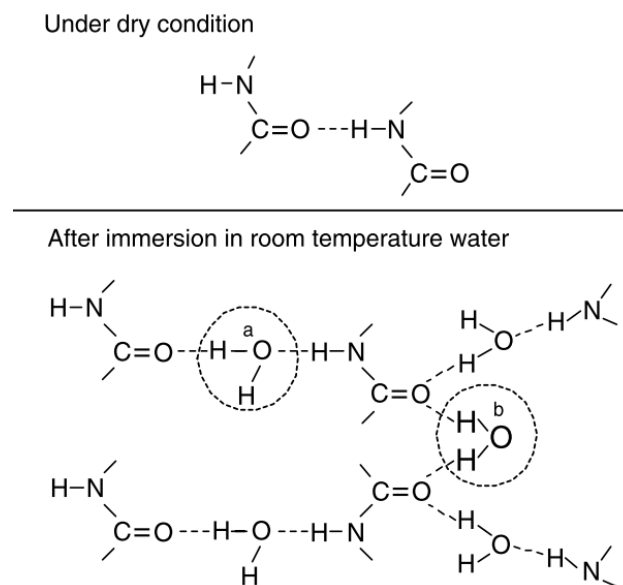
Figure 2.9: Effects of water ingress on the hydrogen bonding in PU SMP [106]

A similar study was carried out by Yu et al (2011), for a PU based SMP foam with the ultimate goal of engineering the SMP material for use in blood contacting environments [107]. The experiments were performed at varying humidity levels (non-immersion and immersion). The SMP exhibited a maximum water uptake of 8% by mass, after exposure to 100% RH for 96hr. A drop in the T_g was also identified by DSC tests and the maximum water uptake shifted the T_g from 67°C to 5°C. The tensile results

demonstrated that water molecules that penetrated the interior structure of the SMP functioned as plasticisers. The plasticisers limited free polymer chain movements and resulted in a failure stress decline [107].

- **Fatigue properties**

Fatigue is a crucial loading condition which can lead to catastrophic failure of components even with a lower stress level. Even though SMPC's mechanical properties were broadly studied, research knowledge on cyclic and fatigue damage behaviours of SMPCs have not been fully explored [108]. Following are the outcomes of fatigue behaviour related SMPC performance findings, according to the only available research article.

As presented in Section 2.3.1 Ohki et al (2004) studied the cyclic behaviour of PU SMPs reinforced with 3mm chopped strand glass fibres. The T_g of the SMPC was 318 K (~45 ^{o}C) [22]. The mechanical cycle tests were performed at room temperature (298 K) under both constant stress and constant strain cycle conditions. For the constant stress cycle, the upper limit stress was set to be 50 % of the maximum static tensile. For the constant strain cycle, the upper limit strain value was set to be 50 % of the strain at the maximum static tensile stress. The specimens were loaded for 20, 40 and 60 cycles. The study investigated the effects of cycle number and fibre weight fraction on the mechanical properties of the PU based SMPC. It was shown that, the inclusion of glass fibre reinforcements have improved the resistance to cyclic loading and crack propagation [22].

- **Fire performance**

Fire based characterisation is another identified aspect of SMPC material performance which was not studied well and consists of very limited research knowledge. However, a couple of researches were carried out very recently, to evaluate the flame retardancy of SMP materials and are described below.

Mehmet et al (2022) enhanced the fire resistance of flax fibre reinforced PU based SMPC with diammonium phosphate, polydopamine and titanium dioxide (TiO_2) [109]. Flax fibres were treated with diammonium phosphate. Then coated with polydopamine (PDA) and SMP matrix reinforced with titanium dioxide. By examining the scanning electron microscope (SEM) images of the produced composites before and after combustion, a protective char layer of PDA was observed. The composite structure preserved its integrity after combustion and the mass loss decreased from 82 % to 69 % because to the protective char layer. The effect of PDA and TiO_2 on the reinforcement and PU SMP matrix was studied by thermogravimetric analysis and differential thermal analysis [109].

The flame retardancy of a 3D printable SMP based syntactic foam was studied by Abedin et al (2022) [110]. The syntactic foam was fabricated by incorporating a high temperature shape memory polymer (HTSMP) as the matrix, with 40 v/v% hollow glass microspheres (HGM) K20, K15, and K1 as fillers. The foam consisting of K20 HGM exhibited excellent flame retardancy compared to other specimens. However, the fire was not extinguished completely during the tests [110].

2.3.3 Applications of SMPCs

In the recent past with the development of SMPCs, the applicability in space applications have been significantly investigated. The effectiveness of outer space exploration missions has reduced as a result of conventional structures having several limitations, such as; heaviness, high cost, large volume consumed in the space vehicle, and high deployable shock impact. As a result, the need for innovative materials capable of improving the efficiency of aerospace products increased by the day. As a result, SMPCs that can be packed into a small space and deployed under a variety of environmental conditions have attracted a lot more attention. After years of SMPC development, unique capabilities of SMPCs could outrace majority

of the conventional materials used at that time. Recently, SMPCs are used in a wide range of applications extending from outer space to automobiles. Recently, they have been developed and qualified particularly for deployable components and structures in aerospace applications [26, 111]. Some of space applications include hinges, trusses, booms, antennas, optical reflectors and morphing skins [23, 26, 112, 113].

- **Deployable structures**

The classic aerospace deployable devices change structural configuration in-orbit by using a mechanical hinge, stored energy devices, or motor driven tools. Traditional deployment devices have certain inherent disadvantages, such as a difficult assembly procedure, heavy mechanisms, large volumes, and undesirable effects during deployment. However, light weight and self-actuating SMPC components can overcome such inherent challenges of deploying devices [26, 114]. Herath et al. (2019) presented shape recovery of a small scale prototype deployable structure (in Figure 2.10) that is suitable for space habitats [33].

| 0 min | 3 min | 6 min | 9 min | 12 min | 15 min | 18 min |
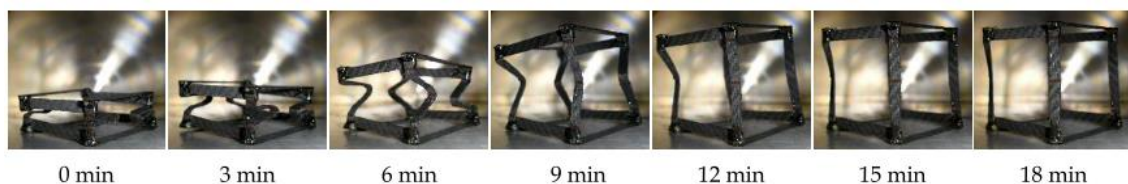
Figure 2.10: Shape recovery of a prototype space deployable habitat with time [33]

- **SMPC hinge**

The traditional hinge mechanism is made up of various moving elements, such as gearboxes, springs, cylinder and mechanical locking systems. During operation, these components might generate noise and cause energy loss. To prevent such drawbacks, lightweight, flexible, reliable and cost effective hinge mechanisms have become highly important for supporting structures, such as; solar arrays, antennas and other devices in

the spacecraft [115]. Several SMPC hinge designs were proposed by researchers as measure of activating the mechanism just by applying the suitable stimulus. Figure 2.11 illustrates how SMPC hinges developed gradually over the time [20, 26, 115-118].
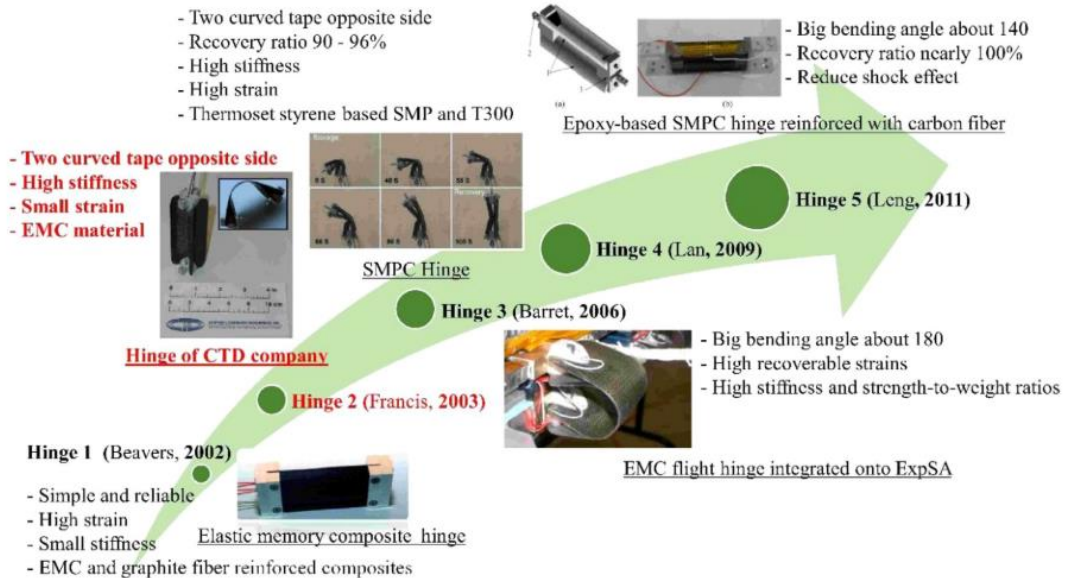
Figure 2.11: Gradual development of SMPC hinges [115]

- **Solar arrays and reflectors**

Figure 2.12 shows an example of an aerospace application where SMPCs are used as actuators in a folded solar panel. The concept of origami has been used to fold the solar panel such a way that the volume is minimized [119]. A similar concept has been used for large aperture antennas which promotes satellite's communication systems and presented in Figure 2.13. The use of SMPCs allows the antenna to be stowed in the spacecraft and then it can be triggered to initiate self-deployment [120].
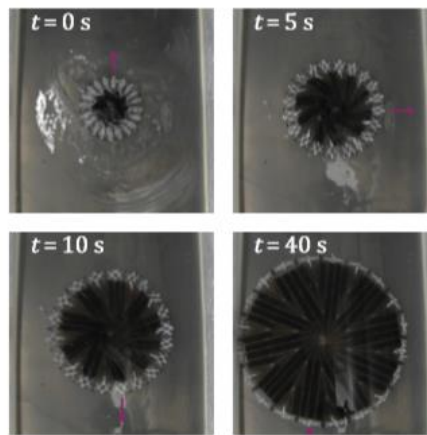
Figure 2.12: Autonomous deployment of
a SMPC solar panel array [119]

(a)   (b)

Figure 2.13: SMPC reflector: (a) Deformed shape and (b)
recovered shape [120]

- **Morphing structures**

Figure 2.14 illustrates the use of SMPCs in a variable camber wing, which is inspired from the ability of birds to change their wing posture depending on the air flow. In order to improve flight performance at take-off, landing and cruising, parameters of the wing such as camber, lift to drag ratio and chord length have to be changed [25]. Self-activating capability of SMPs will minimize the number of mechanical actuators used, making the weight of the aircraft low as possible. A similar concepts was proposed for the application of SMPCs in shape changing unmanned aircraft wings and the concept is presented in Figure 2.15 [121].
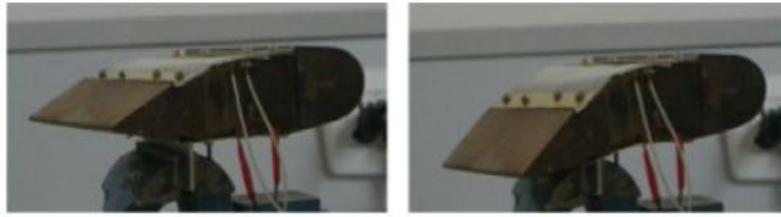
Figure 2.14: SMPC integrated variable camber wing [25]
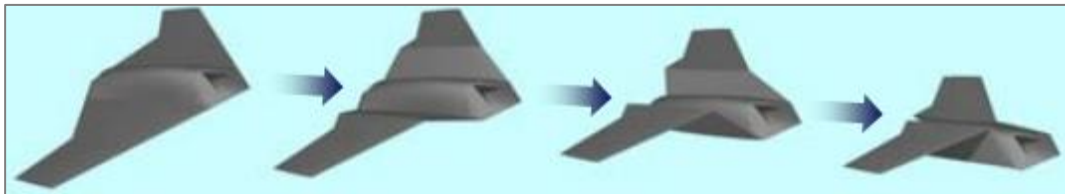
Figure 2.15: Demonstration of a conceptual morphing wing [121]

2.4 Numerical modelling of SME

The SMPs and their composites show variable properties above and below the T_g. Consequently, the constitutive characteristics or modelling techniques of SMPs depend on its temperature. When the temperature is below T_g, the polymer in the glassy state is considered to exhibit an elastic behaviour. While it behaves as a viscous material at a temperature higher than T_g. In the transition temperature, the SMPs show viscoelastic behaviour, in which the polymer properties change rapidly, decreasing the elastic modulus approximately twofold [2]. In this section, research carried relevant to the viscoelastic modelling of SMPs to demonstrate the SMEs are presented.

In the recent past, researchers attempted to develop constitutive models in order to describe the thermomechanical behaviour of SMPs and their composites. There are two common approaches used in the literature for modelling of the thermomechanical behaviour of SMPs. They are purely elastic and viscoelastic approaches. In a purely elastic approach, an amorphous SMP is considered as a two phase material consist of glassy and rubbery phases. Hence, a constitutive model is needed to predict the

30

stiffness of the two phase composite material using the stiffness values of individual phases [122]. Using a two phase approach Diani et al. (2006) proposed a 3D thermos-viscoelastic model which is thermodynamically motivated by using the mechanical understanding of stress, strain and temperature behaviours in SMPs. Also, the model can accurately predict the remaining strain during stress release in the thermomechanical cycle of an SMP [123].
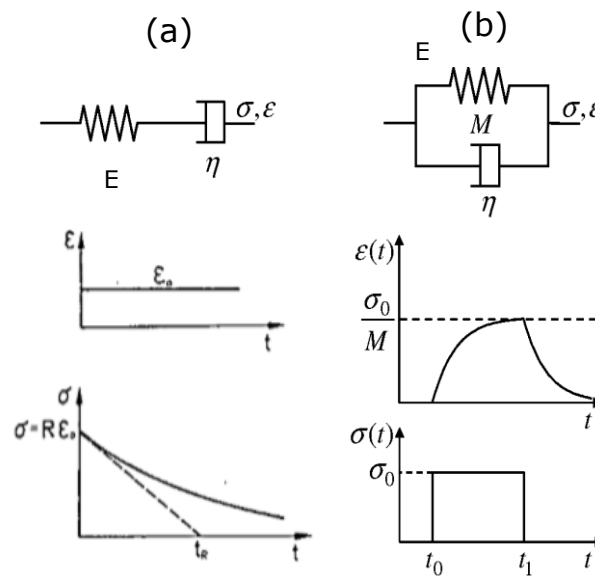
Figure 2.16: (a) Maxwell model and (b)
Kelvin model [21]

The viscoelastic approach was followed by Tobushi et al. (2001) and developed a nonlinear thermomechanical constitutive model by modifying a linear model for SMPs from his previous work. The developed model could describe thermomechanical properties such as fixity ratio (R_f), recovery ratio (R_r) and recovery stress of a PU based SMP well up to 20 % strain [124]. Mechanical spring and dashpot analogy was used in the viscoelastic approach which is represented by models, such as the Kelvin, Maxwell, standard linear model and the generalized Maxwell model. If a constant strain (ε) is applied in the Maxwell model shown in Figure 2.16 (a), there will be an instantaneous extension of the spring creating a stress (σ). But

with time, the dashpot extends decaying the initial stress developed. Therefore, Maxwell model represents the stress relaxation in a viscoelastic behaviour. When a constant σ is applied in the Kelvin model in Figure 2.16 (b), the dashpot prevents any instantaneous deformation. With time it shows increasing strain, which is analogous to creep deformation. Therefore, these two models are combined together to model the general behaviour of a viscoelastic material using the "standard linear model" shown in Figure 2.17. To precisely model the viscoelastic behaviour of a material, the "generalized Maxwell model" (Figure 2.18) has been used. The model considers that the relaxation process does not occur at a single time, but at a distribution of times [21].

In the model E and η represent the elastic modulus and the viscosity coefficient of the elastic and damping element respectively. Thus, the following equations can be obtained, where ε_o and σ_o are the strain and stress of the elastic element E_o. ε_i and σ_i are the strain and stress of the Maxwell model.
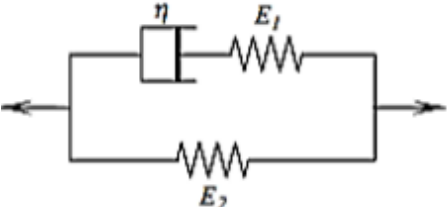
Figure 2.17: Standard linear model of viscoelasticity [21]
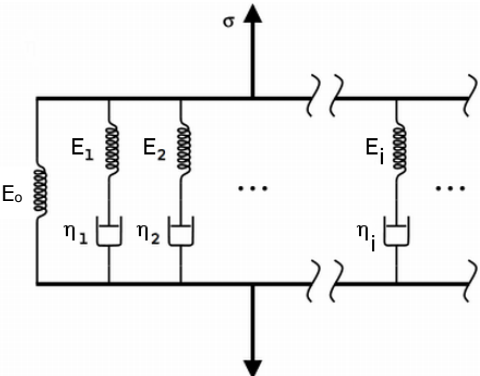
Figure 2.18: Generalized Maxwell model [21]

$$\varepsilon = \varepsilon_0 = \varepsilon_i \ (i = 1,2,3..,n)$$

$$\sigma = \sigma_0 + \sum_{i=1}^{n} \sigma_i$$

$$\sigma_0 = E_0 . \varepsilon$$

For the ith Maxwell model, the following relationship can be derived. Taking Relaxation time = $\tau = \eta/E$;

$$\left(\frac{d}{dt} + \frac{1}{\tau_i}\right) \sigma_i(t) = E_i \frac{d\varepsilon_i}{dt}$$

$$\sigma_i = \varepsilon E_i \exp(\frac{-t}{\tau_i})$$

Then the relaxation modulus R(t) can be given as,

$$R(t) = \frac{\sigma(t)}{\varepsilon} = E_0 + \sum_{i=1}^{n} E_i \exp\left(\frac{-t}{\tau_i}\right) ; (t \geq 0)$$

Using a generalized Maxwell model Diani et al. (2012) modelled the thermomechanical characteristics of SMP and the resulting model was implemented in a commercial finite element code. The capability of the proposed model to simulate and finally predict the shape recovery and shape storage of SMP was compared against experimental SMP thermomechanical torsion data in a large deformation regimen [122]. As an extension to the work proposed by Diani et al. (2012), Azzawi et al. (2017) developed a finite element simulation method to model the thermomechanical behaviour of the SMP composites using ABQUS software. SMPC cantilever beams reinforced with glass fibre were used to prove the correlation between experimental and simulation results.

This technique is based only on material viscoelastic characteristics which were obtained by applying "time temperature superposition" (TTS) method on the material's stress relaxation characteristics (as in Figure 2.19) and fitting resulting master curve with Prony series (Figure 2.20) [125].
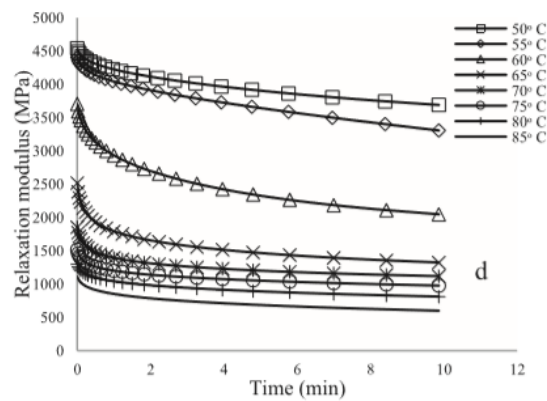
Figure 2.19: Relaxation modulus vs time under varying isothermal conditions for 30% SMPC [125]
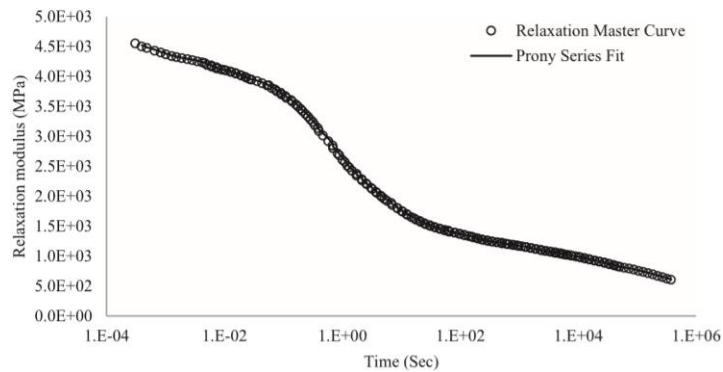
Figure 2.20: Relaxation master curve and Prony series fitting curves for the 30% SMPC sample obtained for 0.25 % stain at reference temperature 68 °C [125]

2.5 Basalt fibre

Glass and carbon fibres are the most widely used types of reinforcements in the polymer composite industry. It is generally known that when carbon fibre is merged with a polymer matrix, excellent mechanical properties such as high strength, stiffness, high elastic modulus, and low weight can be obtained. But, high cost of carbon fibre led to a growing interest on alternative fibres with reasonably good mechanical properties at a cheaper price. Recent experimental studies and analytical approaches revealed that basalt fibre reinforced materials may be effective for structural applications in civil engineering [126]. Basalt has many

excellent properties such as high strength, electrical insulation, corrosion resistance, impact resistance [127] and high temperature resistance. Properties of basalt fibres are similar to that of glass fibres, but have better physical and mechanical properties than glass fibres. Also, it is significantly cheaper than carbon fibres [128].

Moreover, Basalt fibre has the advantages of strong anti-oxidation capability, low thermal conductivity and high melting temperature. Basalt fibre has a higher Young's modulus and tensile strength compared to E glass fibre [128]. In Table 2.1, a comparison of the basic mechanical properties of basalt and E-glass fibres are given [129]. In addition, Lopresto et al. (2011) have investigated the performance of basalt and E-glass fibre in an epoxy matrix and the results obtained for the Young's modulus in tensile, flexural and compressive tests are demonstrated in Figure 2.22. Even though basalt fibre composites show better mechanical properties compared to E glass fibre, Kessler et al. (2016) have reported (as shown in Figure 2.21) that the strength of basalt fibre is lower than that of E-glass fibre above 300 ^{o}C. Tests were carried out to evaluate the effect of thermal and mechanical loads on basalt, glass and carbon fibre reinforced polymer composites [130]. It is important to note that no one has ever used basalt fibre as a reinforcement in SMPC applications despite of its better properties over glass fibre.

Table 2.1: Comparison of mechanical properties of basalt and E-glass fibre [128]

Properties	Basalt	E-glass
Density (kg/dm^3)	2.8	2.54
Tensile strength (MPa)	4800	3200
Elastic modulus (GPa)	90	70
Elongation at break (%)	3.15	4.0
Max. Service temp. (^{o}C)	650	460
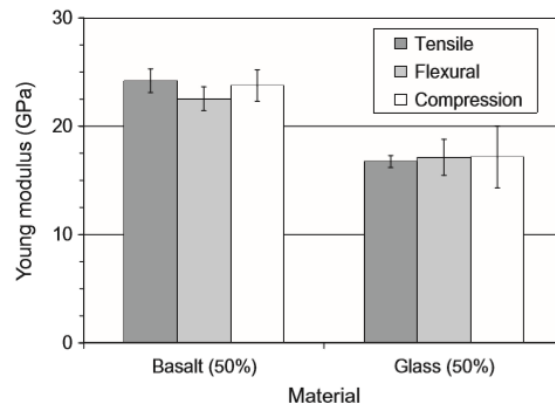
Figure 2.22: Comparison of tensile, flexural and compressive modulus of basalt and E-glass fibre composites with 50 v/v% [129]
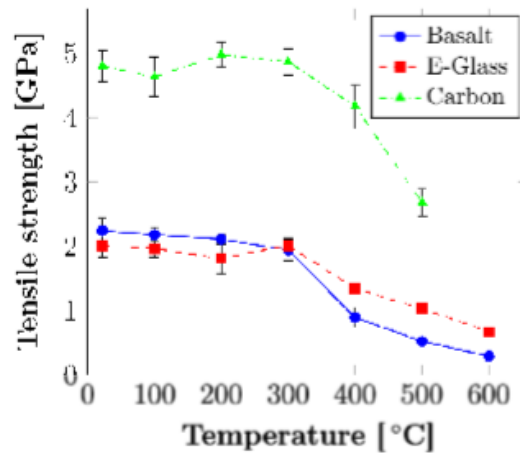
Figure 2.21: Tensile strength of basalt, E-glass and carbon fibre rovings after a 2 hr heat treatment [130]

2.6 GFRP in constructions

In recent decades, implementation of glass fibre reinforced polymers (GFRPs) in civil engineering applications have been increased. High strength and stiffness, lightweight, corrosion resistance and water resistance are GFRPs key advantages [131, 132]. Typically, GFRPs are used in three aspects of civil engineering; (1) GFRP structures, (2) GFRP bars and (3) strengthening/repairing systems [133].

2.6.1 Pultrusion process

GFRP components can be manufactured using different processes. However, the most common fabricating method of GFRP is pultrusion. The procedure is a very cost effective method of manufacturing structural profiles, such as; I-beams, channels and tubular profiles. and involves drawing raw fibres through a resin solution and then through a heated die. As the resin and fibres pass through the heated die, the resin initiates its curing cycle. As a consequence, the polymer solidifies into the shape of the die creating a structural component [134, 135]. A schematic of the pultrusion process is presented in Figure 2.23 [133]. Due to its effectiveness and common usage, pultrusion machines have been developed and are now equipped with high pressure resin injector dies, instead of messy resin baths. In addition, rotating winders are used nowadays to incorporate angled fibre rovings which enables alteration of directional GFRP properties as per intended application. The cured GFRP component is then pulled using two reciprocating pullers, alternatively. Once, the required length is achieved, the sensor triggers the cutting saw which separates the profile form the production line. Further, the overall process is automated and the programme settings can be easily tailored to cater any product length [134].
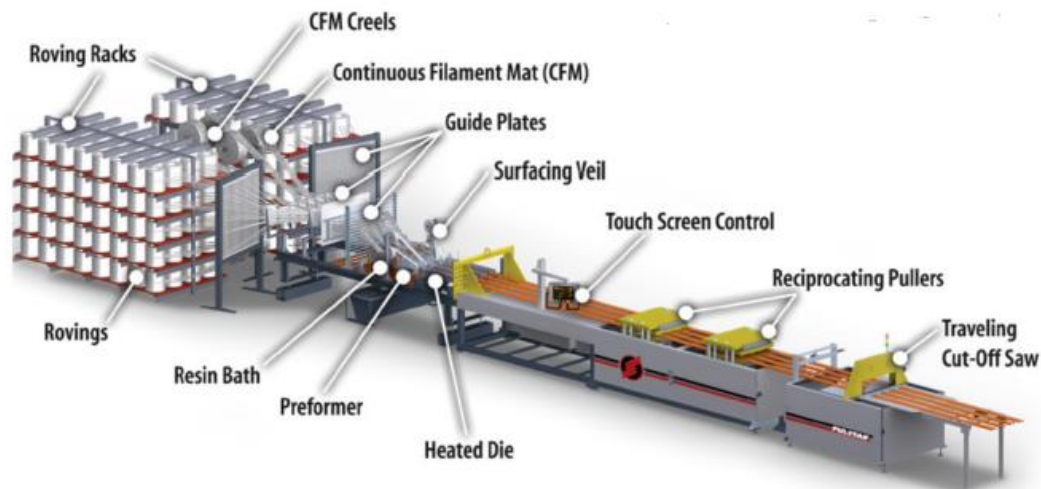
Figure 2.23: Pultrusion process and components [133]

2.6.2 Civil engineering applications

Recently, there has been a major growth in the application of GFRP in infrastructure, either completely using GFRP or combining it with steel or concrete as a reinforcement [136]. The single story gable frames were the first GFRP-based building structures, utilised in developing computer and electronics industries for electromagnetic interference (EMI) test facilities. The main advantage of using FRP profiles is their electromagnetic transparency, as the EMI building was designed to have a magnetically neutral structure [137]. A 15 m tall five story building (Figure 2.24 (a)) which comprised trapezoidal load bearing GFRP A frames, was constructed for the Swiss building fair in 1998 [134, 138]. Further, GFRP components are employed in cooling towers used for heating, cooling, ventilation and other industrial purposes, due to their corrosion resistance. Figure 2.24 (b) presents a pultruded GFRP cooling tower [133]. Bridge decking is another prominent application area for GFRP. In Germany, a 27 m long bridge was constructed with two steel beams and a multicellular GFRP deck made out of pultruded profiles [139].
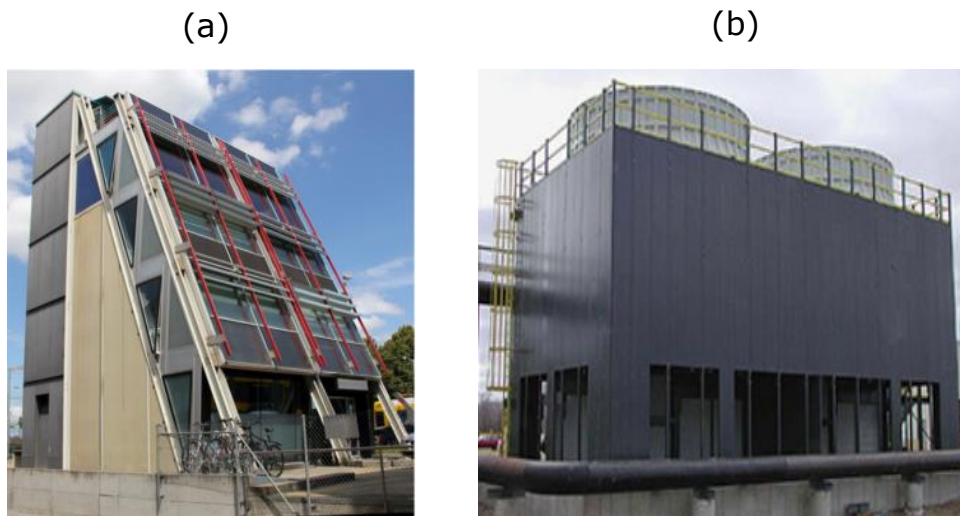
Figure 2.24: Applications of GFRP profiles in constructions; (a) 15 m tall building in Switzerland and (b) pultruded GFRP cooling tower [134, 138]

A leading GFRP manufacturer in Australia, Wagners Composite Fibre Technologies (CFT), has been supplying composite fibre material for civil engineering construction industry since 2002 [140]. Interestingly, as a well-established industry in GFRP, they have been successful to export their products to the USA, Malaysia, the United Arab Emirates and New Zealand. Their pultruded GFRP profiles are used for a variety of construction applications such as; pedestrian boardwalks and bridges, road bridges, viewing platforms, shelters, marine infrastructure, electrical crossarms and light poles (shown in Figure 2.25) [140].

(a)   (b)

(c)   (d)

(e)
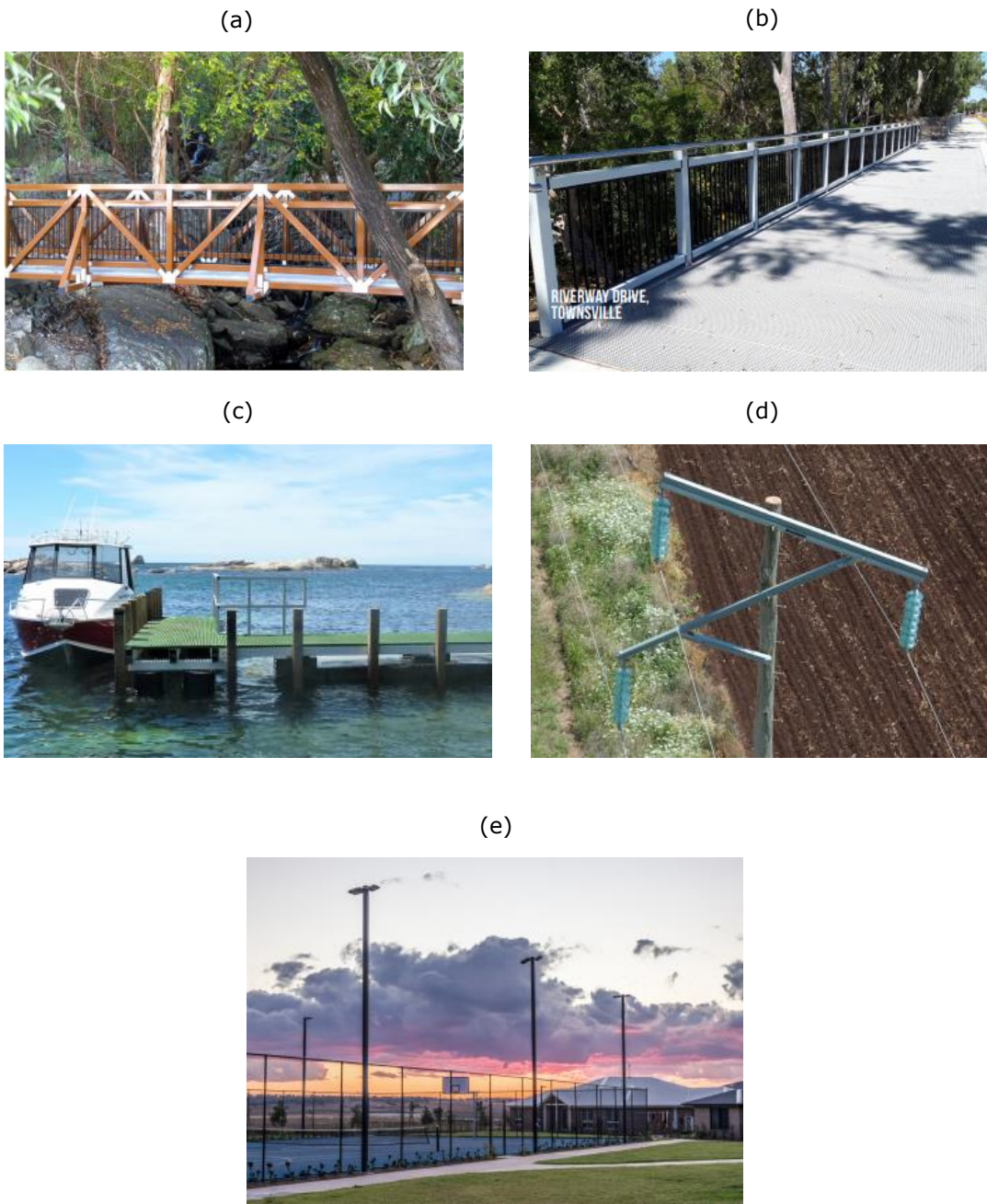
Figure 2.25: Applications of GFRP profiles; (a) pedestrian bridges, (b) boardwalks, (c) marine infrastructure, (d) crossarms and (e) light poles [140]

2.7 Prefabricated modular constructions

2.7.1 Introduction to prefab modular constructions

The modular construction of building structures has gained substantial interest form the construction sector in recent years due to its benefits over conventional construction methods, which include: faster and safer building practices, higher quality, improved predictability of completion time, reduced labour demand, less wastage of resources and less environmental sensitivity [30, 141-143]. Prefabricated housing comprises the offsite fabrication and assembly of components prior to their ultimate installation at a specified location [144]. While some prefabricated items are used in typical onsite construction, such as plasterboard sheets or finished doors, the phrase "prefabrication" is normally reserved for more extensive products, such as the fabrication of structural volumetric spaces, including complete houses or enclosed modules, and non-structural volumetric spaces [145]. Further, past studies utilized several terminology and acronyms connected with prefabricated construction, such as off-site prefabrication, precast concrete building, off-site constructions and industrialised building [146-148]. Figure 2.26 illustrates different approaches of modular constructions in terms of complexity and scale of application [149]. Prefabrication construction is often classified into four categories based on the degree of prefabrication used on the product [144, 150, 151];

  I. Manufacturing and sub assembly of components that are always done in a factory and are not considered for on-site production

 II. Non-volumetric pre-assembly refers to pre-assembled items that do not enclose useable space, such as wood roof trusses

III. Volumetric pre-assembly refers to pre-assembled units enclosing useable space that are typically created inside factories but do not form part of the building's structure, such as bathrooms and restrooms

IV.   Entire buildings refer to pre-assembled volumetric pieces that create the building's physical structure and fabric, such as motel rooms
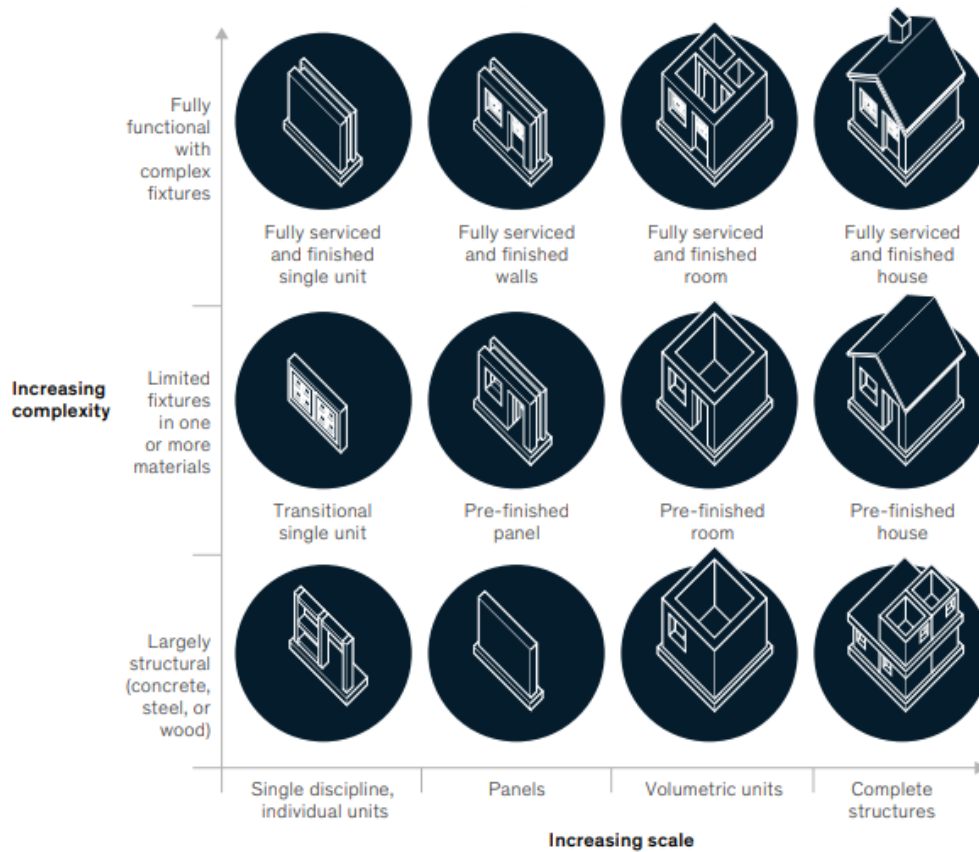
Figure 2.26: Comparison of modular construction approaches by complexity and scale [149]

2.7.2 Applications of prefab modular constructions

In recent years, modular constructions have been widely used in the construction of low-rise buildings as well as high-rise skyscrapers up to 44 stories tall (La Trobe Tower in Melbourne Australia) [30, 152]. The modular structure construction in Croydon, South London, is expected to be completed as the world's tallest modular building which combines two residential towers of 38 and 44 floors in height [153]. Figure 2.27 presents an application of prefabricated construction of a family house in Tasmania, Australia, made out of hollow timber box modules [154]. Further, a completed 12 floor student accommodation modular construction in Bristol,

built using concrete cores, is demonstrated in Figure 2.28 [152]. In addition, some of the other similar applications for prefabricated modular constructions include: low rise 'Little Hero' apartment building in Melbourne, 'SOHO' apartment building in Darwin, 'One9' apartment building in Melbourne, 'Katrina Cottage' housing in Mississippi, housing for Haiti earthquake victims, etc [155].

(a)	(b)	(c)
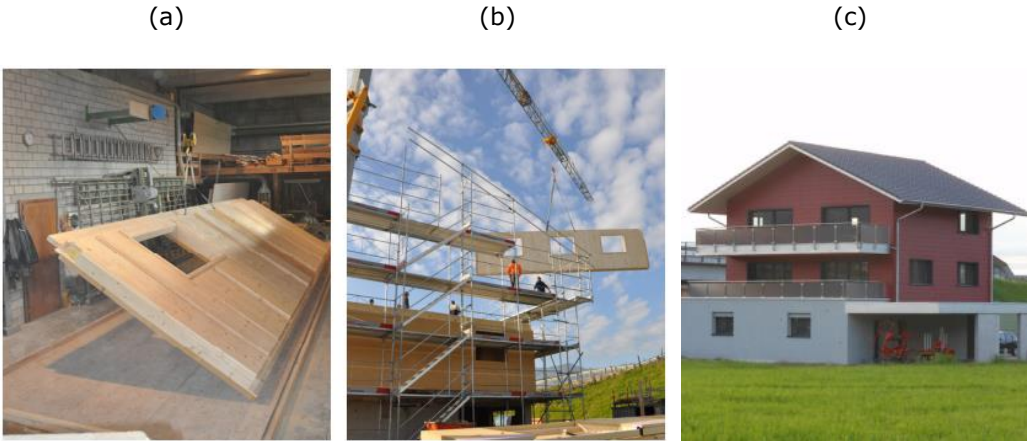
Figure 2.27: Constructions steps of family house; (a) fabrication of panels, (b) on site assembly and (c) completed house [154]

Figure 2.28: Modular twelve floor student accommodation building in Bristol [152]

2.7.3 Limitations and future developments

Despite prefabrication's inherent advantages, its application has resulted in a wide range of drawbacks and challenges, ranging from inadequate design guidelines, investor and training shortages, unfavourable public opinion, capital requirements and most importantly, shipping, handling and assembly difficulties [151]. To remedy such limitations, the potential of FRP composites to replace conventional timber, concrete, and steel materials in prefabricated building applications is currently being studied by researchers [156-158]. However, due to inadequate understanding of the performance of new substitute construction materials under long term and extreme loading conditions, the field of prefabricated modular construction technologies is progressing slowly [30].

2.8 Summary

According to the literature survey, a few of the identified key research gaps related to the field of SMPCs are listed below. As SMPs and their fibre composites were mainly focused on biomedical and space applications, there has been no considerable research done on the usage of fibre reinforced SMPs for civil infrastructure development. In addition, majority of the SMPC research have incorporated glass and carbon fibre for reinforcing the SMP matrix, but have not studied any natural fibre types. Importantly, the phenomenon of programming damage of SMPCs has not been well understood and knowledge on the FEA based viscoelastic study of the programming stage was found to be lacking. Even though thermomechanical and mechanical properties of SMPCs were well researched, the durability based characteristics such as fire exposure and fatigue performance have not been thoroughly studied.

The methodologies and outcomes of the research work carried out to address the identified knowledge gaps in the field of SMPCs and related applications, are elaborated in chapters 3 to 5.

CHAPTER 3: MATERIAL PREPARATION AND CHARACTERIZATION

3.1 Introduction

To date, a variety of functional SMPs with exceptional SME have been developed. Cyanate, styrene, PU and epoxy based SMPs are few of such improved smart materials [51]. Cyanate thermoset resin is a highly thermally stable material with a very high T_g of up to 400 ^{o}C. Moreover, with its low dielectric loss and low hydroscopic level, cyanate based polymer is a suitable material for electronic circuit boards, dielectric coatings, aerospace applications and wave transmitting [54]. Due to low T_g, Styrene based SMPs are of interest for low temperature applications [58]. PU SMPs have a narrow range of T_g around room temperature. Thermoplastic PU SMPs can be moulded to the required shape from injection, extrusion and blowing. They are highly focused on biomedical applications as a result of its low deformation temperatures [159].

As a result of superior mechanical properties, better fatigue resistance [160, 161], good thermal stability [68], ease of processing and excellent chemical resistance [162, 163], an epoxy based resin was selected for this research work to derive SMPs. As epoxies are cheap and readily available in the market, SMPs derived from epoxy resins could be a cost effective solution providing benefits in demanding structural applications. Hence, Chapter 3 gives a detailed analysis on the synthesisation and optimization of epoxy based neat SMP followed by its reinforced composite.

The new knowledge presented in this chapter significantly contributes towards the development and optimization of high strength competent SMPCs for large scale structural components. The material synthesis, manufacturing, characterization techniques, damage quantifying and

optimization procedures elaborated herein can be effectively implemented in further SMPC developments.

3.2 Materials preparation

In this chapter, development of the SMPC is presented in two phases. In Phase I, Bisphenol A epoxy based SMP was synthesised with two amine based hardeners to obtain properties required for a construction material while maintaining superior shape memory properties. Subsequently, in Phase II, continuous fibre reinforcements were integrated within the synthesised SMP matrix to enhance mechanical performance. Further, shape memory characteristics, structural properties, undesirable influence on shape programming and optimization of SMPC constituents are presented in Phase II.

3.2.1 Bisphenol A Epoxy Based SMPs and SMPCs

Three types of chemicals were used for the synthesis of SMP matrix. They were Bisphenol A diglycidyl ether (DGEBA) epoxy resin, Triethylenetetramine (TETA) and Jeffamine D230 amine based hardeners. The epoxy resin DGEBA was supplied by Huntsman, Australia. The two hardeners TETA and Jeffamine D230 were supplied from Sigma Aldrich, Australia. The chemical formulas of DGEBA, TETA and Jeffamine D230 are illustrated in Figure 3.1. These three selected chemicals were mixed in a selected ratio to fully cure the thermoset SMP matrix undergoing complete reaction. The stoichiometric ratio was evaluated using the epoxy equivalent weights 190 g/eq, 24.3 g/eq and 59.5 g/eq, of DGEBA, TETA and D230, respectively. The resultant chemical mixing ratio from Phase I study was used when synthesising the SMP matrix for all specimen preparation. Hence, DGEBA: TETA: D230 were mixed in the weight ratio 13.03: 1: 1.63 respectively. The chemical reactions between DGEBA and the two hardeners are presented in Figure 3.2 [164] and Figure 3.3 [165]. Importantly, the synthesised SMP matrix was degassed in a vacuum oven for 15 min prior

to moulding. Degassing is a vital procedure in SMP related manufacturing as it removes trapped air bubbles during synthesisation which can hinder structural properties of the fully cured SMP. Moreover, the vacuum oven was kept at room temperature to prevent triggering of SMP's chemical reaction.
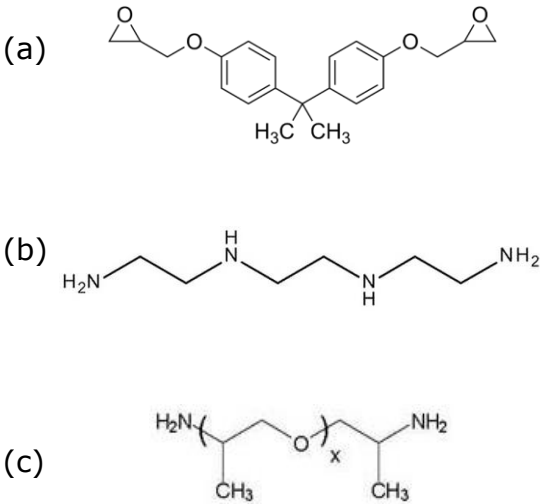
Figure 3.1: Chemical formulae; (a) DGEBA epoxy resin (b) TETA hardener (c) Jeffamine D230 hardener [164][165]
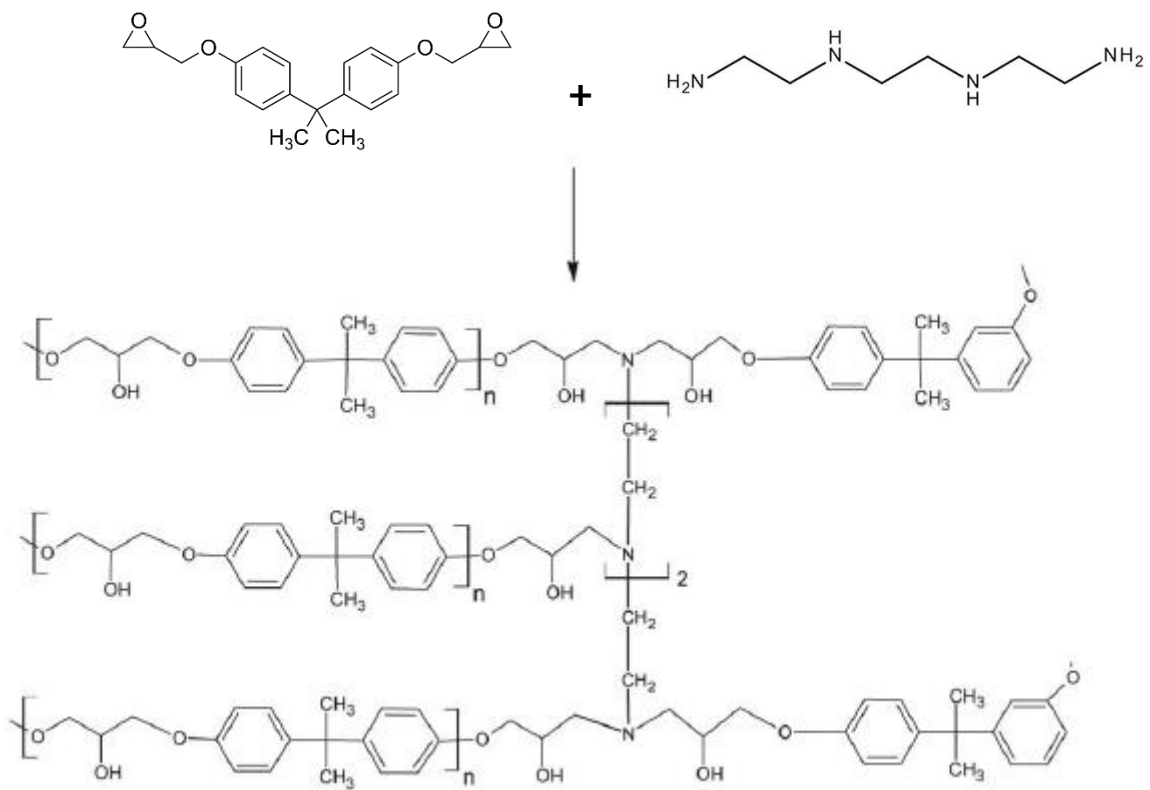
Figure 3.2: Chemical reaction between DGEBA and TETA [164]
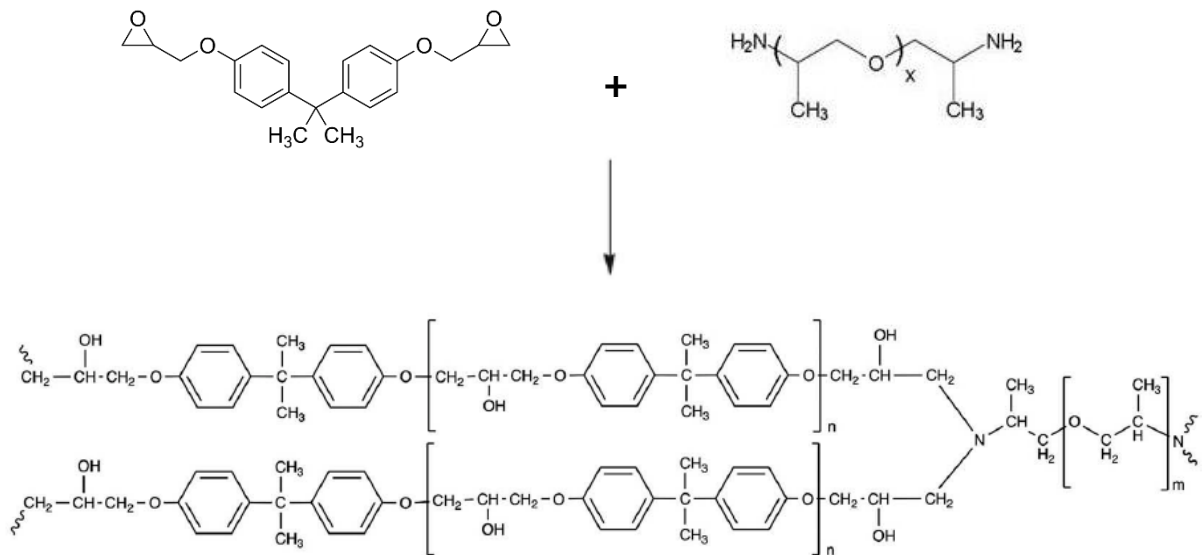
Figure 3.3: Chemical reaction between DGEBA and Jeffamine D230 [165]

A mould made out of two 400 x 400 mm^2 glass plates was used in the manufacturing process specifically to control the thickness of each sample precisely. To facilitate easy demolding and avoid sticking, a layer of PTFE coated non-stick release material was pasted on each glass plate. Required fibre layers were placed at the centre of the mould. Steel spacers of selected thicknesses were then placed between two plates and the sides were properly sealed keeping an opening on the top using a high temperature resistive silicone. The silicone sealing transforms the setup into a tank with required sample thickness and reinforcements. Binder clips were used to keep the plates intact during the fabrication process. The mould was kept a side for a day to dry prior to SMP pouring. A schematic of the mould and its components are shown in Figure 3.4 and Table 3.1

Then, the degassed SMP was poured into the mould held upright, gradually from one side allowing air to escape from the other side. This was done to ensure no air trapes within fibre layers creating voids. After allowing the sample to cure for 24 hr, post curing was done at 100 °C for 1.5 hr followed by 130 °C for 1 hr.

(a)   (b)
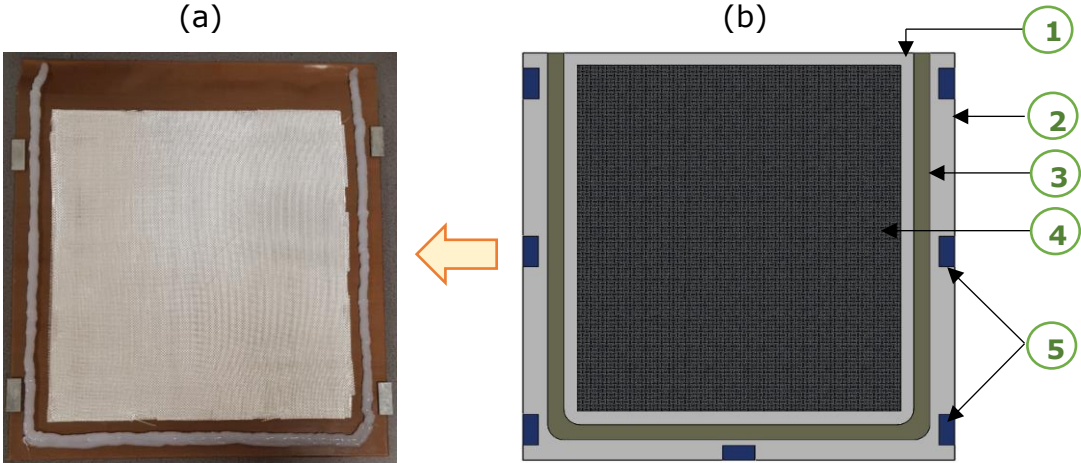
Figure 3.4: Glass sheet mould used for SMP and SMPC
fabrication; (a) actual and (b) schematic
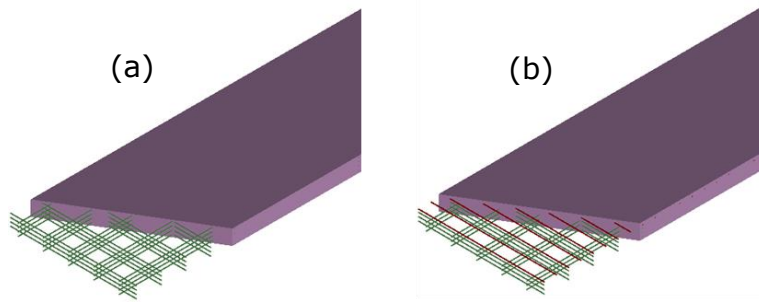
Figure 3.5: Arrangement of fibre reinforcement layers: (a) first stage; for Taguchi optimization, and (b) second stage; fibre architecture modification

Table 3.1: Components of the mould

Part No	Components
1	SMP inlet
2	Glass with release material
3	Silicone seal
4	Fibre fabric
5	Metal spacers

In Phase II, SMPCs were fabricated by integrating 200 gsm plain weave glass, basalt and carbon fibre fabrics as primary reinforcements (as in Figure 3.5(a)). In addition, for second stage optimizing, a stitched unidirectional glass fibre fabric of areal density 500 gsm was used for reinforcement refinements as shown in Figure 3.5(b), to diminish recognized defects presented in Section 3.5.6

3.2.2 Specimen dimensions and cutting

Once the fabricated SMP and SMPC sheets were fully cured, they were demoulded and cut into specific dimensions for testing. Test standards (ISO/ASTM) for polymer composites were used to select sample dimensions for each test. Table 3.2 presents a summary of sample dimensions along with respective standards. Figure 3.6(a) and Figure 3.6(b) illustrate sample

cutting procedure using a waterjet and a cutting layout used to generate '.dxf' files that were fed into the waterjet cutter.

(a)   (b)
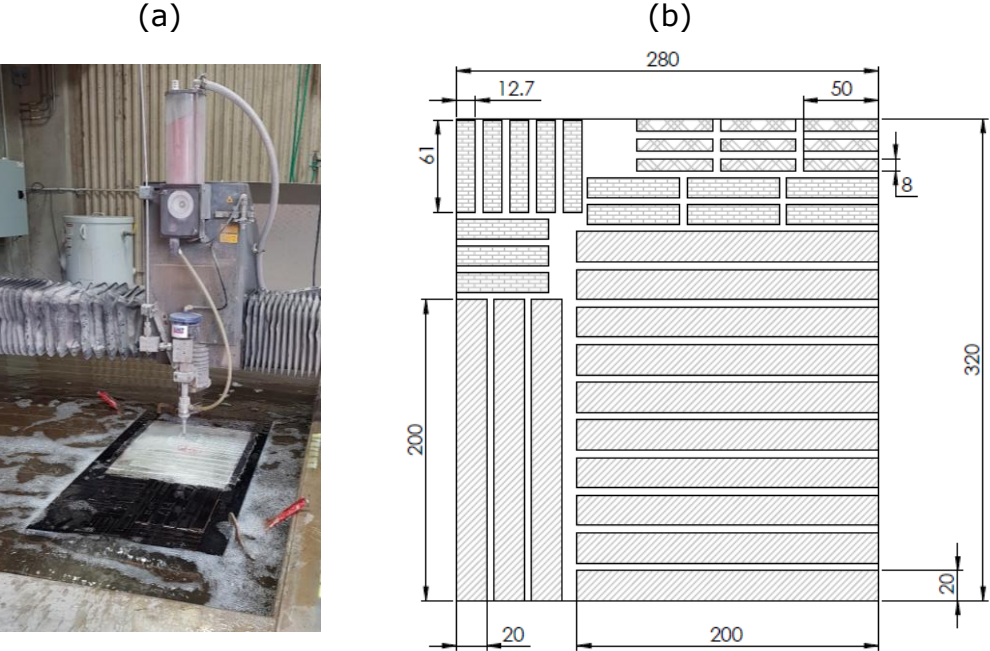
Figure 3.6: SMP and SMPC specimen cutting; (a) waterjet cutter and (b) cutting layout

Table 3.2: Specimen dimensions for standard tests

Experiment	Dimension (mm)		No of specimens tested	Standard
	Length	Width		
DMA	50	8	3	Instrument's specification
Tension	250	25	5	ISO 527-4:2009
Compression	140	12.7	5	ASTM D6641
Flexure	61	12.7	5	ASTM D7264

3.3 Experimental Methods

a) Dynamic Mechanical Analysis (DMA)

Glass transition temperatures, T_s and T_δ of materials were evaluated using TA Instruments HR-2 Discovery Hybrid Rheometer with a dual cantilever fixture. 8 x 50 mm^2 sized samples were used to characterize the storage modulus by means of an Oscillation (temperature ramp) mode. A Displacement of 25 μm was applied at a frequency of 1 Hz. During the test, samples were heated from 20 °C to 120 °C with a temperature ramp of 5 °C/min.

b) Fourier-transform Infrared Spectroscopy (FTIR) experiments

The FTIR analysis was conducted in a Thermo Fisher Scientific, Nicolet iS50 spectrometer. The uncured SMP mixture was analysed with an attenuated total reflection module. The spectrum data were recorded through 500-4000 cm^{-1} wavenumbers with a resolution of 0.5 cm^{-1} and analysed in the OMNIC software.

c) Tension, compression and flexure testing

Tensile tests were conducted according to standards ISO 527–4:2009 using MTS 100 kN uni-axial testing machine. In addition, ASTM D6641/D6641M test standard was followed to carry out compression tests on the same MTS testing machine. Similarly, flexural properties of SMPs and SMPCs were evaluated in a MTS 10 kN testing machine according to ASTM D7264.

d) Shape memory properties

Shape memory properties of neat SMPs in Phase I were evaluated by means of R_f, R_r and long term shape fixity. As the neat SMPs get flexible when heated to T_g, a custom made hand tool was used for programming.

Neat SMP specimens were programmed by bending to 90°. Photos of the fixed and recovered shapes of the SMPs were taken and used to quantify R_f, R_r and long term shape fixity. Equations 3.1 and 3.2 were used to evaluate

Shape memory properties of SMPCs were studied and analysed in terms of R_f, R_r and areal damage percentage (ADP %). Samples of size 100 mm x 20 mm were used to evaluate SME characteristics of each SMPC. The thermo-mechanical cycles of SMPCs were implemented in MTS 10 kN testing machine along with its compatible thermal chamber as shown in Figure 3.8. Programming of SMPCs were carried out at two temperatures: (1) the onset of storage modulus (T_S) and (2) tan δ peak ($T_δ$). Figure 3.7 illustrates the shape programing steps of the SMPCs and specific angles used to evaluate R_f and R_r [166].
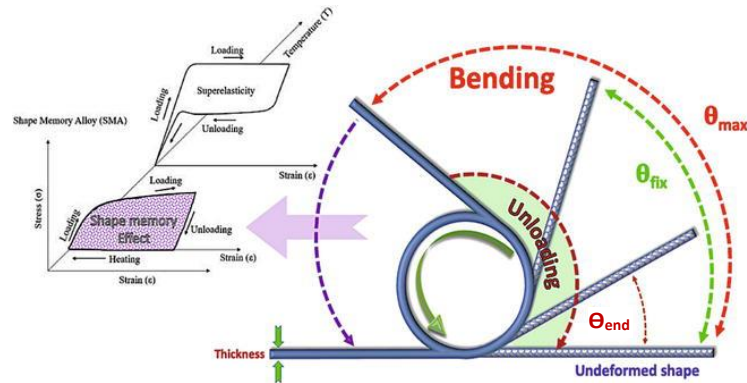
Figure 3.7: Shape programming test and angle representation [166]

$$R_f = \frac{\theta_{fixed}}{\theta_{max}} \times 100\%$$

3.1

$$R_r = \frac{\theta_{max} - \theta_{end}}{\theta_{max}} \times 100\%$$

3.2

First a sample was placed on the bending fixture with a support span of 50 mm and was allowed to heat up to its programming temperature for 30 min. Then, the programming stage was initiated with two selected

deformation rates: (1) 1 mm/min and (2) 60 mm/min. Each SMPC was deformed bending up to a depth of 15 mm at the centre of its span. A piece of rubber of size 50 x 25 x 6 mm^3 was placed on the top face of the SMPC during programming to increase bend radius and minimize stress concentration. After programming, thermal chamber was switched off allowing the sample to cool down to room temperature. The sample was cooled for 30 min with thermal chamber door opened to facilitate accelerated cooling. The force applied on the SMPC was maintained throughout the cooling process. Once the sample has properly cooled, force was released to attain its fixed temporary shape. Then, the deformed SMPC was placed in an oven set to its T_δ for 15 min to recover initial shape. During this testing procedure, photographs of the programmed, fixed and recovered shapes were taken using a camera and microscope
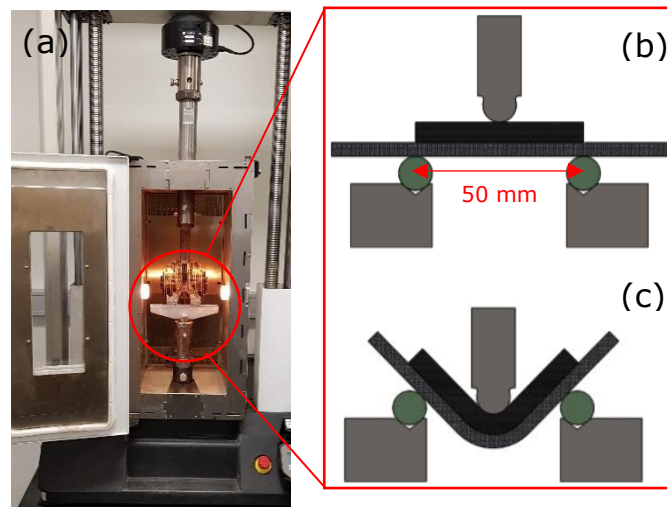
Figure 3.8: Shape programming; (a) experimental setup (b) initial shape of the sample and (c) programmed shape

e) Damage quantification

The damage levels of tested SMPCs were quantitatively analyzed in a macro scaled perspective to identify optimum material parameters. Scanning electron microscope (SEM) is a well-known instrument used for

inspection of materials. However, SEM can only be carried out for a very small part of the sample. In addition to that, tedious SEM sample preparation requires specialized equipment and the process of cutting a tiny test piece from the damaged area can further damage and distort the SMPC. Consequently, the reliability of test results will impede. Hence, the proposed user-friendly technique enables damage analysis of the programmed SMPC reliable and quick. The side view of the bent SMPC was used for the analysis, as it evidently displays the through thickness behaviour of the material due to induced stresses while bending. Thus, a dimensionless quantity ADP % has been introduced to assess sample's through thickness damage levels. ADP % given in Equation 3.3 compares the ratio of damaged area (A_D) to the total deformed area (A_T). Figure 3.9 shows (a) the programmed shape of SP-1 at T_δ ($\sim$ 84 ^{o}C), (b) total deformed area (A_T) and (c) damaged area (A_D). ADP % values were evaluated by measuring A_T and A_D values using the measure tool in SolidWorks.

$$\text{ADP \%} = \frac{A_D}{A_T} \times 100\% \qquad\qquad 3.3$$
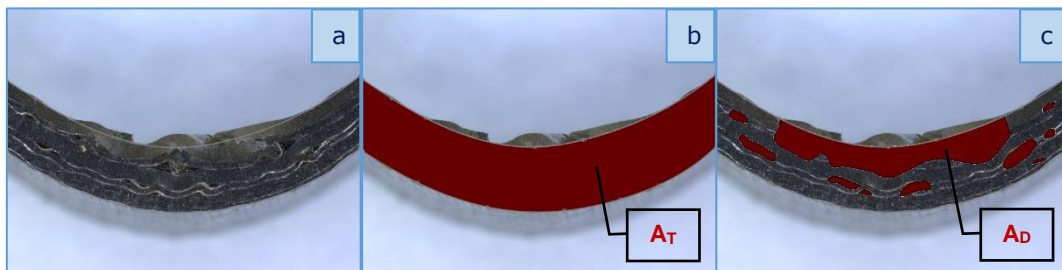
Figure 3.9: Evaluation of ADP % of SP-1; (a) programmed shape (b) total deformed area and (c) damaged area

3.4 Phase I - Synthesisation of chemical composition of the neat SMP

The SMP matrix used in my research was a thermoset polymer. Thermosets undergo a chemical reaction between mixed chemicals to form the final solid polymer. Therefore, during the synthesisation of SMPs, the stoichiometric ratio of the mixed chemicals were considered to assure a

complete reaction. By varying the proportions of reacted hardeners with the base resin, the chemical weight ratios of the synthesized SMPs given in Table 3.3 were calculated. Then, the material properties: T_g, R_f, R_r and long term shape fixity, of the SMP specimens were evaluated to find the most suitable chemical ratio.

Table 3.3: Chemical weight ratios of the synthesized SMPs

SMP Type	DGEBA	TETA	D230
A	7.82	1.00	-
B	3.19	-	1.00
C	9.77	1.00	0.61
D	13.03	1.00	1.63
E	19.55	1.00	3.67
F	39.09	1.00	9.79

3.4.1 T_g analysis of SMPs
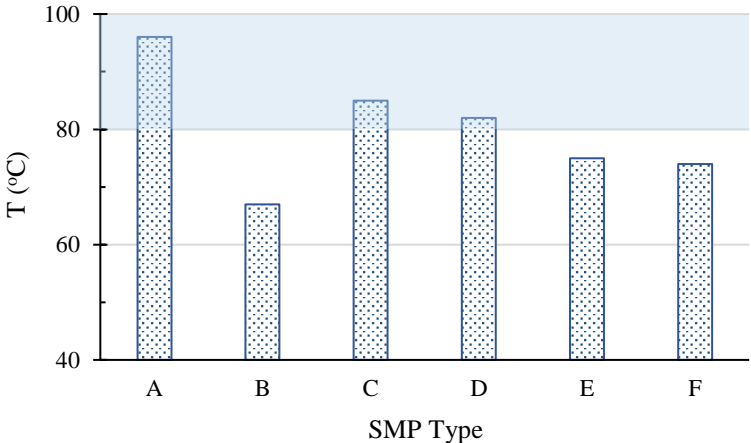
Figure 3.10: Glass transition temperature values of SMP

For SMPCs to be used in structural components of modular constructions, having a T_g higher than average environmental temperature is mandatory. In addition, properties of SMP's and SMPC's start dropping

when heated beyond T_g. Thus, the T_g of a SMP is one of the key characteristics which outline material's performance range and limitations. Therefore, DMA tests were carried out to identify this critical temperature value. Chemical compositions with the highest T_g were preferred for our analysis. According to Figure 3.10, SMP types A, C and D have shown T_g values higher than 80 °C. The values denote temperatures at the peak of Tan δ curves.

3.4.2 Shape memory properties: Fixity and recovery ratio

Shape memory performance of SMPs is commonly studied in terms of R_f and R_r [28, 167, 168]. Shape fixity ratio shows the extent to which a material can hold its deformed shape when the external force is removed, while recovery ratio relates to the amount of shape recovered. To ensure proper application with expected shape changing properties, it is vital for the synthesized SMPs to have higher R_f and R_r values. Respective ratios of the SMP types are presented in Figure 3.11. Interestingly, all synthesized SMPs except Type A, showed over 95 % shape memory performance in both fixity and recovery.
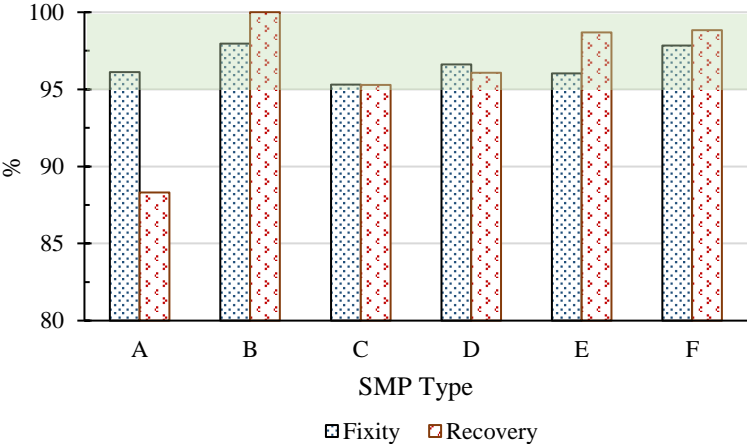
Figure 3.11: Shape fixity and recovery ratios of the synthesized SMPs

3.4.3 Long term shape retention properties

Once the SMP was deformed, ability of the material to maintain the modified shape was also tested during the selection of the best SMP matrix. Comprising better shape holding ability can further enhance the effectiveness of SMP applications, because no other locking mechanisms are required. In addition, that makes the developed SMP components lightweight and easy to handle. Figure 3.12 illustrates the variation of R_f of the synthesized SMPs within eight days. Interestingly, majority of the SMP types demonstrated negligible change in shape fixity after five days. Consequently, for clarity, results are shown only up to a timeframe of eight days. Moreover, it can be seen that Types B, D and F have shown the best shape retention properties with minimal decline in R_f.
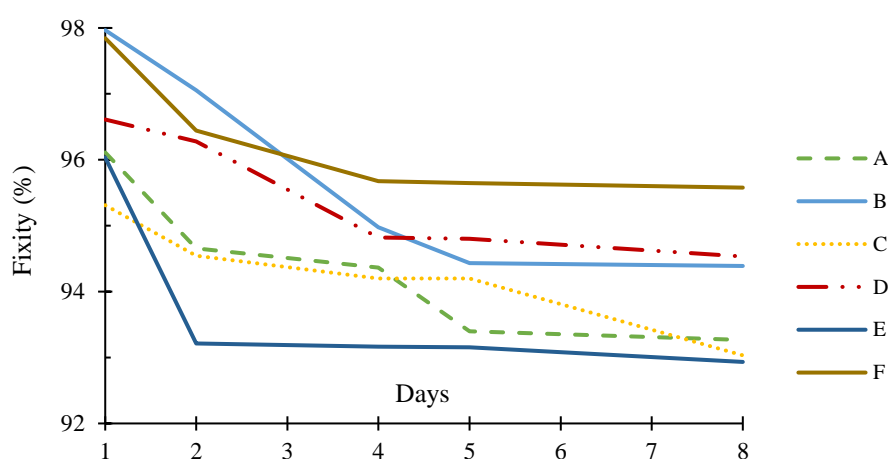
Figure 3.12: Variation of shape fixity with time

3.4.4 SMP chemical composition selection

Based on the material property tests described above, a summary of the selected SMP specimen types are presented in Table 3.4. Even though most of the SMP types performed well in two property tests at most, the Type D chemical composition displayed consistent performance. Hence, the chemical weight ratio of Type D SMP was selected and implemented in the synthesisation of the SMP matrix in further studies of my research.

Table 3.4: The summary of the SMP composition selection

Material property	Selected specimens
T_g	A, C, D
R_f and R_r	B, C, D, E, F
Long term fixity	B, D, F

3.4.5 FTIR characterisation of the SMP
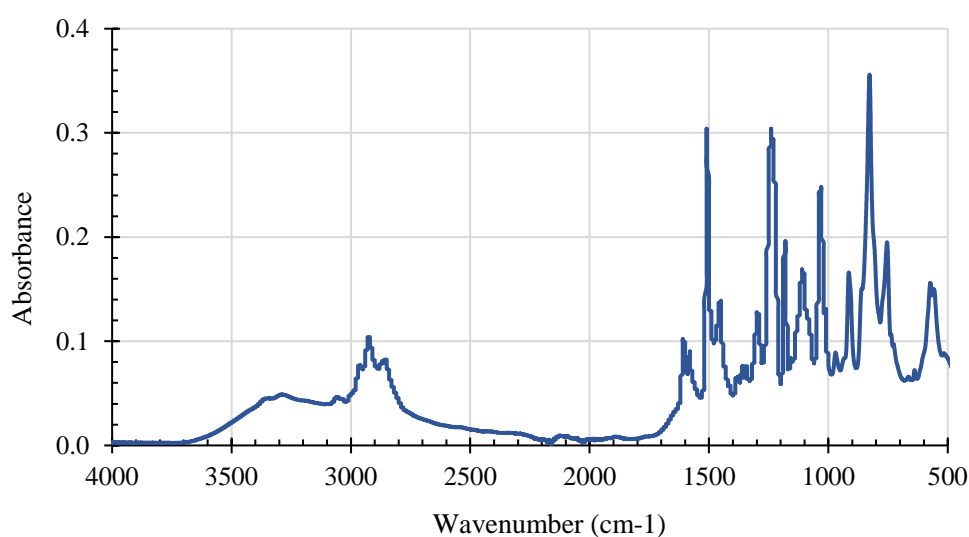
Figure 3.13: Absorbance spectra of the optimized SMP

A FTIR analysis was performed by generating the absorbance spectra of the optimized SMP type D liquid polymer. The Figure 3.13 shows the absorbance peaks of the SMP at respective wavenumbers. To confirm the constituent base material of the SMP, a library search was performed and the results are shown in Figure 3.14. Accordingly, the search results demonstrated a good match to DGEBA mixture (85 %) and epoxy resin (83 %). As the characterised liquid SMP consist of two other chemicals (hardeners), a perfect match cannot be attained.
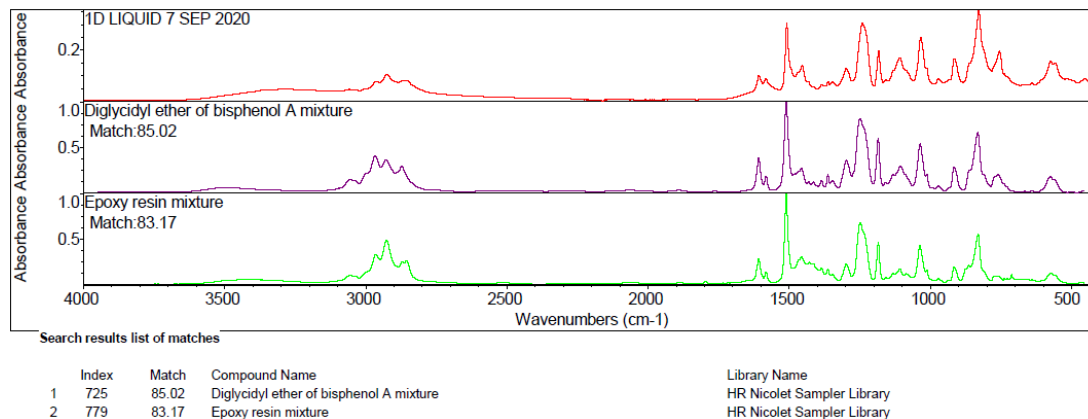
Figure 3.14: OMNIC software library search results

3.4.6 Mechanical properties of the optimized neat SMP

Structural performance of the developed SMP was evaluated to determine its strength under tensile, compressive and flexural loads. Calculated ultimate strength (UTS) values of the pristine SMP are given in Table 3.5. Importantly, the results were consistent with minimal variation, thus, indicates homogeneity of the SMP and excellent fabrication practice. Average stress – strain behaviour of the SMP during tested three loading conditions are presented in Figure 3.15.

Table 3.5: Mechanical properties of the neat SMP

Test type	UTS (MPa)	E (GPa)	ε at failure
Tension	55.4 ± 1.9	2.9 ± 0.0	0.06 ± 0.01
Compression	74.7 ± 1.0	0.8 ± 0.3	0.21 ± 0.05
Flexure	103.4 ± 3.1	3.0 ± 0.4	0.07 ± 0.01
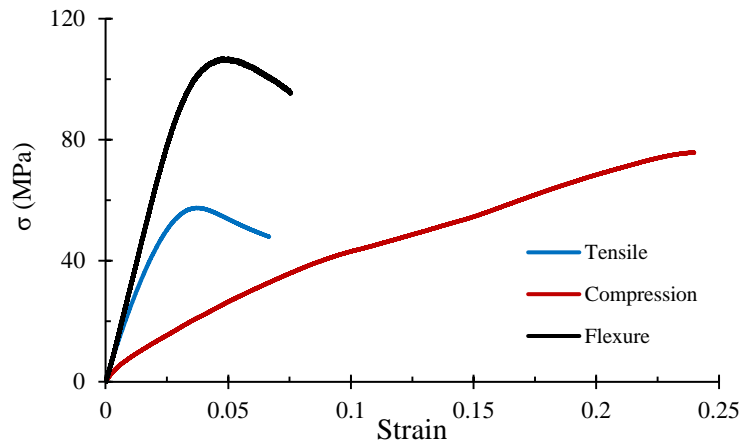
Figure 3.15: Tensile, compressive and flexural stress -
strain curves of the selected neat SMP

3.5 Phase II - SMPC optimization: Taguchi L9 array

Once the chemical composition was selected, a Taguchi array was introduced with identified parameters as a statistical approach to decide on thickness and high fibre fraction effects on the desired properties. Taguchi method is a robust design method highly used in engineering applications particularly to improve processes or designs by identifying best process parameters. Table 3.6 illustrates the created 3 x 3 experimental design with three identified parameters or factors, (1) fibre type, (2) thickness and (3) number of reinforcement layers. Furthermore, selected levels of each factor are also given in Table 3.6.

Table 3.6: Selected test parameters and levels

	Factors	Levels		
		1	2	3
1	Fibre type	Basalt	Glass	Carbon
2	Thickness (mm)	3	4	5
3	Number of reinforcement layers	6	8	10

According to Table 3.7, nine SMPC samples were fabricated as described in Section 3.2 with respective thicknesses, reinforcement type and number of layers. Minitab 18 software was used to generate sample configurations required for the analysis. The mould shown in Figure 3.4 was used with the fabrication process mentioned in section 3.2.1 to manufacture SMPCs. Fibre mass fractions (w/w %) of SMPCs were evaluated by burnout tests and are given in Table 3.8.

Table 3.7: Developed L9 Taguchi array

Specimen (SP)	Fibre type	Thickness (mm)	No. of reinforcement layers
1		3	6
2	Basalt	4	8
3		5	10
4		3	8
5	Glass	4	10
6		5	6
7		3	10
8	Carbon	4	6
9		5	8

Table 3.8: Fibre mass fractions of specimens

Specimen (SP)	Fibre mass fraction (w/w %)	Fibre volume fraction (v/v %)
1	29.4	14.3
2	28.7	13.9
3	28.8	13.9
4	48.3	28.8
5	47.0	27.7
6	25.3	12.8
7	38.2	29.8
8	19.0	13.9
9	20.7	15.2

3.5.1 T_g analysis SMPCs

In SMP context, T_g is also referred to the temperature at which both programming and recovery can be undergone. However, the definition of T_g is not certain among SMP researchers. In general, for all one way SMPs higher the temperature of the sample, easier the programming. Conversely, programming at higher temperatures is not always favourable due to higher consumption of energy and time. Thus, research suggests that SMP shape training can be categorized in to three different temperature ranges as cold (below T_S), warm (T_S to $T_δ$) and hot programming (above $T_δ$) [169, 170]. Feldkamp et al investigated the effect of deformation temperature on the ultimate deformation strain ($ε_{UL}$) of an epoxy shape memory pristine polymer under tension and concluded that $ε_{UL}$ can be increased 3 to 5 folds at T_S [68]. Hence, T_S and $T_δ$ which lie within the borders of warm temperature region were selected for this study. Figure 3.16 shows the characterization of the storage modulus and Tan δ of SP-1. The transition values T_S and $T_δ$ of SP-1 were found to be 58 °C and 83.8 °C respectively. According to Table 3.9, it can be seen that respective transition

temperatures have changed with the specimen constituents. This suggests that SMPC's thermomechanical characteristics depend on material composition defined by their thickness, fibre type and number of reinforcement layers.
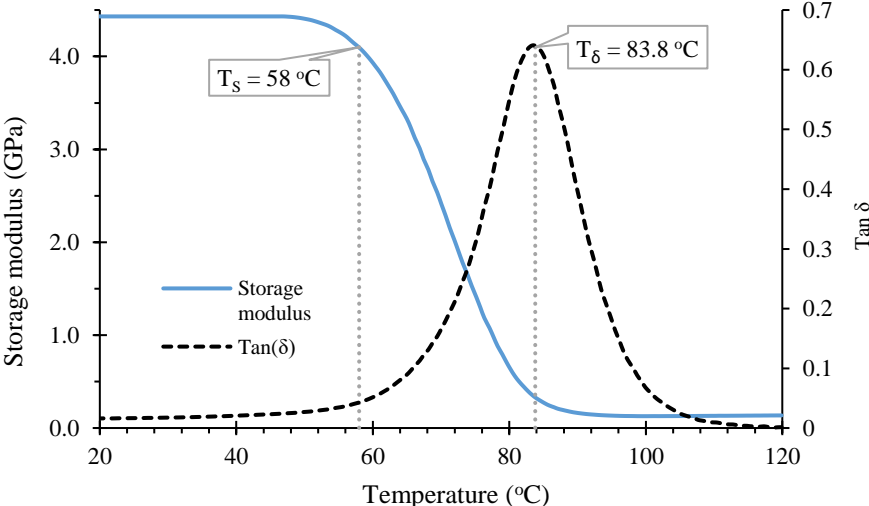
Figure 3.16: DMA results characterizing the storage modulus and Tan δ of SP-1

Table 3.9: Transition temperatures of SMPC samples

Specimen (SP)	T_S (°C)	T_δ (°C)
1	57.6	83.8
2	59.7	86.9
3	57.6	88.4
4	60.0	81.9
5	55.4	82.5
6	58.9	85.9
7	59.5	83.9
8	53.2	84.7
9	59.4	85.2

3.5.2 Shape memory properties

Study of shape memory parameters R_f and R_r is vital in proposed SMPC applications. That is, deformed SMPC structural components in production factory should be capable of retaining the deformed shape during transportation to construction site. Then, upon heating in the site, maximum recovery is expected for module assembling. Hence, these crucial parameters of the developed test samples were measured and analysed to attain maximum shape memory performance of the optimized material.

Table 3.10 demonstrates evaluated R_f % and R_r % values of all 9 SMPC specimens. During SME testing, some of the samples have undergone cracking with fibre damage mostly at the lower temperature T_S (given by "X"). The reasons for such phenomenon and other possible damage types are discussed in the "damage analysis" section of this thesis. At a given temperature (as in Table 3.10), evaluated values are different to one another and it is evident that material composition defined by the thickness, fibre type and fibre content has affected shape memory performance despite of having the same polymer matrix. This can be attributed to the changes in fibre matrix bond characteristics, reinforcement mechanical properties and bending stress distribution through the thickness. In addition to that, higher R_f % and R_r % values were obtained at the higher temperature T_δ compared to T_S. That is due to high loss of material stiffness as it gets closer to the rubbery phase [171], allowing the material to store more strain energy when deformed. However, programming at higher temperatures has caused material defects in SMPC specimens, which is a significant drawback in terms of SMPC material performance and application.

Table 3.10: Fixity and recovery ratios of samples at two selected transition temperatures

Specimen (SP)	Programming			
	At T_S (°C)		At T_δ (°C)	
	R_f %	R_r %	R_f %	R_r %
1	91.7	93.0	99.0	95.4
2	X	X	95.3	96.9
3	X	X	96.7	97.3
4	91.4	90.4	95.8	91.5
5	96.4	86.4	79.2	90.6
6	X	X	92.9	92.6
7	X	X	86.2	95.2
8	X	X	93.9	94.7
9	X	X	X	X

3.5.3 Mechanical properties: Tensile, compressive

Superior shape memory properties alone cannot transform SMPCs highly competent compared to traditional materials. Having adequate mechanical properties is a vital factor for SMPCs to outrace performance of other common materials in proposed engineering applications. Consequently, SMPC's tensile and compressive properties were analysed and considered as output variables of the Taguchi L9 analysis. Figure 3.17(a) shows tensile properties of the test samples in terms of tensile strength and elastic modulus. Among all test samples, carbon fibre reinforced SMPCs have shown best tensile properties due to superior material properties of the carbon fibre reinforcement [33]. However, basalt SMPCs have almost similar tensile properties compared to glass fibre even with comparatively low fibre fractions. That is because of better structural properties of the basalt fibre compared to E glass reinforcement [128]. A slight variation among the tensile values of basalt SMPCs can be seen due to almost similar fibre weight fractions (29.4 %, 28.7 % and 28.8 %).

Moreover, SP-4 and SP-5 with the highest fibre weight fraction among glass samples have similar tensile properties while SP-6 with the lowest fibre content of 25.3 % has shown weakest properties. Interestingly, both tensile strength and elastic modulus have shown a similar trend and have demonstrated a proportional relationship between tensile characteristics and fibre content.

The variation of compressive strengths and moduli of the test samples are illustrated in Figure 3.17(b). Compared to tensile properties, carbon fibre SMPCs have not shown a significant improvement under compressive loading with respect to other reinforcements. However as in tensile properties, an almost identical trend can be seen between compressive strength and its modulus. Thus, these results agree with the claim that increase in fibre content (or fraction) results in enhancement of SMPC's mechanical properties [172]. Most importantly, evaluated tensile and compressive properties of the specimens have shown better mechanical properties and structural capability compared to structural characteristics of other previously studied SMPCs [173, 174] exhibiting their potential to be integrated in deformable structural components.
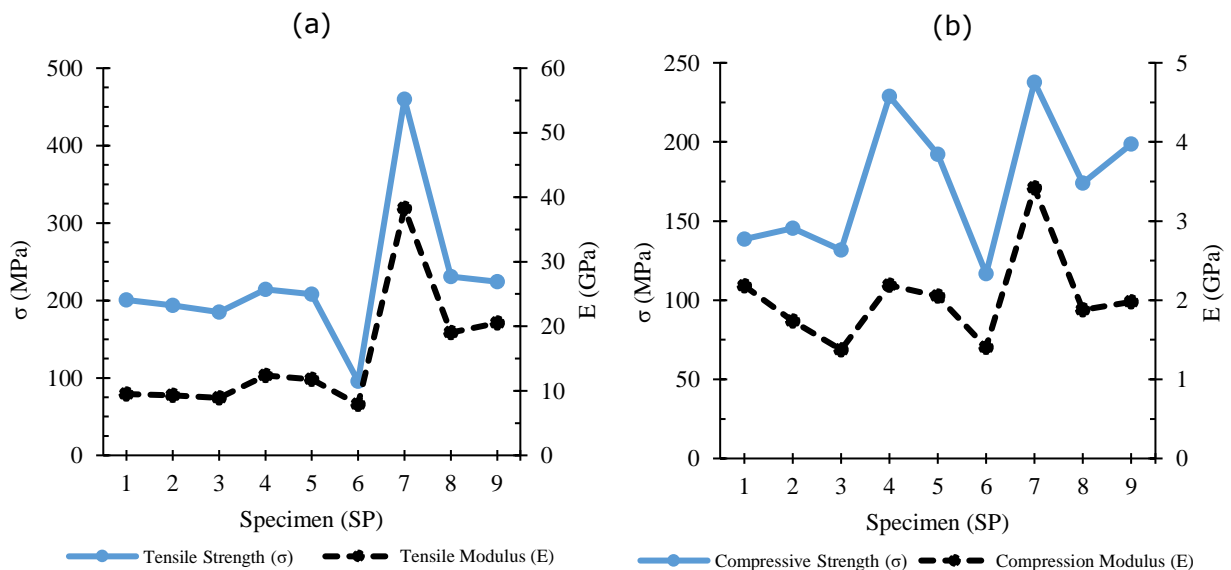
Figure 3.17: Mechanical properties of SMPC specimens; (a) Tensile and (b) compressive material properties

3.5.4 Damage analysis

The SME of a shape memory material makes it distinct and competent compared to traditional materials. Hence, the SME of these functional materials should be flawless to be effectively used in challenging applications. The SMPs and their composites are expected to deform at a suitable transition temperature under the applied load, making no damage to the shape memory component. Such undesirable damage during programming can result in weakening of SMPC components.

During the shape training process, the heated SMP will be in its flexible but weak rubbery state due to matrix softening and degradation [175]. Hence, the matrix-fibre interface which supports fibres and engage in stress transfer when loaded, will also get weakened [176-178]. Consequently, the interfacial bond strength between matrix and fibre will be in a weak state during programming. In addition, the failure mode and strength capacity of the polymer composite will rely on the interfacial bond strength [176, 179] which is a crucial factor for SMPC programming.

Interestingly, the stress at the onset of damage has been introduced as a measure of interfacial bond strength of the composite [176]. Hence, even reinforced SMPCs might not have enough strength to withstand the deformation strain levels. In such cases, the material is prone to damage due to deformation strains induced whilst programming. In addition, these undesirable effects become prominent as the material thickness increases. Hence, the investigation of material damage in the programming stage of SMPCs is vital to develop versatile future smart components.

According to the results, SMPCs with high thickness and fibre layers have resulted in high damage levels. Specially, irrespective of the temperature, carbon SMPCs have shown weakest programmability due to high stiffness. That is due to significant improvement gained in stiffness and

other mechanical properties by carbon fibre integration compared to other fibre types.

Even though most of the samples cracked with severe material damage at T_S, few glass and basalt SMPCs have displayed significantly low ADP % values. The damage levels of the specimens SP-1, SP-4 and SP-5 which performed best during the programming process with better damage resistance are presented in Figure 3.18 for comparison. Hence, T_S can be concluded as the best transition temperature to program SMPCs to minimize possible material damage. This was also suggested by Feldkamp et al [68] for a neat flexible SMP under tensile loading.
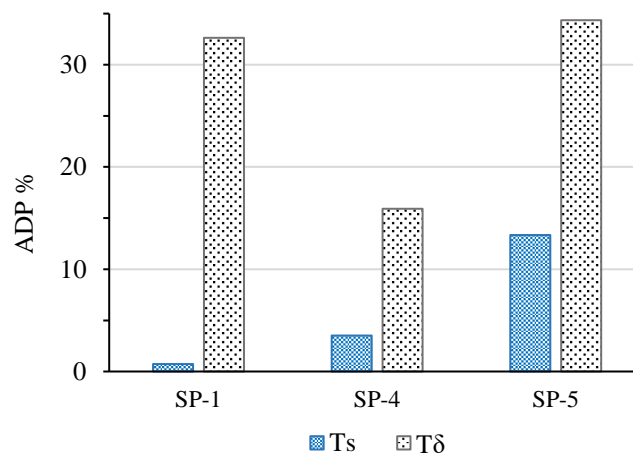
Figure 3.18: Comparison of ADP % values of SP-1,
SP-4 and SP-5 at two transition temperatures

- **Types of damages and locations**

By studying the behaviour of SMPCs during programming, three types of damages were identified. They are (1) Type 1 - Internal fibre micro-buckling and debonding (2) Type 2 - Delamination and (3) Type 3 - Through thickness cracking. Type 1 damages were observed at both temperatures T_S and T_δ, but only on the compressed side of the sample. Moreover, higher temperatures have facilitated Type 1 damage due to soften polymer matrix. Type 2 SMPC damage was also detected at both temperatures, mostly at the central region closer to the compressed side of the specimen. However,

samples have shown severe Type 2 damage at the higher temperature T_δ. High SMP stiffness at the lower temperature T_S has resulted Type 3 damage in samples with high thickness and fibre fraction. The chance of Type 3 damage increases at lower temperatures and it initiates at the tensioned side of the specimen. Among identified three damage types, Type 1 and 2 damages were the most common as they have occurred at both temperatures.

3.5.5 Taguchi optimization

Taguchi optimization can be carried out to maximize or minimize responses by larger-the-better or smaller-the-better criteria respectively. For our application, maximizing almost all material parameters are favourable for SMPC performance. However, ADP % the damage quantifying factor should be minimized to achieve best SMPC functionality. Therefore, a modified response $(1/\text{ADP \%})_{MAX}$ was introduced as an alternative to $(\text{ADP \%})_{MIN}$. Thus, by modifying the response for damage as 1/ADP, optimization analysis was easily carried out with the principle larger-the-better. Minitab 18 software was used to perform the Taguchi analysis and generate signal to noise ratio (S/N) plots.

- **For best overall material properties**

Taguchi optimization was also carried out for the test series considering T_S, T_δ, R_f, R_r, 1/ADP %, σ_T, E_T, σ_C and E_C as responses to investigate most suitable SMPC parameters and achieve best overall material properties (both shape memory and mechanical). Table 3.11 presents evaluated S/N of the analysis and the respective plot is given in Figure 3.19. Interestingly, the material parameters; Glass fibre, 3 mm and 6 layers were found to be the best constituents to achieve both shape memory and structural performance. Consequently, further tests included in this research were based on these selected SMPC parameters.

Table 3.11: Response table for signal to noise ratios for overall SMPC performance considering T_S, T_δ, R_f, R_r, 1/ADP, σ_T, E_T, σ_C and E_C

Level	Fibre type	Thickness	No of layers
T_S, T_δ, R_f, R_r, 1/ADP, σ_T, E_T, σ_C and E_C: S/N ratios (Larger is better)			
1	-16.718	-7.041	-16.718
2	-30.459	-24.632	-20.782
3	-14.956	-30.459	-24.632
Delta	15.503	23.417	7.914
Rank	2	1	3
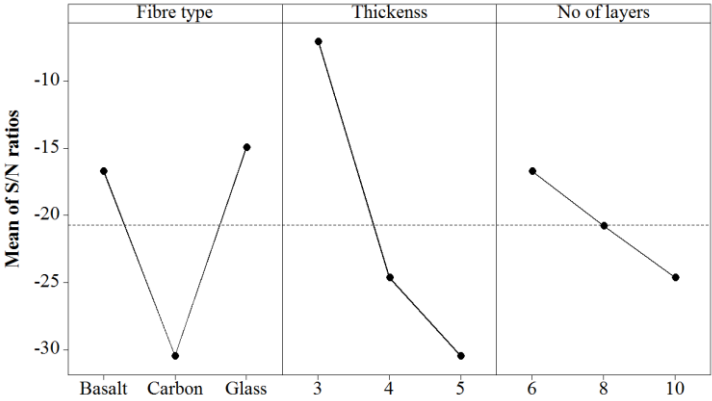
Figure 3.19: S/N ratios of T_S, T_δ, R_f, R_r, 1/ADP, σ_T, E_T, σ_C and E_C for overall SMPC performance

3.5.6 Refinement 1: Reinforcement architecture modification

From the above Taguchi analysis, properties of specimens were optimized within the selected factors and levels. The analysis was done using the same reinforcement architecture in all tested samples. From this analysis, optimum material parameters were proposed to achieve a lowest possible damage level (but not ADP % = 0). However, even a minor damage level resulted in a programming stage could lead to a considerable drop in material's mechanical properties and hinder performance of SMPC structural

components. Therefore, having zero ADP % is mandatory for successful SMPC integrated applications. As a result of that, the fibre reinforcement architecture of the optimized SMPC was modified as a further refinement to enhance SME without experiencing a reduction in strength. These further modifications aim to achieve two objectives. They are (1) prevent any visible cracks (through thickness) and (2) make no change to material's ultimate strength after shape programming. Two selected refinement strategies were implemented in order to achieve above mentioned objectives, (1) reinforcement orientation and architecture adjustment and (2) programming method parameter change. The optimum thickness of 3 mm and total number of layers (6 layers) were maintained along with the above refinements.

a) Performance of two unidirectional fibres on either side (SP-10)

As explained in Chapter 3.5.4, to avoid buckling or wrinkling of fibres, a new specimen (SP-10) was tested with unidirectional fibre layers placed on outermost faces in the transverse direction, as illustrated in Figure 3.20. Then, programming efficiency of SP-10 sample was also tested at T_S and T_δ. ADP % of SP-10 at T_S and T_δ were calculated as 1.1 % and 19.6 % respectively. As predicted, the damage level was lowest at T_S. Interestingly, sample SP-10 has shown an outstanding improvement with no damage on the compression side preventing formation of reinforcement wrinkles with micro-buckling. However, few cracks on the tension side of the bent SP-10 sample were noticed (as shown in Figure 3.20). This can be attributed to the fibers oriented perpendicular to the tensile loads which has created a directional weakness allowing SP-10 to crack on the tensioned side. Hence, SP-11 with only one unidirectional reinforcement on the compression side was fabricated and tested to achieve zero ADP %.
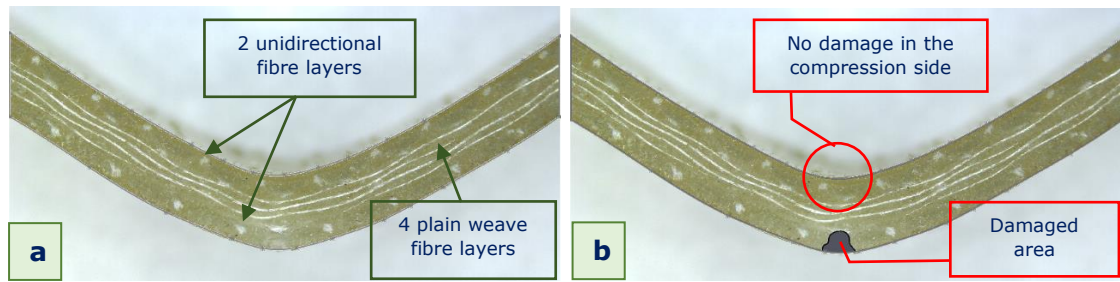
Figure 3.20: Visible damage analysis of SP-10 with a reinforcement refinement; (a) deformed shape and (b) area of damage

b) Performance of an unidirectional fibre on the compression side (SP-11)

Figure 3.21 shows a deformed SP-11 specimen with a unidirectional reinforcement layer positioned on the compression side of the sample. Rest of the five layers were not changed and maintained as plain weave fabrics. According to the findings above, specimen SP-11 was programmed at the most effective temperature T_S. As depicted in Figure 3.21, a single unidirectional layer has made a significant improvement in terms of damage resistance and resulted a zero ADP %. Hence, visible damage (in objective 1) was effectively prevented by means of appropriate adjustments in reinforcement architecture. However, the SMPC should be able to retain its initial strength once going through a complete shape memory thermomechanical cycle.
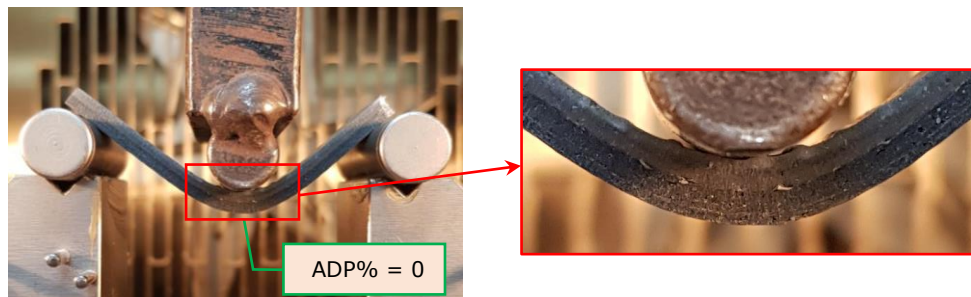
Figure 3.21: Programming of SP-11 with no visible damage

73

c) Evaluation of tensile properties after shape programming and recovery

Tensile tests were carried out to evaluate retained strength of the programmed and recovered samples. That is to understand the impact of material programming on structural characteristics of SMPCs. Stress (σ) – strain (ε) curves of programmed SMPCs after recovery and original sample are given in Figure 3.22. According to Taguchi optimization, basalt fibre was found to be the second best option for a low ADP % value. Hence, tensile test results of both glass and basalt SMPCs are included in Figure 3.22 for a comparison. Also, the same programming conditions used for the Taguchi damage and SME analysis were used in the shape training process of SP-11 specimen. The notation "GL" and "B" stand for glass and basalt SMPCs.
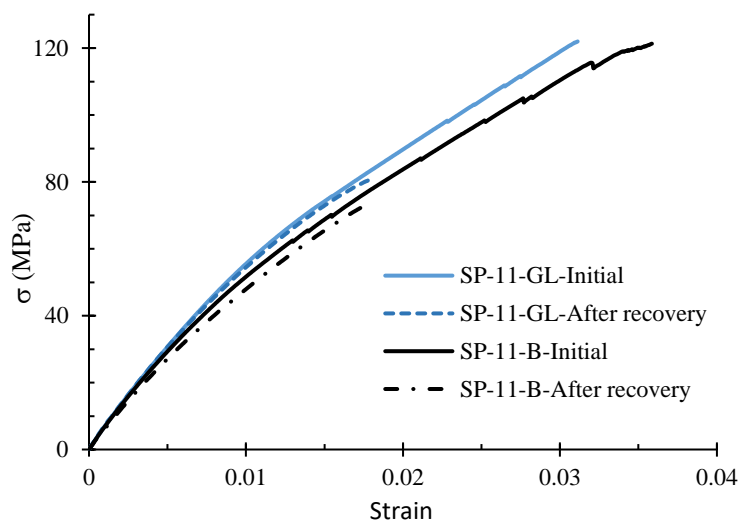
Figure 3.22: Tensile σ-ε curves of glass and basalt SP-11 before and after programming

As in Figure 3.22, both glass and basalt fibre composites have shown similar properties and σ-ε behaviour under tensile loading. Glass and basalt fibre composites have displayed almost identical initial tensile strength of 122.9 MPa and 121.3 MPa respectively. Additionally, initial elastic moduli (E) were evaluated as 9.2 GPa and 9 GPa respectively for glass and basalt SMPCs. However, a drastic drop in tensile properties was observed in both

programmed and recovered specimens. Table 3.12 gives a summary of the test results of both types of SMPCs before and after undergoing a complete thermomechanical cycle. Glass SMPC has shown a 37 % and 10 % reduction in tensile strength and elastic modulus respectively. Moreover, basalt SMPC has resulted in a 40 % and 18 % decline (UTS and E) in tensile properties after programming. This can be attributed to internal minor loosening (Type 1) and separating of fibres (Type 2) due to concentration of stress and loss of adhesion with the polymer matrix during SMPC programming. This phenomenon has reduced the amount of effective reinforcement in the SMPC which can withstand tensile loads and hence resulted in a premature failure. Interestingly, the reinforcement refinement has minimized the severity of Type 1 and 2 damages which had occurred in a small scale. Additionally, these minor flaws exist between laminae inside the material which does not affect visible damage quantifier ADP %. Hence, having a zero ADP % does not guarantee a perfect retainment of mechanical properties after recovery. Even though ADP % = 0 is mandatory to prevent visible cracks in the sample, identified minor flaws such as debonding between fibres and matrix must be eliminated during the programming stage to avoid any drop in mechanical properties.

Table 3.12: A summary of tensile test results of SP-11 samples before and after programming

SMPC	Initial		After programming		Reduction %	
	UTS (MPa)	E (GPa)	UTS (MPa)	E (GPa)	ΔUTS	ΔE
Glass	122.9	9.2	78.0	8.3	37	10
Basalt	121.3	9	72.7	7.4	40	18

3.5.7 Refinement 2: Programming process modification
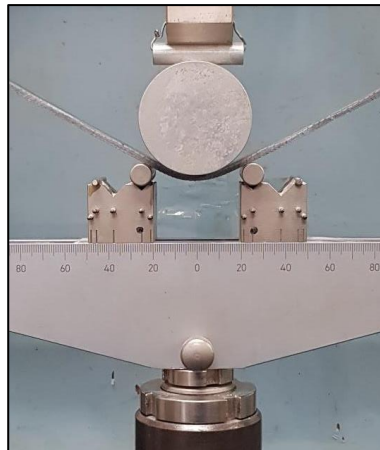
Figure 3.23: Programming of SP-11-D50
with the refinement in programming

Stress concentrated to the bending region facilitate debonding of fibres with the soft polymer matrix at the programming temperature. To achieve both ADP % = 0 and ΔUTS % = 0, a further refinement is required which will eliminate internal fibre debonding and hence retain initial material structural properties. As the thickness of SMPC is constant throughout the sample, stress concentration can only be reduced through an adjustment to programming process parameters. Increasing the support span or bend radius of the specimen will help to distribute bending stresses throughout the sample allowing it to deform easily with minimal internal damage. Figure 3.23 illustrates the adjusted programming process with a 50 mm (5 folds higher than previous) diameter deforming tool. Figure 3.24 presents σ-ε curves of glass and basalt SMPCs programmed under the modified process and named as "D50". Most importantly, recovered samples have shown almost identical tensile strength as their initial properties. Both composites have displayed a negligible drop in tensile strength of 0.9 % and 0.1 %. Moreover, strain at break of both SMPCs have increased which evidently proves an improvement in material elasticity. The drop in elastic modulus has also shown an improvement compared to the previous tests. However, recovered glass and basalt fibre composites have shown 9 % and 10 %

modulus reduction respectively. Existence of few locations with minor Type 1 damage with internal fibre debonding (as in Figure 3.25 (c)) has caused this slight drop in modulus. This claim has been validated numerically with the help of developed FEA approach in Section 4.6 . In addition, increased elasticity of the material has also adversely affected the reduction in elastic modulus of SMPCs. Figure 3.25 depicts a deformed glass SMPC with new programming process parameters. Table 3.13 and Figure 3.26 present a summary of the evaluated results and clearly demonstrate significant improvement in SMPC performance even after shape recovery. With the refinements introduced, both visible damage level and strength drop could be mitigated which will eventually enhance SMPC performance in future prospective applications.
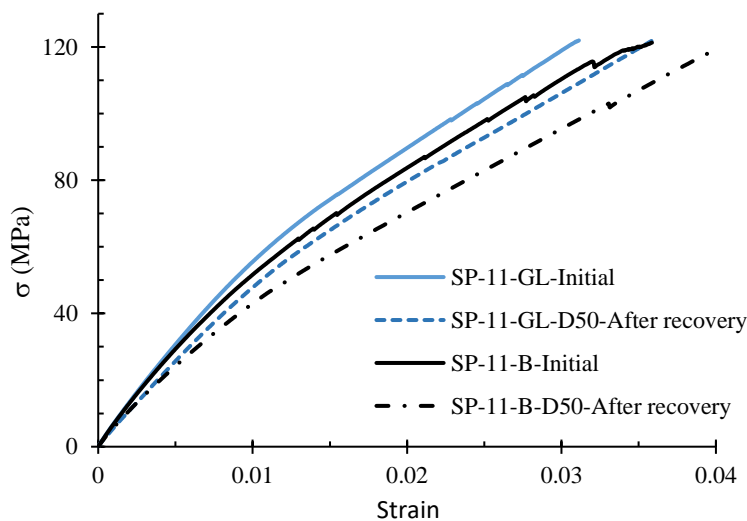
Figure 3.24: Tensile σ-ε curves of glass and basalt SP-11-D50 before and after programming
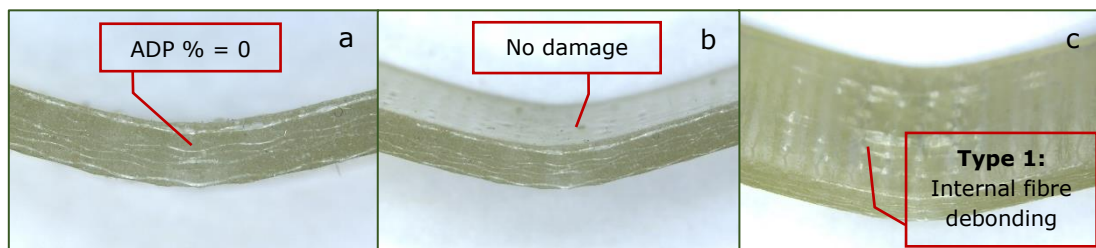
Figure 3.25: SP-11-GL-D50 sample photographs after programming

Table 3.13: A summary of tensile test results of SP-11-D50 samples before and after programming

SMPC	Initial		After programming		Reduction %	
	UTS (MPa)	E (GPa)	UTS (MPa)	E (GPa)	ΔUTS	ΔE
Glass	122.9	9.2	121.8	8.4	0.9	9
Basalt	121.3	9	121.2	8.1	0.1	10
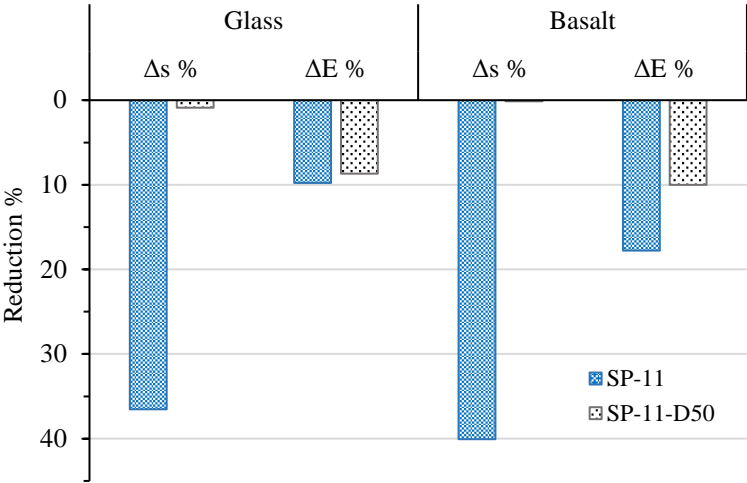
Figure 3.26: Comparison of reductions in tensile strength and modulus of SP-11 and SP-11-D50 glass and basalt SMPCs

3.5.8 Material properties of the optimized SMPC
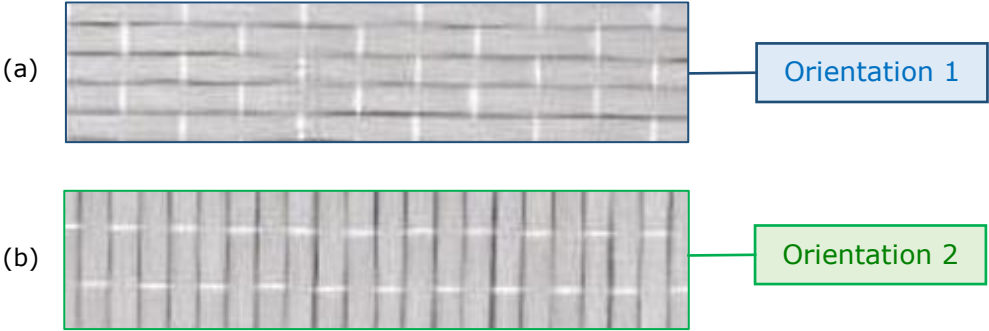
Figure 3.27: SMPC fibre arrangements; (a) orientation 1 and (b) orientation 2

The unidirectional fibre reinforcement modification mentioned previously in section 3.5.6 affects the directional uniformity of the composite. Consequently, the mechanical properties of the optimized SMPC was evaluated in both longitudinal (orientation 1 = O1) and transverse (orientation 2 = O2) directions as shown in Figure 3.27. The structural performance of the developed SMPC was investigated in terms of tensile, compressive and flexural properties. The stress–strain relationships for the loading conditions are illustrated in Figure 3.28, Figure 3.30 and Figure 3.29, respectively. Additionally, material properties of the basalt fibre reinforced SMPC are also included for a comparison. Interestingly, for both fibre types, strength values in the longitudinal direction were higher than that of transverse direction. That is due to the intervention of the unidirectional fibre allowing the SMPCs to withstand more load acting parallel to its length. In contrast, due to the directional weakness in the transverse direction, performance of the SMPCs dropped under all considered load types. However, integration of reinforcements in the SMP matrix resulted in improved structural performance mitigating weaknesses of the neat SMP. A summary of the mechanical properties of the SMP and the optimized SMPCs are presented in Table 3.14.
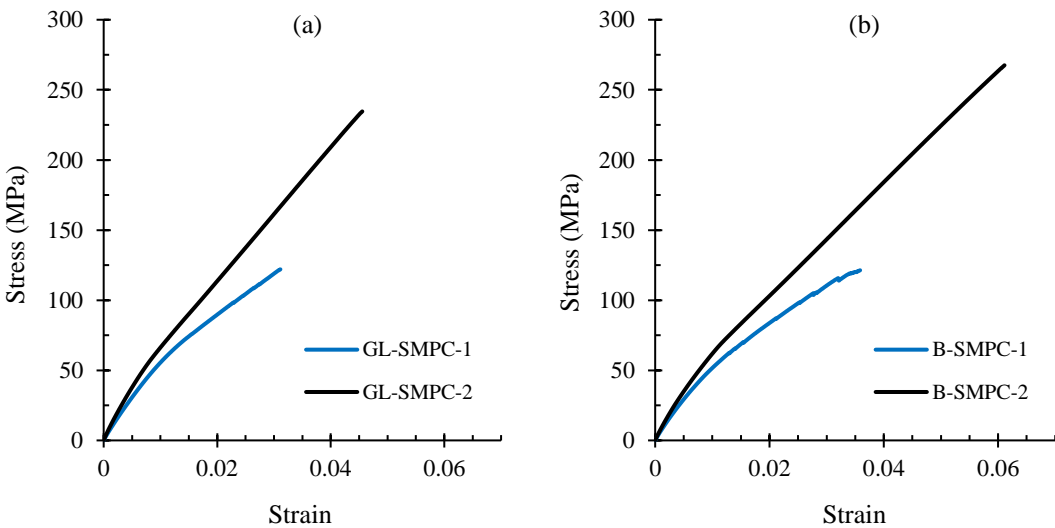
Figure 3.28: Tensile behaviour of; (a) glass and (b) basalt SMPCs in orientations 1 and 2
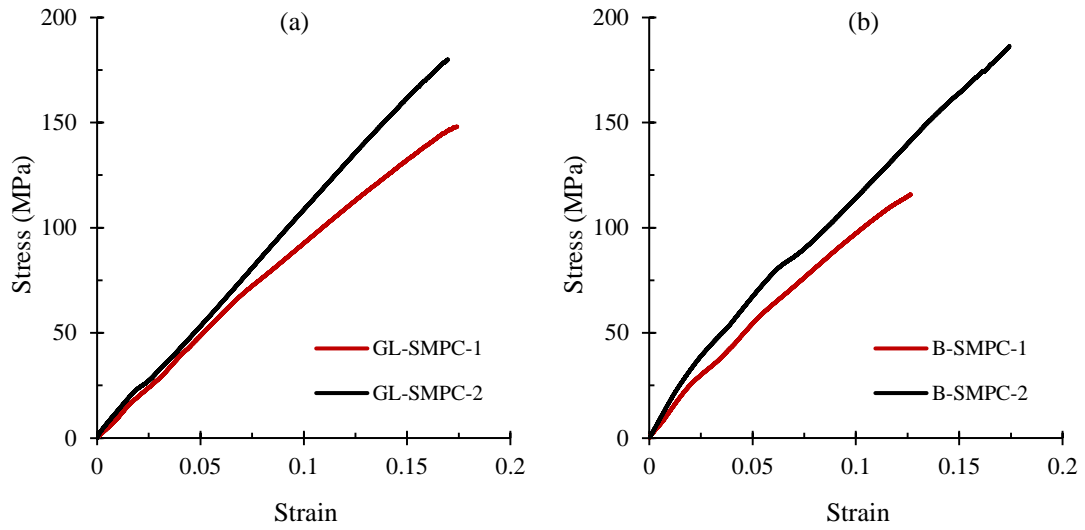
Figure 3.30: Compressive behaviour of (a) glass and (b) basalt SMPCs in orientations 1 and 2
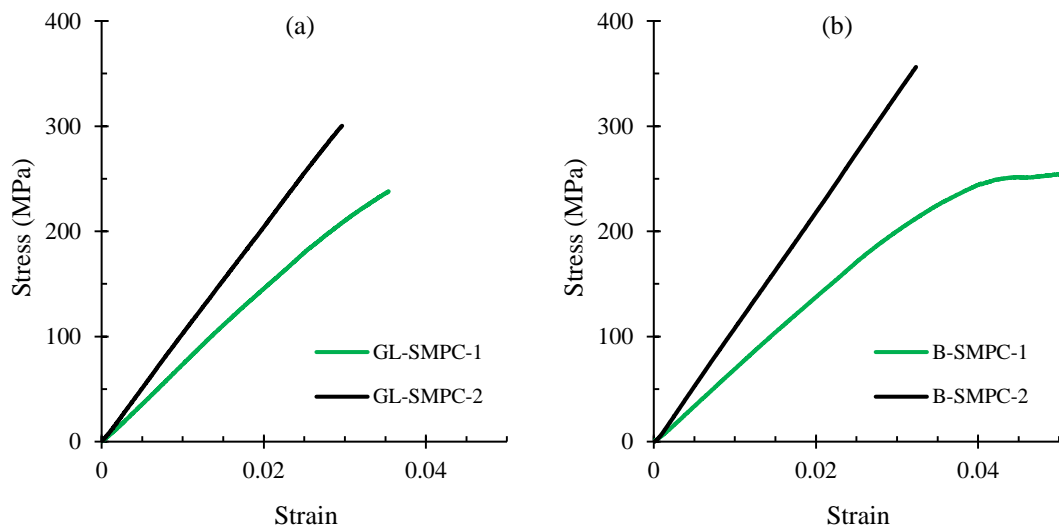
Figure 3.29: Flexural behaviour of (a) glass and (b) basalt SMPCs in orientations 1 and 2

Table 3.14: Summary of mechanical properties of the neat SMP and the optimized composites

Property	Material	Initial UTS (MPa)	E (GPa)
Tensile	Neat	55.4 ± 1.9	2.9 ± 0.0
	GL-SMPC-1	122.9 ± 1.7	9.2 ± 0.7
	GL-SMPC-2	231.9 ± 29.6	14.1 ± 0.4
	B-SMPC-1	121.3 ± 8.0	9.0 ± 0.4
	B-SMPC-2	267.3 ± 4.9	12.2 ± 0.2
Compressive	Neat	74.7 ± 1.0	0.8 ± 0.3
	GL-SMPC-1	149.6 ± 2.6	1.4 ± 0.4
	GL-SMPC-2	184.0 ± 6.5	1.8 ± 0.2
	B-SMPC-1	106.2 ± 4.8	1.4 ± 0.4
	B-SMPC-2	181.5 ± 6.8	1.6 ± 0.7
Flexural	Neat	103.4 ± 3.1	3.0 ± 0.4
	GL-SMPC-1	232.0 ± 6.9	7.5 ± 0.1
	GL-SMPC-2	307.8 ± 19.4	10.8 ± 1.0
	B-SMPC-1	252.1 ± 4.5	7.3 ± 0.4
	B-SMPC-2	354.7 ± 23.6	9.3 ± 2.2

3.6 Summary

In this chapter, the approach of developing a SMP has been presented using the base chemicals. The thermoset epoxy based SMP was synthesised as per the required material properties for structural engineering applications. In addition, research work relating to the optimization of the SMPCs, implementing a Taguchi optimization array has also been presented. A novel user-friendly approach to quantify damage has been introduced and implemented in this research to identify damages incorporated in SMPCs during shape programming.

It was revealed that, high SMPC thickness and reinforcement content adversely affect the effectiveness of the shape programming process resulting in material flaws. A new dimensionless quantity (ADP %) has been introduced and can be used by researchers as a user friendly through thickness visible damage quantifier in SMPCs when programming. A robust Taguchi L9 array was implemented to attain the lowest ADP % along with best possible mechanical properties. Further two refinements in the reinforcement architecture and programming process were proposed and tested to achieve ADP % = 0 and no drop in ultimate tensile strength (ΔUTS = 0 %).

From the analysis, three types of SMPC damages, were identified and material's compression side was identified as the most critical location susceptible to damage while programming. Best programming characteristics were shown at the low temperature T_S ($\sim$ 60 ^{o}C) coupled with a higher deformation rate (60 mm/min). The best combination of SMPC material parameters were evaluated as glass fibre reinforcement, 3 mm thickness and 6 layers (5 plain weave + 1 unidirectional layer on the compression side with fibres in the transverse direction) for optimum performance. Subsequently, Chapter 4 focus on the numerical analysis of programming, damage onset identification and application of SMPCs in structural profiles.

CHAPTER 4: DESIGN AND APPLICATION OF SMPCS IN STRUCTURAL COMPONENTS

4.1 Introduction

In Chapter 3, the development of an epoxy based structural SMPC was presented with comprehensive elaborations on SMP matrix synthesisation, SMPC parameter optimization, programming efficiency and structural performance. Further, previous studies were primarily based on material characterisation, and improvements were made to meet civil engineering application demands. This chapter mainly focuses on the design and application of the developed SMPCs in potential large scaled components and structures, to demonstrate their suitability and key benefits.

To date, the major application interests for SMPCs have been a variety of outer space applications [180]. Due to unavoidable drawbacks of conventional structures made of common materials, such as high cost, heaviness, requirements of actuators and high volume consumed, research interests to explore alternative materials and methods increased day by day [26]. As a consequence, shape changing and self-actuating SMPCs were developed to fabricate lightweight components to be used for space explorations [20, 33]. Structural performance is important for space structures, due to significant dynamic loads during launch which require demanding specific stiffness, and thermal cycling requirements after deployment. To design such outer space components, numerical models were developed in order to simulate the shape memory cycle of SMPCs [18, 122-124]. But, much emphasis was not given to evaluate the depletion of programming efficiency which can adversely affect the material's structural performance. Therefore, research knowledge on the identification of the onset of programming damage via FEA is clearly lacking. Thus, the research

findings presented in this chapter will assist to fill the knowledge gap linked to in-depth FEA analysis of the SMPC thermomechanical cycle.

To the author's knowledge, less attention was given to incorporating SMPCs in structural members used for civil infrastructure. In this study, common structural member sections such as CHS and SHS were selected and fabricated from the developed SMPC described in Chapter 3. Interestingly, the SME of these structural members and the validity of the introduced FEA based damage onset identification technique, were presented. Ultimately, the suitability of the developed SMPC for space cramped and time critical civil engineering applications [30, 181], was demonstrated by simulating SMPC large scaled long beams and deployable structures. The key findings of this chapter stress on the proof of concept of the proposed applications and demonstrate the comparability of SMPC member sectional capacities.

4.2 Materials preparation

4.2.1 Fabrication of CHS and SHS members

Two specially designed molds (shown in Figure 4.1) were used to fabricate the glass fibre reinforced SMPC CHS and SHS structural members of length 250 mm. The CHS and SHS sections were selected for this study because they are the most commonly used members in many structural applications. The wall thickness of these hollow sections was based on the 3 mm laminate thickness selected by Taguchi method in Section 3.5.5, and the refined laminate developed in Section 3.5.6. The mandrels and outer fixtures were precisely machined to maintain a 3 mm constant thickness in all SMPC components. Additionally, 3 mm spacers were used to position the inner mandrel and restrict its movements inside the mold.

Table 4.1: Components of the customized mold

Part no	Description
1	Funnel
2	Mandrel with mold release
3	Fibre reinforcements
4	8 mm tube
5	Silicone seal
6	3 mm steel spacers

To avoid air bubbles becoming trapped in dry patches and to monitor the resin level inside the mold, a resin infusion tube connected to the bottom of the mold was used for pouring the polymer. The pressure differential in the resin infusion tube facilitated an effective and trouble free resin flow when casting the SMPC structural components. Once the molds were filled with SMP, the curing cycle mentioned in Chapter 3.2.1 was utilized to fully cure the SMPC components. The key components of the developed mold are listed in Table 4.1. Subsequently, the fabricated CHS and SHS components were demolded and cut into the lengths required for shape memory testing. Three specimens were tested in each experiment. Figure 4.2 presents manufactured the SMPC CHS and SHS specimens along with their cross sectional dimensions.
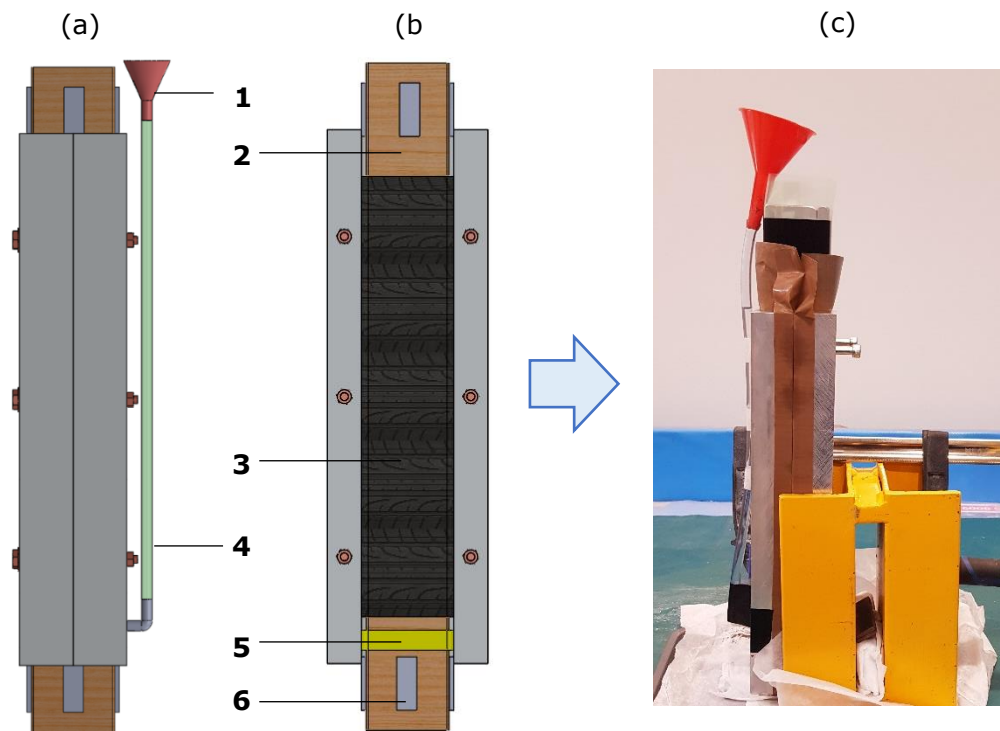
Figure 4.1: Solid model and actual manufacturing technique of SHS SMPC members; (a) side view (b) inside view of the mold (c) actual fabrication setup
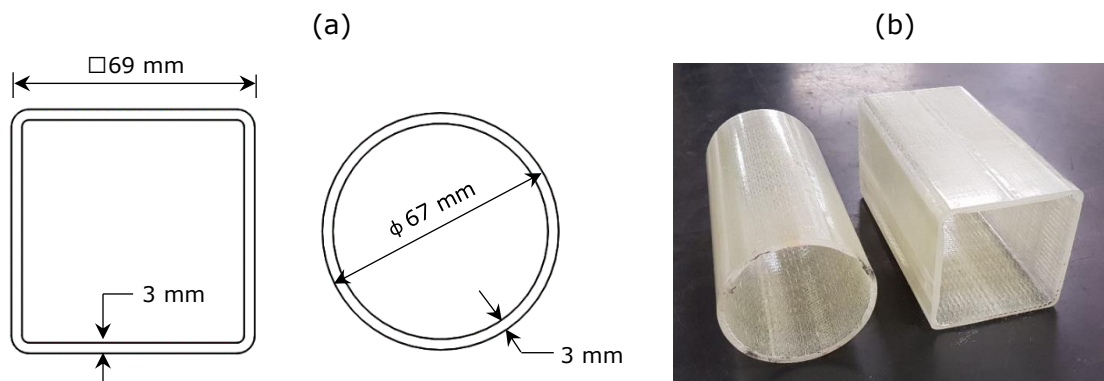
Figure 4.2: Fabricated CHS and SHS components; (a) cross sectional dimensions and (b) 60 mm long components tested for SME

4.3 Experimental methods

4.3.1 Stress relaxation

Stress relaxation tests were carried out in a DMA Q800 for neat and reinforced SMPs. A dual cantilever fixture was used to evaluate the stress relaxing behaviour of materials within the temperature range 50 °C to 80 °C with 5 °C increments. Once the chamber temperature was set to a specific value, a 10 min isothermal step was used to achieve thermal equilibrium. Then, a constant strain of 0.2 % was applied and relaxation data were recorded for 15 min. The time-temperature superposition (TTS) principle was applied to characterize the viscoelastic properties of materials over an extended time period [18]. The relaxation data were analyzed with the Advantage Software (v5.5.22) rheology module, and Prony relaxation master curves were generated using Williams-Landel-Ferry (WLF) curve shifting technique [125]. The master curve was fitted with the Prony series formula described by the Generalized Maxwell Model given in Equation (4.1), and was used to evaluate Prony coefficients. The shear and bulk moduli required to fully define the viscoelastic properties in ABAQUS were evaluated using Equations (4.2) and (4.3).

$$E(t) = E_\infty + \sum_{i=1}^{n} E_i e^{-\frac{t}{\tau_i}} \qquad\qquad (4.1)$$

$$G(t) = \frac{E(t)}{2(1+v)} \qquad\qquad (4.2)$$

$$K(t) = \frac{E(t)}{3(1-2v)} \qquad\qquad (4.3)$$

4.3.2 Shape memory effect test of SMPC members

To demonstrate the shape memory behaviour of the fully cured SMPC structural components, 60 mm long components were cut and programmed by a radial force along their lengths. Programming was carried out at a storage modulus onset (T_S = 60 °C) which was concluded from previous studies [29]. The experimental setup including the thermal chamber,

fixtures and specimen positioning are illustrated in Figure 4.3. Prior to the application of programming force, the SMPC structural components were held inside the thermal chamber of the MTS 100 kN for 30 min to achieve thermal equilibrium. Next, force was applied with a crosshead movement of 1 mm/s. During the programming stage, the time taken to initiate damage and specific locations were monitored and used to validate the FEA predictions based on the critical stress margins (CSMs) proposed in our recent studies [29]. The programming stage was terminated when the load reading on the MTS began dropping rapidly due material failure such as cracks. Then, the chamber was opened for natural cooling allowing the specimen to cool gradually from 60 ^{o}C to room temperature. Next, the applied force was removed allowing the component to spring back and fix its shape. Finally, the specimen was placed in an oven heated to 90 ^{o}C, allowing it to recover the initial shape. Photographs of the initial, fixed and recovered shapes of the components were taken to evaluate the SME properties R_f and R_r. Moreover, Equations (4.4) and (4.5) were used to evaluate R_f and R_r. The notations D1, D2, L1 and L2 denoted specific dimensions of the specimens, and are illustrated in Figure 4.4.
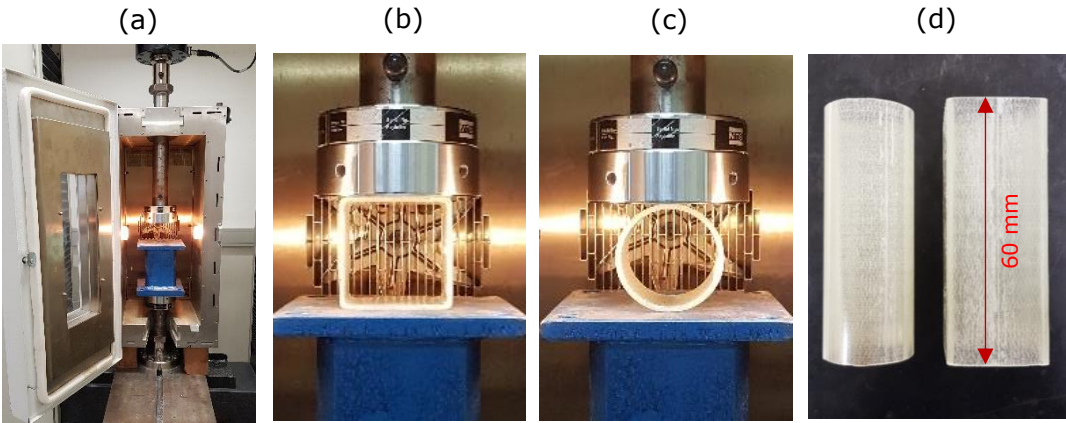
Figure 4.3: SME testing of SMPC components; (a) experimental setup (b) SHS and (c) CHS components prior to programming, and (d) top view

$$R_f = \frac{L_2}{L_1} \times 100\ \%$$

<div align="right">(4.4)</div>

$$R_r = \frac{D_2}{D_1} \times 100\ \%$$

<div align="right">(4.5)</div>
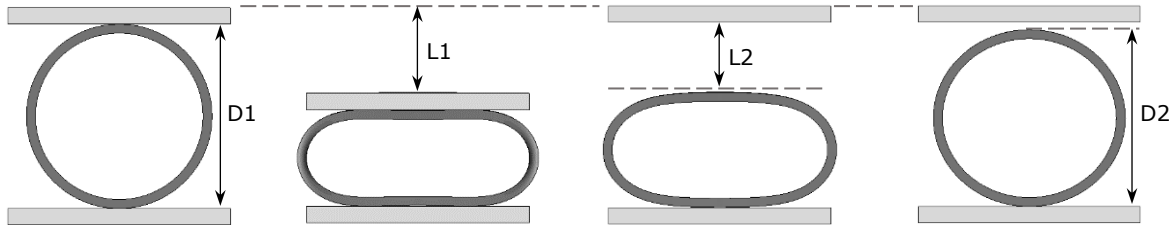
Figure 4.4: Parameters used for evaluation of R_f % and R_r %

4.3.3 Axial compression of SMPC components

The compressive strength and failure method of the glass SMPC CHS and SHS components were evaluated in the MTS 100 kN. The length to diameter ratio (L/D) of the SMPC components was approximately 2. A displacement rate of 1.3 mm/min was used to apply a compressive load. All compressive tests were performed at room temperature. The axial load was applied until damage was initiated and the respective damage types were recorded for analysis.

4.4 Relaxation and viscoelastic properties
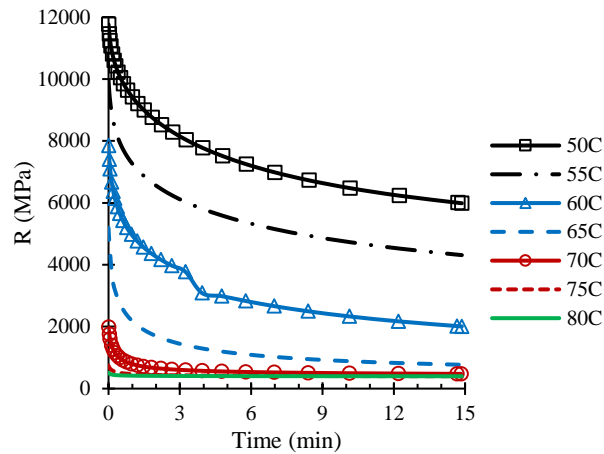
Figure 4.5: Glass SMPC relaxation moduli at tested temperatures

When the SMP is heated to its T_g, the material transforms its state from solid to rubbery through a transition phase. Hence, in order to simulate the behaviour of the SMP within the phase transition region, characterization of the viscoelastic properties is essential. Figure 4.5 illustrates how the relaxation modulus (R) of the glass reinforced SMPC falls with time at different temperatures. The generated Prony series curves for all tested specimens are presented in Figure 4.6. The relaxation values taken from the Prony series of a certain material at different time values were used to define viscoelastic properties of the SMPCs in ABAQUS software. Importantly, it can be seen that both the glass and basalt fibre SMPCs showed higher relaxation moduli compared to the neat SMP. This can be attributed to the high stiffness attained with improved mechanical performance by reinforcement inclusion and low matrix content. The viscoelastic FEA modelling enables simulation of the complete thermomechanical cycle of SMPCs, and was inspired by a study conducted by Azzawi et al. [125]. In our recent studies [29], modelling of the general shape memory cycle was modified by the inclusion of tensile properties at the programming temperature to study the stress variations during programming and identify damage onset.
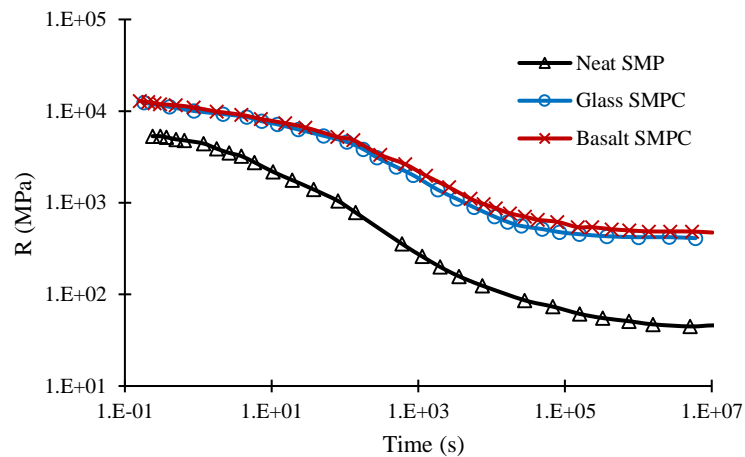
Figure 4.6: Relaxation Prony series curves for neat SMP and SMPCs

4.5 Simulation methods

4.5.1 ABAQUS modelling of the thermomechanical cycle

The programming stage was simulated in ABAQUS (2019) FEA software to analyze the stress distribution within the sample. As SMP/SMPC programming takes place within the transition region, the material will have a mix of both elastic and viscous properties. Hence, the programming step was defined as a "visco" step with "viscoelastic" material property which was previously studied by Azzawi et al (2017) [125]. As suggested, Prony series relaxation data extracted from DMA Q800 were used to define the viscoelastic properties of the material. In addition, tensile properties at the programming temperature were required to define SMPC material properties. The experimental results of elevated temperature tensile properties are presented in Section 5.9. The exact experimental programming test given in Chapter 3, was simulated in ABAQUS for a SMPC of size 100 mm x 20 mm x 3 mm. A summary of the FEA analysis setup of the SMPC thermomechanical cycle, is described below;

I.   Parts and assembly

The labelled FEA model used for the analysis is presented in Figure 4.7. The model replicates the exact experimental process with same dimensions for all parts. Only a half of the steel roller supports were considered to minimize computational power. All the parts were partitioned in order to build up the assembly using proper mates, define boundary conditions and loads. Created datum planes were used to generate the partitions. For SMPC meshing, 3000 "Quad" type mesh elements were used.
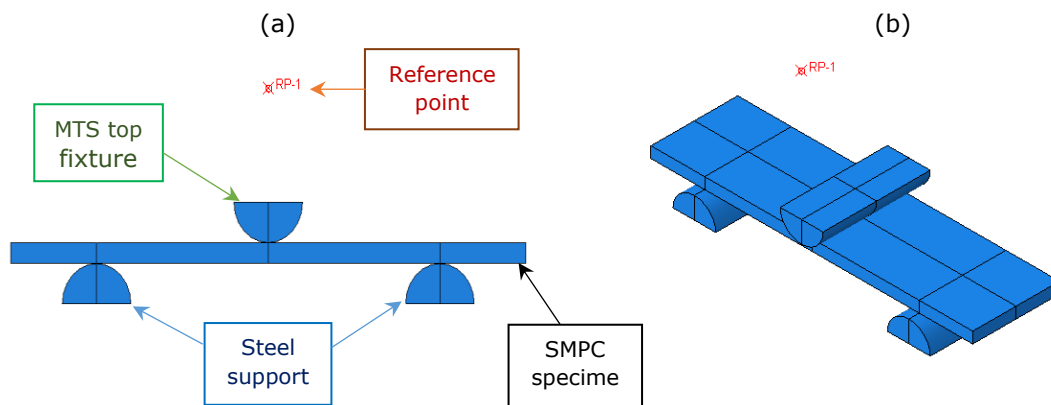
Figure 4.7: Created solid assembly model for analysis; (a) front view with part names and (b) isometric view

II.   Materials

The material of support rollers were defined as steel. The viscoelastic properties of the SMPC were defined using the G and K moduli coefficients, evaluated through relaxation data and Prony series. In addition, the density and elastic properties of the SMPC at the programming temperature were also defined. Density was essential to generate the effect of gravity. An overview of the defined SMPC's material behaviour properties are presented in Figure 4.8.
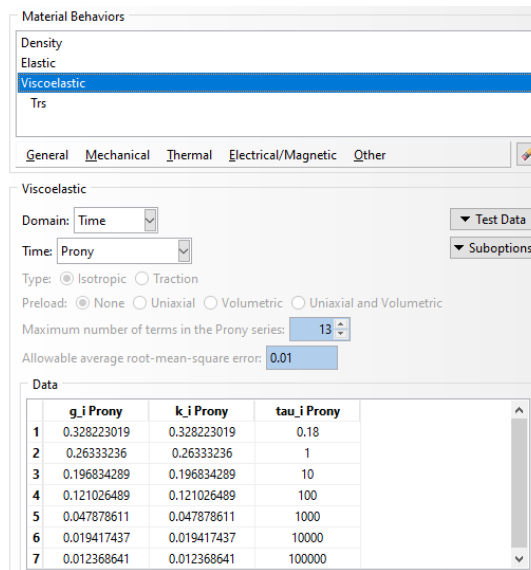
Figure 4.8: Defined viscoelastic properties
of the glass fibre SMPC

III.   Steps

In ABAQUS software, how the defined boundary conditions, predefined fields, loads, etc, are controlled or changed within the FEA, were defined through programme steps. The sequential procedure of the thermomechanical process were defined in terms of five steps, including 4 visco steps. Table 4.2 describe the list of programme settings defined via five steps.

Table 4.2: List of steps with their respective control settings

Step	Reference point displacement	Predefined field	Boundary conditions
Initial step		Created Direct specification Constant through region; 60 °C	Created
Visco step 1	Created Ramp loading; 0 m to 0.015 m in 15 s	Propagated	Propagated
Visco step 2	Propagated Maintained at 0.015 m	Modified Cooling; 60 °C to 25 °C, in 300s	Propagated
Visco step 3	Modified Ramp unloading; 0.015 m to 0 m, in 2s	Propagated Maintained at 25 °C	Propagated
Visco step 4	Propagated Maintained at 0 m	Modified Final heating; 25 °C to 90 °C, in 450 s	Propagated

IV.   Interactions

To define the surface to surface interactions between the steel rollers and SMPC, the following settings were used. As the stronger material, steel was considered as the 'master surface' and the surfaces of SMPC were defined as 'slave surfaces'.

- Surface to surface contact, contact interaction property;
  Frictionless tangential behaviour
  Hard contact normal behaviour
  Separation after contact was allowed

V. Loads and boundary conditions

A reference point (RP) was defined equidistant to the top fixture, using an interaction equation, to apply the external load at a displacement rate of 1 mm/s. A displacement boundary condition was used to define the movement of RP, as shown in Figure 4.9. All the degrees of freedom (DOF) of the bottom supports were restricted to move with "ENCASTRE; all DOF = 0" displacement condition. Also, gravity effect was activated with 9.81 ms^{-2} acting downwards.
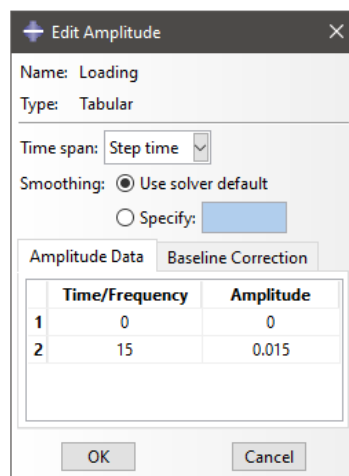
Figure 4.9: Displacement ramp amplitude of
RP for loading step

VI. Post processing

The 'Results' module of the ABAQUS software was used for post processing results of the analysis. The applied programming load and displacement were plotted using the 'history outputs' defined for RP. The stress, displacement and temperature contours which were defined via 'field outputs', were also analysed.

4.6 Identification of damage onset and validation

A numerical simulation was implemented in ABAQUS to investigate induced stress distribution in the optimized SMPC during the programming stage and develop a damage prediction strategy. In keeping with the scope of the study, only the programming stage of SMPCs is analysed here. Figure 4.10 presents the modelled assembly with initial and programmed shapes. Experimental results (load versus time) extracted from the MTS 10 kN
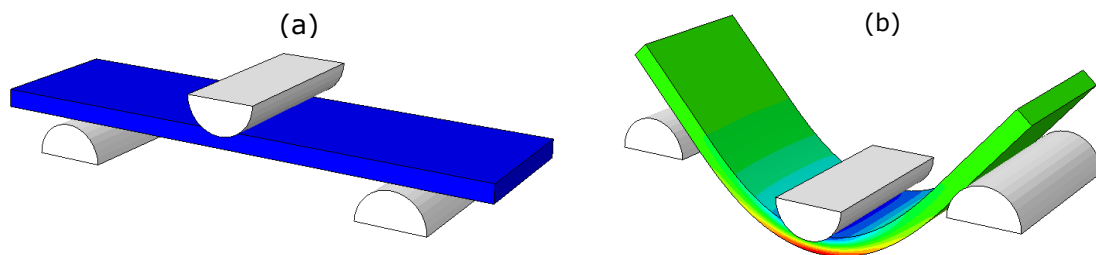
Figure 4.10: Shape programming in ABAQUS; (a) initial shape
(b) programmed shape

testing equipment and calculated flexural stress during the programming stage of SP-11 were used to validate the FEA approach implemented in ABAQUS. Figure 4.12 (a) and (b) show the comparison of the maximum flexural stress magnitude and load due to the programming of the glass sample SP-11-GL. The curves fit perfectly until Point 1 (Figure 4.12) where the Type 1 SMPC damage begins. Type 1 damage developed until a displacement of 7 mm (Point 2) where Type 2 damage occurred, further reducing the load. Hence, by matching this scenario, CSMs can be introduced to predict the occurrence of Types 1 and 2 damage from FEA results.

Most importantly, for the best SMPC performance, a zero damage level is mandatory. Thus, a numerical analysis should be developed to predict σ_o which can then be used as a tool to predict whether damage in the programming stage is likely or not. Hence, it can be concluded that σ_o as the most critical factor for SMPC programming. As the model does not take into account the behaviour of post damage, interfacial bond properties

and progressive failure of SMPCs, FEA results do not match with the experimental data beyond Point 1. However, if needed, properties of the nanoscale matrix-fibre interface and mechanics of stress transfer can be analysed using shear lag theory and traction-separation law as previously studied by Budurapu et al (2019) [182] and Skovsgaard et al (2021) [183]. This analysis is not included here as it is not within the scope of the study.

Therefore, a compressive stress of 70 MPa (= σ_o) should not be exceeded during programming to avoid all types of damages at T_S. Thus, the interfacial bond strength of the SMPC can also be described as 70 MPa [176]. Moreover, stress values from 70 MPa to 100 MPa will cause Type 1 damage, and Type 2 damage will develop beyond 100 MPa (given in Figure 4.13). Hence, the selected CSM facilitates prompt prediction of programming effectiveness of the SMPC, enables selection of the most suitable programming parameters through FEA, and saves time. Figure 4.14 illustrates the FEA stress results of the SP-11-GL-D50 with 60 mm span described in Section 3.5. According to the proposed CSM, it is evident that the SMPC reached the Type 1 damage region which resulted a decline in modulus. However, as the maximum stress is well below the Type 2 region, no change in strength can be expected. The respective FEA results of SP-11 and SP-11-GL-D50 are given in Figure 4.11, where $S_{11} = S_{xx}$ = flexural stress. These FEA results and damage predictions validate the experimental observations and outcomes which can be effectively applied in future SMPC developments.
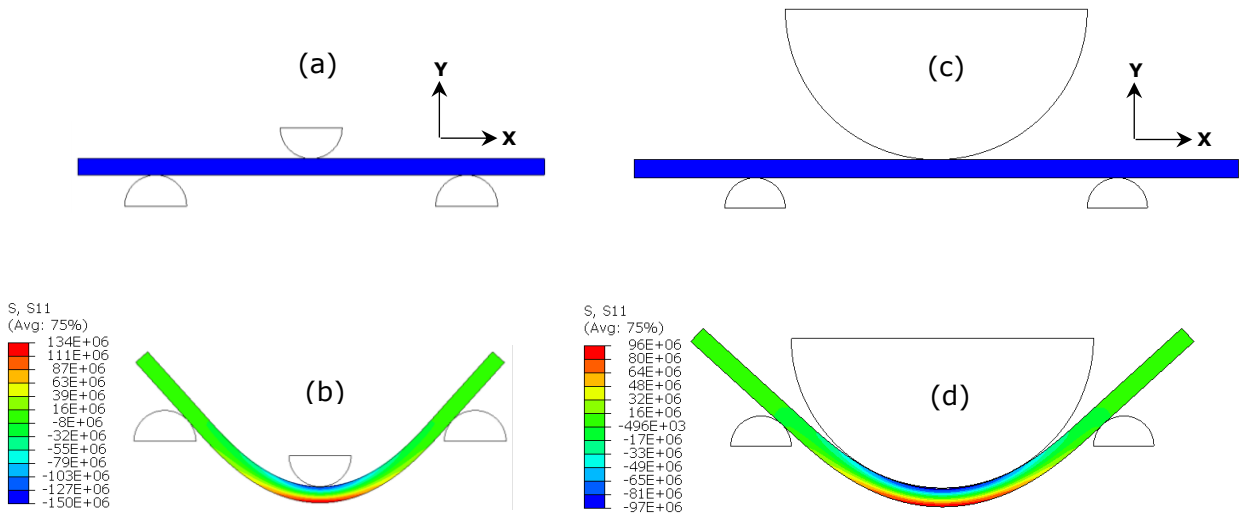
Figure 4.11: Stress (xx) variation of programmed samples; (a) SP-11 before programming (b) programmed SP-11 (c) SP-11-D50 before programming and (d) programmed SP-11-D50
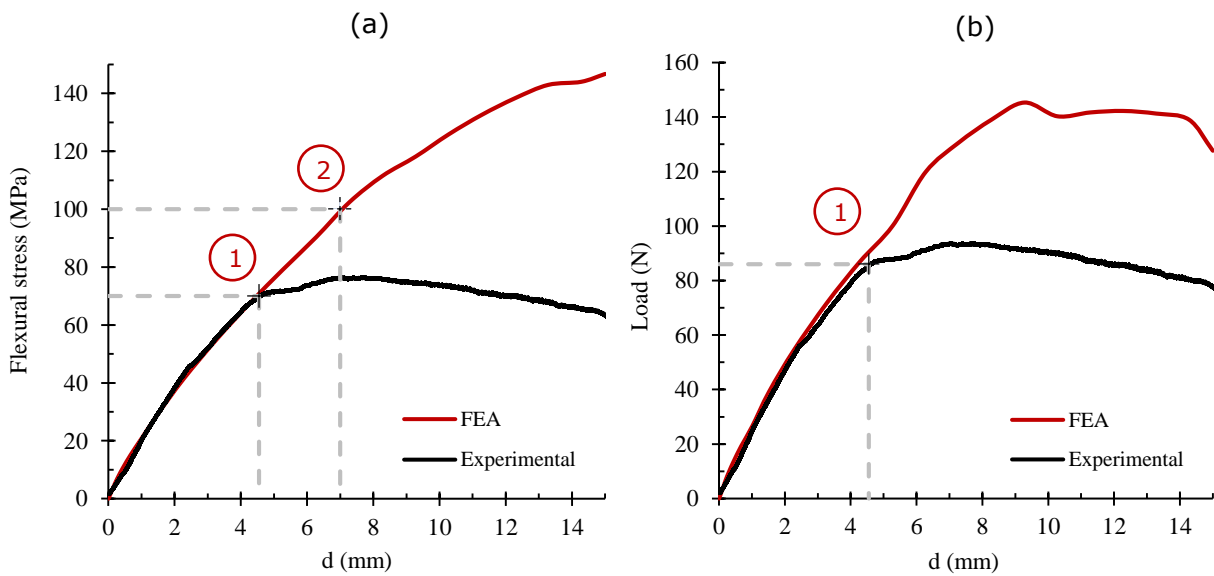
Figure 4.12: Comparison of experimental and FEA; (a) average compressive stress magnitude at the most critical location of the SMPC and (b) applied load for programming
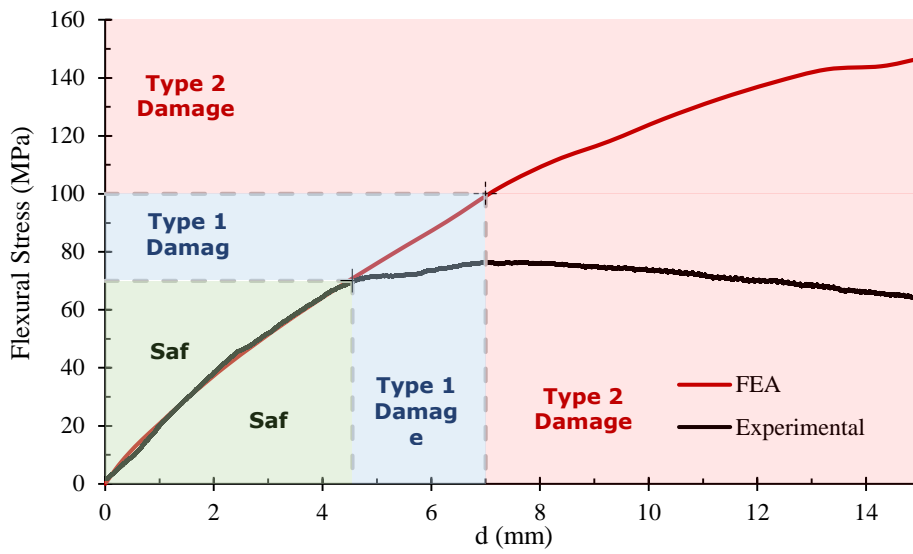
Figure 4.13: Critical stress margins introduced to predict programming effectiveness through FEA
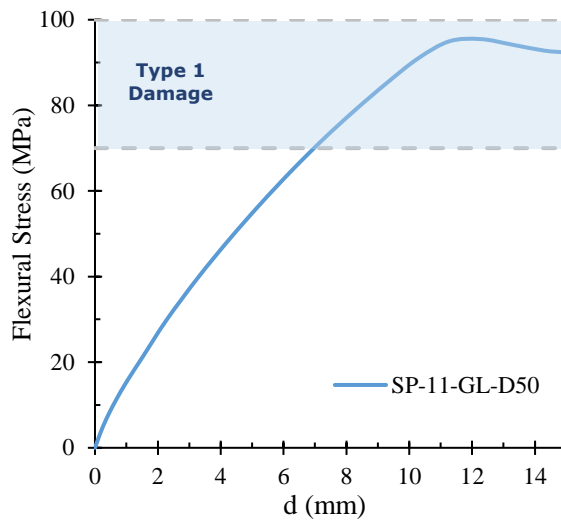
Figure 4.14: FEA stress results for the shape programming process of SP-11-GL with 50 mm bend diameter

4.7 Modelling SME of CHS and SHS components

To improve SMPC component design and applicability in a broad spectrum of civil engineering applications, the programming stage modelling of the SMPC members is vital. FEA analysis of the SMPC component's programming stage allows the prompt prediction of any damage through stress build up, detection of critical locations prone to high stresses, determination of fibre orientation (at compressed side), evaluation of required external forces and optimization of programming process parameters, saving both time and cost. FEA and experimental shape comparisons of CHS and SHS SMPC components during programming are presented in Figure 4.15 and Figure 4.16, respectively. The shapes of the deformed components during the first 12 s of programming are presented. It is evident that the shapes predicted by FEA matches well with experimental deformed shapes of both tested components. In addition, the FEA model was able to demonstrate the spring back effect during shape fixing and recovery of the initial shape once thermal load is reapplied. Fixity and recovery ratios evaluated according to Equations 1 and 2 are given in Table 4.3. The evaluated ratios show a good match among FEA and experimental results, with an error percentage less than 5.6 % and 3.5 % for fixity and recovery, respectively, further validating the FEA model used. The slight difference between these results can be attributed to the material damage experienced during experimental programming.

| t = 1 s | t = 3 s | t = 6 s | t = 12 s |
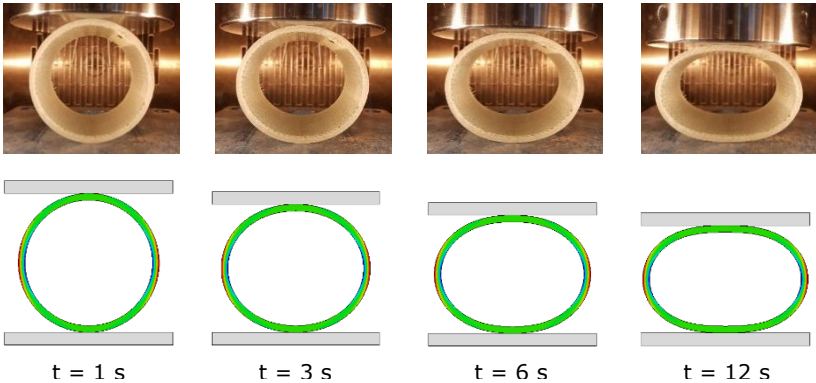
Figure 4.15: Shape comparison of CHS SMPC components during first 12 s of programming

| t = 1 s | t = 3 s | t = 6 s | t = 12 s |
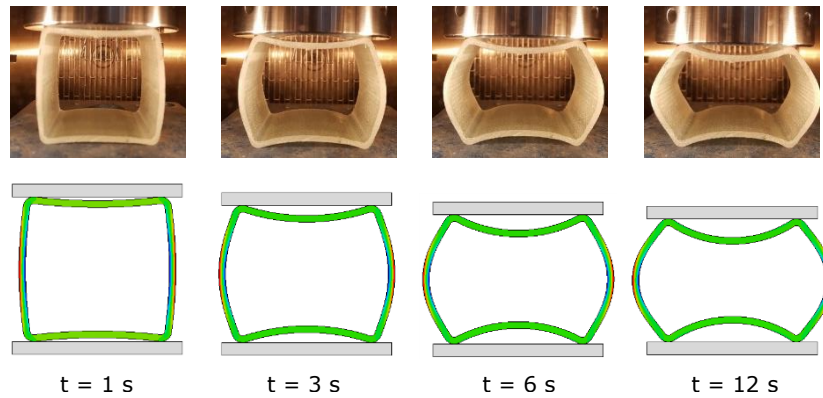
Figure 4.16: Shape comparison of SHS SMPC components
during first 12 s of programming

4.7.1 Damage prediction of structural components during programming

As per the guidelines proposed in our previous study [29], 70 MPa and 100 MPa were proposed as the critical stress limits for the SMPC during programming. In addition, Type 1 damage which corresponds to matrix-fibre debonding due to interfacial failure dominates in the stress range 70 MPa to 100 MPa. Beyond 100 MPa, the material can experience delamination and also cracks initiating on the tensioned side. Consequently, these CSMs were used to predict whether damage had occurred during the programming stage or not, and to further determine the validity of the model by comparison with the experimental data. For clarity, only the damage prediction of the CHS components are presented.

Figure 4.17 illustrates the variation in externally applied load (experimental) during the CHS sample programming and numerical normal stress results at the top (S11) and side (S22) of the specimen. The MTS load reading was utilized in order to recognize the initiation of material damage. As per previous studies, it was suggested that Type 2 delamination and Type 3 cracks could occur beyond a 100 MPa stress level. The material damage Types 2 and 3 refer to delamination and through thickness cracking, respectively. The sudden drop in the experimental load curve in Figure 4.17 is a result of the initiation of a crack or considerable material

damage. The CHS specimen has experienced material damage during the process of programming when it was deformed by 31.2 mm. The FEA stress level on the side of the CHS sample reached 100 MPa close to 32 mm. As per developed stresses (Figure 4.17) on top and side of the CHS, the top should experience Type 1 and the side should undergo damage Types 2 and 3. Interestingly, these simulation based results showed good consistency with experimentally experienced damage types and are shown in Figure 4.18. This proves the effectiveness of the proposed CSMs to numerically investigate and predict the likelihood of material damage during programming. Moreover, most critical locations of the SMPC component prone to damage can also be detected with ease.

In the SHS SMPC samples, a rapid drop in applied test load was seen at a displacement of 11.3 mm, whereas from the FEA results, normal stress on the damaged side achieved 100 MPa at 10.6 mm, demonstrating good consistency with the proposed framework (damage onset at 70 MPa). According to the radial deformability results of the SMPC sections, the SHS showed a quick damage onset at a lower deformation. Hence, the SHS sections can be categorized as more critical compared to CHS which can result in programming damage easily. Consequently, SMPC application suggestions are presented considering only SHS SMPC members.

Table 4.3: Experimental and FEA fixity and recovery values

Component	Programming displacement (mm)	Method	R_f %	R_r %
SHS	15	Experimental	72.6	96.5
		FEA	68.5	99.9
CHS	32	Experimental	82.1	98.1
		FEA	78.8	99.8

Figure 4.17: Comparison of external load applied during experimental programming test and FEA compressive stress results on side and top faces of CHS components
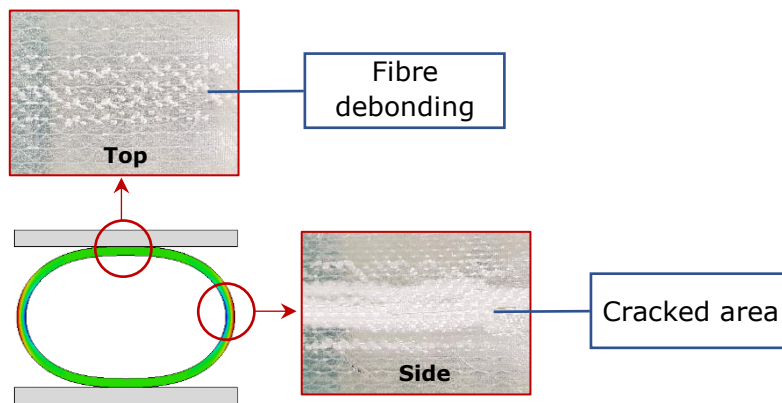
Figure 4.18: Damage types on radially deformed CHS components

4.8 Application of SMPCs in long beams and deployable structures

4.8.1 Shape memory effect of long beams

SMPC SHS and CHS structural components can be used in many challenging civil engineering applications because of their unique intrinsic properties. They can be deformed easily at low cost and with minimal labour to a temporary or confined shape, and then transported to the construction site with ease. Finally, by applying the external stimulus, the deformed SMPC components and structures can be recovered to their initial shapes wherever required. Some suitable engineering applications for these smart SHS and CHS structural components are prefabricated modular constructions, construction of footbridges in remote areas, constructions in challenging terrain, as an alternative to expensive and heavy curved steel beams, for deployable lunar habitats and outer space structures.

Figure 4.19: Programming of SHS SMPC member with 3 m span, for mid span displacements; (a) 0 mm, (b) 250 mm, (c) 500 mm and (d) 750 mm.

The shape memory performance of a large scale 5 m long SHS SMPC member, with the cross section given in Figure 4.2 (a), was also investigated via FEA. A displacement boundary condition was applied at the mid span of the SMPC member at 1 mm/s deformation rate. The deformation rate was identified from our recent studies [29]. To demonstrate the shape deformability of the SMPC members, only the FEA analysis for the SHS SMPC is presented here for clarity. The SHS components initiated damage at a lower radial displacement as described in Chapter 4.7.1 . The FEA analysis was performed for different support spans (S) and mid span displacements (D). Subsequently, the developed

maximum compressive bending stress and bend radius (r) of the SMPC member was evaluated for analysis. As the compressive side of the SMPC is prone to damage during the programming stage, the compressive stress was used as the tool to predict damage onset. Figure 4.19 demonstrates the programming of the SHS component up to D = 750 mm from its initial shape.

FEA viscoelastic simulations were performed for five S values and deformed to a maximum of D = 1000 mm. The summary of FEA results is presented in Figure 4.20. Interestingly, for S > 1000 mm, the compressive stress was below 70 MPa for all D values. However, the evaluated stress exceeded damage onset stress (σ_o) when S = 1000 mm. Hence, the span of 1000 mm can be identified as the critical span (S_C) value for SHS programming. Moreover, for the configuration with S_C, the r values of the deformed SMPC members were evaluated (in Figure 4.21) to determine the limiting bend radius. According to the recognized relationship between r and compressive stress, 650 mm was revealed as the critical bend radius (r_c) for SHS SMPC member programming. Hence, it demonstrates the ability of the fabricated SMPC SHS components to be deformed or wrapped to a compact temporary shape with a bend radius of 650 mm (1.3 m diameter). Similarly, from the FEA study performed for a 5 m long CHS SMPC beam, the r_c was evaluated as 420 mm (0.84 m diameter) for the same S_C. Further, it is clear that CHS SMPC members showed better shape memory performance in comparison to SHS sections, with respect to undamaged shape deformability. These tightly wrapped long SMPC CHS and SHS members can even be stored in a car for transportation as the average width of a passenger car is around 1.75 m [184].

Figure 4.20: FEA results summary; (a) variation of compressive stress with D and S values and (b) test parameters
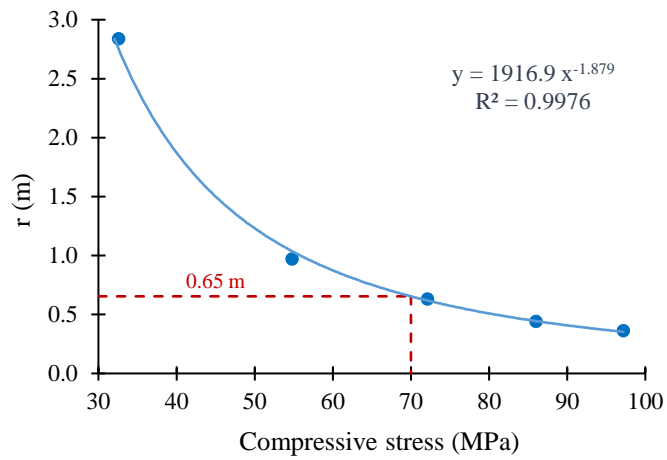
Figure 4.21: Relationship between r and compressive stress for configuration with S_C

4.8.2 Deployable SMPC structures
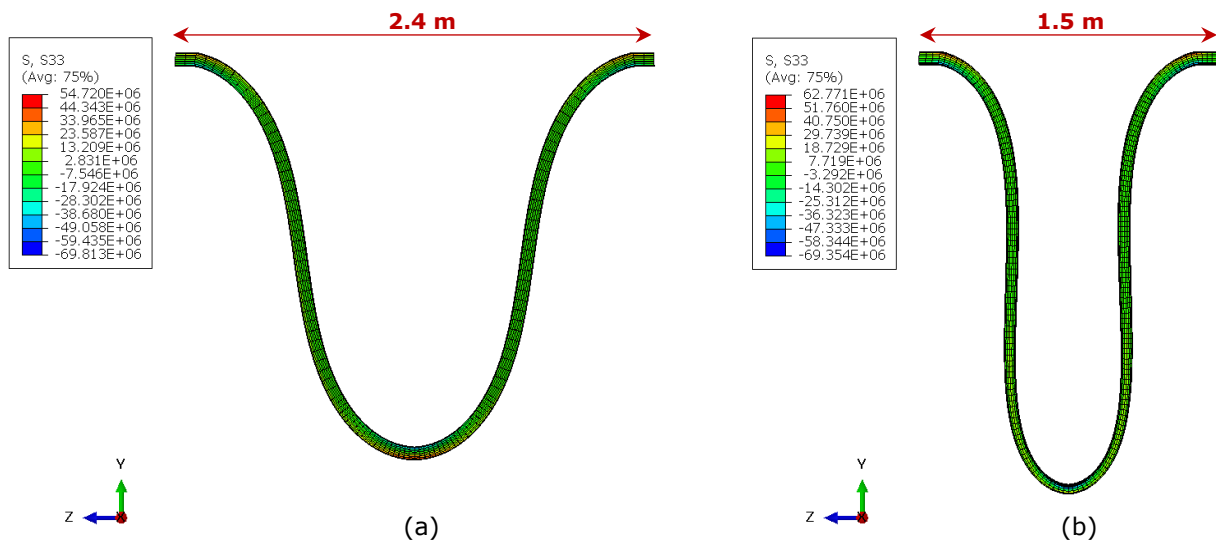
Figure 4.22: Shape programming of vertical member in frame structure;
(a) SHS and (b) CHS

To demonstrate the application of large scale SMPC structural components in deployable structures, a 5x5x5 m³ frame structure was analysed numerically with CHS and SHS members, separately. Figure 4.22 illustrates the shape programming of a single SHS and CHS vertical strut of the structure, up to a maximum compressive stress of approximately 70 MPa to ensure no damage occurred. The initial lengths of both members were 5 m. According to the results, the SHS and CHS SMPC members experienced overall length reductions of 2.6 m and 3.5 m, respectively, with no programming damage. Thus, the height of the SMPC structure has reduced to 2.4 m and 1.5 m, respectively for SHS and CHS. The overall compact configuration of the SHS and CHS structures each with four programmed struts is presented in Figure 4.23. A volume reduction of 52 % and 70 % was achieved by the SHS and CHS structures, respectively. Table 4.4 presents the initial (Vi) and final (Vf) bonding volumes of the two SMPC structures. Importantly, the results clearly show the space saving advantage that can be achieved by SMPC integration into structural components. In contrast to traditional construction materials and technologies, the use of SMPC structural members can be a game changer

for prefabricated modular constructions, heavy curved steel structures, space deployable structures, lunar habitats, foot bridges, etc.
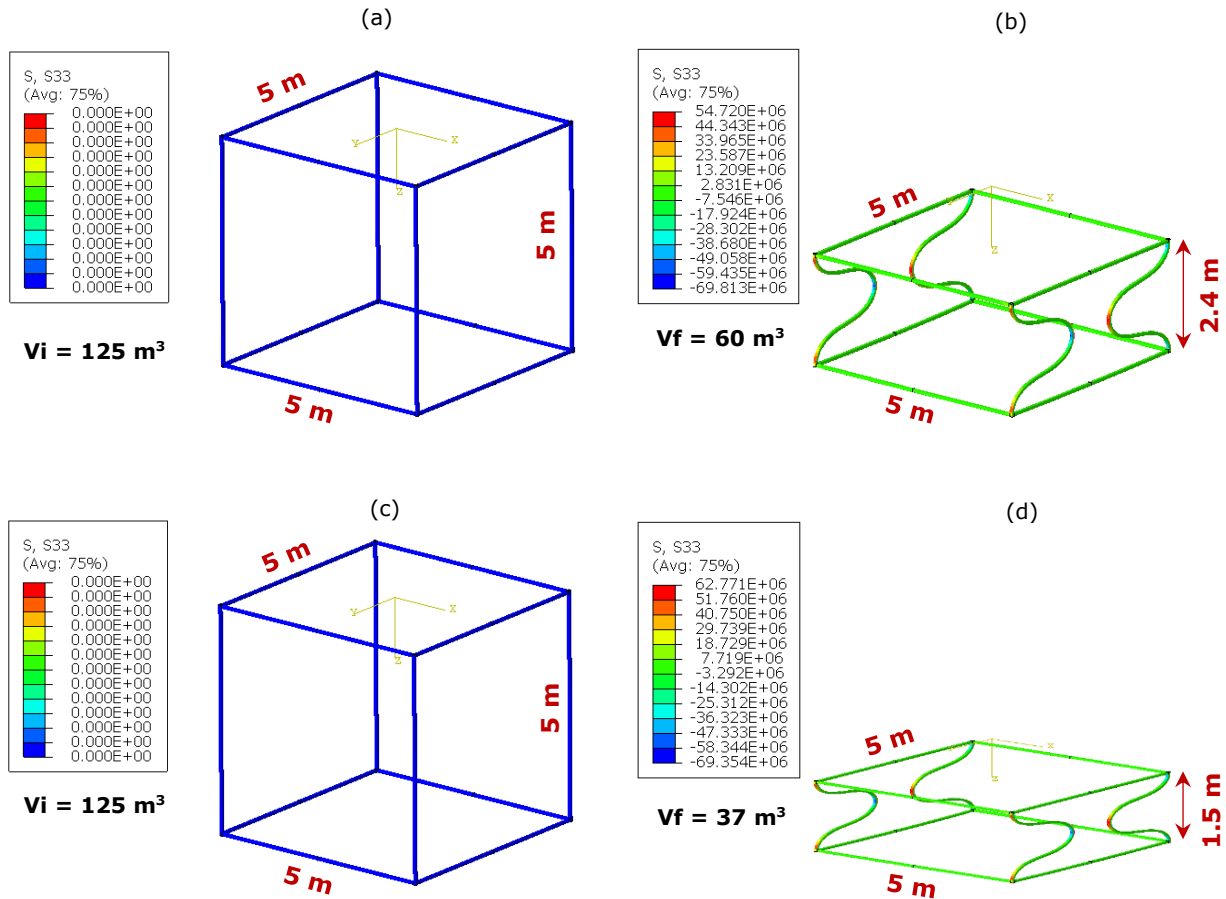
Figure 4.23: SMPC structure configurations; (a) initial SHS, (b) programmed SHS, (c) initial CHS and (d) programmed CHS

Table 4.4: Volume savings of (a) SHS and (b) CHS SMPC structures

SMPC member	Vi (m³)	Vf (m³)	Volume saving (%)
SHS	125	60	52
CHS	125	37	70

4.9 Structural performance of SMPC members

4.9.1 Behaviour of axially compressed SMPC components

Depending on their application, structural components often experience compressive loads. Thus, buckling is an important phenomenon that needs to be investigated when components are exposed to compressive stresses. Consequently, the behaviour and damage mode of the SMPC CHS and SHS components was investigated for components with L/D = 2, and are shown in Figure 4.24. The CHS SMPC components showed a compressive strength of 124.7 MPa when the edges began to experience damage due to crushing. However, the SHS SMPC components experienced local buckling due to compression, and initiated damage at 69.6 MPa. Importantly, recent studies of glass fibre reinforced geopolymer concrete beams used as construction materials showed similar compressive strengths in the range 40 MPa - 85 MPa [185-187]. The comparability of the experimentally evaluated compressive strengths of the SMPC components can be further validated with respect to the results presented for FRP, concrete (~40MPa) and steel integrated, tubular and SHS components [188, 189]. Thus, the results of the compressive behaviour analysis indicate that the comparative loading capacity of the SMPC components is suitable for construction applications.
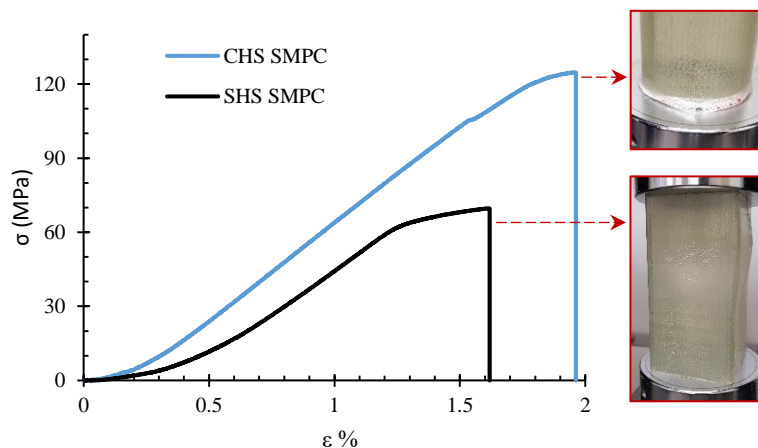
Figure 4.24: Behaviour of CHS and SHS
glass SMPCs under axial compression

4.9.2 Nominal section capacities of SMPC members

According to the steel designer's handbook [190] and Australian standard AS 4100 [191], the suitability of structural members of a particular material can be assessed by calculating the nominal section capacities. The sectional capacities are categorized according to the subjected loading such as bending (AS 4100-5.2) and axial compression (AS 4100-6.2). To further demonstrate the applicability of SMPCs, the CHS structural capacity to weight ratio (specific strength) was evaluated and compared with steel. Equations (4.6) and (4.7) illustrate the nominal section capacity equation for bending and axial compression, respectively. M_S = Nominal section capacity for bending (AS4100-5.2.1), f_y = Yield strength used in design, Z_e = Effective section modulus, N_S = Nominal section capacity for axial compression (AS4100-6.2.1), k_f = Form factor, A_n = Net cross sectional area, d_o = Outer diameter, t = Thickness, ρ = Density). For both loading criteria, the CHS SMPC components demonstrated higher "specific sectional capacities" showcasing their structural potential as lightweight components in comparison to heavy steel sections. The calculation results for the CHS sections are presented in Table 4.5. However, the shear induced corner failures due to confining effects of hollow profiles were not studied, but are recommended as future work.

For bending:
$$M_S = f_y Z_e \tag{4.6}$$

For axial compression:
$$N_S = k_f A_n f_y \tag{4.7}$$

Table 4.5: CHS specific section capacity for mild steel and SMPC

CHS	d_o (mm)	t (mm)	ρ (kg/m³)	f_y (MPa)	M_S (Nm)	M_S/ρ	N_S/ρ
Mild steel	60.3	2.9	7800	380 [192]	4082	**0.5**	**25.5**
SMPC	67	3	1320	232	3215	**2.4**	**57.0**

4.10 Summary

In this chapter, experimental programming damage results given in Chapter 3 were validated using FEA analysis. A FEA based framework was implemented to ascertain the onset of damage and CSM guidelines were proposed to predict possible damage levels during programming. Hence, 70 MPa was found to be σ_o or interfacial bond strength of the optimized glass SMPC to undergo perfect programming. The results showed that Type 1 damage occur in the compressive stress range 70 MPa to 100 MPa, while Type 2 damage develop beyond 100 MPa.

Further, the applicability of SMPCs in real scale CHS and SHS structural components with unique SME, was demonstrated. The integration of SMPCs in commonly used members can transform their current capability, allowing them to be deformed to a compact shape for easy transportation and handling, or incorporate curvy shapes into constructions. Importantly, FEA based damage predictions of the SMPC components were consistent with the experimental results. In addition, it was found that long SHS and CHS SMPC structural members can be wrapped to a minimum radii of 650 mm and 420 mm, respectively, without undergoing any damage during programming. Further, the application of shape deformable SMPC members was presented in a deployable structure which showcased exciting volume savings of 52 % and 70 % for SHS and CHS SMPCs, respectively, for easy handling and transportation.

Overall, this chapter provides first hand comprehensive programming damage investigation of SMPCs through a novel numerical approach and a framework to incorporate the SME of SMPCs in construction components. However, it is vital to understand the durability of the developed SMPC in conditions typical construction materials are subjected to. Accordingly, a comprehensive durability and long term performance study is elaborated in Chapter 5 to further characterise the performance of the SMPC as a construction material.

CHAPTER 5: DURABILITY OF SHAPE MEMORY POLYMER COMPOSITES

5.1 Introduction

In Chapter 3 and 4 of this thesis, comprehensive deliberations were presented on the material synthesisation and optimization, characterisation, FEA modelling and applications of SMPC materials. In this research, as the SMPC materials were developed for structural engineering applications, the durability of the developed SMPC under a variety of environmental conditions were analysed.

Materials used for constructions, often get exposed to different environmental conditions. Hence the effects such as; (a) light/radiation absorption, (b) elevated temperature, (c) moisture, (d) exposure to fire and extreme heat, and (d) fatigue loading, were analysed. As different materials showcase their own behaviour under such effects, the specific SMPC characteristics were studied to evaluate its limitations and capacity.

Moreover, as the SMPC structures get exposed to long term sunlight when in use, it might impose adverse effects on the polymer matrix. Long term UV exposures can affect and degrade the polymeric structure eventually hindering structural performance of the SMPC. Hence, light absorbance properties of the SMPCs were investigated to understand their potential and applicability as a construction material. Importantly, fire safety is also a major concern in all types of civil constructions. Tough design requirements and material performance expected in building codes for construction materials reflect the high level of concern for fire safety. The behaviour of a material when exposed to fire can be assed considering many critical factors. However, smoke generation can be identified as the most prominent and crucial aspect, as it can cause fatalities with loss of visibility and difficulty in breathing due to toxic materials in smoke [193]. Consequently, the properties of the SMPCs under fire were analysed and

the evolving gases due to thermal decomposition were characterised via FTIR spectroscopy.

On the other hand, structural components may experience fluctuating loads depending on the application. These fluctuating loads can lead to premature catastrophic failure putting lives of people at high risk. Therefore, fatigue properties of the optimized SMPC were also studied and material specific fatigue parameters used for predictions were also evaluated.

In practise, the materials will often get exposed to natural phenomena such as rain and humidity which may result in degradation of strength, stiffness etc. Thus, the study of moisture effects on SMPC properties was also performed. Additionally, the environmental temperature changes with respect to the weather condition, location, time etc. Thus, elevated temperature effects were investigated as the properties of polymers are highly dependent on the environmental temperature.

The new knowledge presented in this chapter significantly contributes towards the characterisation and investigation of the durability of SMPCs under different environmental factors. Hence, the research work and procedures elaborated herein can be effectively implemented in further SMPC developments and aid in successful implementation of SMPCs in structural components.

5.2 Materials preparation

In this study, two types of SMPC materials are presented based on two SMP types; A and D (in Table Table 3.3). They are; i) glass, basalt and carbon fibre/SMP (Type A) and ii) glass, basalt fibre/SMP (Type D). During the author's preliminary research work, the light absorption properties, smoke density based fire properties, thermal decomposition and gas characterisation were performed for the SMPC with type A SMP reinforced with glass, basalt and carbon fibre reinforcements. A summary of the

presented materials, fabrication method and experiments performed are illustrated in Table 5.1

Table 5.1: Summary of the presented materials and specific studies conducted

SMP type	Reinforcements	Fabrication method	Tests performed
A	Glass Basalt Carbon	Hand lay up	Light absorption Fire and smoke density Thermal decomposition Gas characterisation
D	Glass Basalt	Mould method	Tension-tension fatigue Moisture exposure Temperature effect

5.3 Experimental methods

a) UV-VIS light absorption

Figure 5.1: UV-VIS spectrometer

The optical transmittance spectra of carbon, glass and basalt fibre reinforced SMPCs were measured using Evolution 220 UV-VIS spectrometer (Thermo Scientific) with an integrating sphere (ISA-220), in 220 nm - 1100 nm wavelength range. SMPC samples with a surface area of 40x40 mm^2 were positioned under spring clamps on either side of the transmission port.

The transmittance measurements of SMPCs were recorded using INSIGHT software. Three transmittance tests were performed for each type of material, but for clarity only one spectrum is shown due to the consistency of the results. The apparatus is shown in Figure 5.1.

b) Smoke density tests

The smoke generating behaviour of SMPCs in a fire was analysed using a Deatak Model SD-2 smoke density tester (shown in Figure 5.2), pertaining to the guidelines given in ISO 5659-2 testing standard. Samples were cut into 75 mm ± 1 mm square shapes and wrapped with a single layer of Aluminium foil to limit the flame exposed area to 65 mm^2. Also, it was ensured that no residue falls out from the sample during fire, making weight loss readings erroneous. SMPC samples were tested at a heat flux of 25 kW/m^2 with pilot flame. The heating coil temperature was set to 616 ^{o}C. During the test, the apparatus recorded and plotted the light transmittance (T) and specific optical density (D_S) inside the testing chamber. The relationship between T and D_S is given in Equation 5.1. In addition, the load cell connected to the sample holder recorded the mass readings by which overall mass loss has been evaluated.

Moreover, during testing key parameters such as time of ignition, duration of fire and smoke characteristics were observed and recorded manually. Three specimens from each type of SMPC were tested and for clarity only the average curves are presented here.

$$D_S = 132 \ log_{10} \left[\frac{100}{T} \right]$$

5.1

Figure 5.2: Deatak smoke density testing apparatus

c) Thermogravimetric analysis-Infrared spectroscopy (TGA-IR)

Thermal decomposition of SMPCs was ascertained by Thermogravimetric characterization using a TA instruments (SDT 650) as per test standard ASTM E2550. The TGA-IR module of Nicolet iS50 spectrometer was coupled with the TGA to identify evolving gases due to thermal decomposition and three specimens were tested. In each test, about 20 mg of composite sample was placed in a ceramic pan inside the furnace and heated at a temperature ramp of 10 ^{o}C/min from room temperature to 600 ^{o}C. Simultaneously, the loss of sample's weight as a function of temperature was monitored. To investigate how materials can decompose in a natural environment, the tests were conducted taking air as the carrier gas. The flow rate of air through the furnace was set to 50 mL/min. The temperature of both flow cell and transfer line of the TGA-IR module were set at 300 ^{o}C and allowed to run for few hours prior to testing. This was done to make sure the components of TGA-IR module are free from moisture. Spectrometer readings were taken within 4000-600 cm^{-1} wavenumbers. Figure 5.3 presents the coupled apparatus to perform TGA-IR tests.

Figure 5.3: Apparatus used for TGA-IR testing; (a) FTIR and (b) TGA

d) Fatigue testing

Fatigue behavior of the optimized SMPCs under tension-tension cyclic loading was investigated in MTS 810-100 kN according to ASTM D3479/D3479M-19 [194] and is shown in Figure 5.4. Five samples were tested for each material type and experiment. The specimens were cycled between their minimum and maximum tensile load (stress) at 1 Hz frequency (f). A low frequency was selected to avoid temperature rise in the sample. Fatigue lives of SMPC samples were studied for a stress ratio (R = ratio of minimum and maximum stress) of 0.1 and for five selected load levels (L) which are 40, 50, 60, 70 and 80 % of UTS. Tabbed SMPC samples were used to avoid premature failure within grips along with a 10 Hz data acquisition rate. The load mean (L_M) and amplitude (L_A) were used to define the 'Sine' wave form in the test setup and respective values for glass SMPCs are given in Table 5.2.

Table 5.2: Load values for glass SMPC fatigue test setup

SMPC	UTS (MPa)	R	L %	L_M (kN)	L_A (kN)
Glass	231.9	0.1	80	7.7	6.3
			70	6.7	5.5
			60	6.0	4.9
			50	5.0	4.1

| | 40 | 4.0 | 3.3 |

(a) (b)
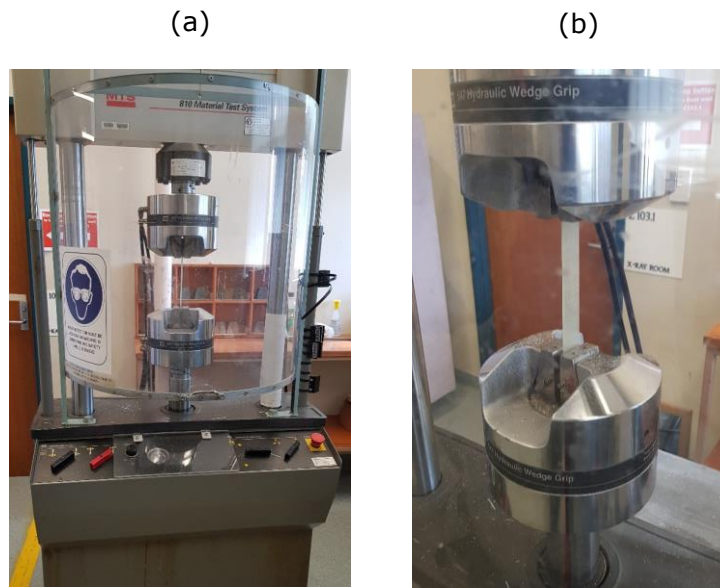
Figure 5.4: Fatigue testing equipment; (a) apparatus
setup and (b) SMPC specimen under testing

e) Moisture exposure

To study the effect of humidity or moisture exposure on SMPC's tensile, compressive and flexural properties, samples cut to required dimensions for each test were placed inside the 'Votsch-technik environmental chamber' (Figure 5.5) for 1000 hrs. During this time, all samples were exposed to 98 % RH (relative humidity) and 60 ℃

Figure 5.5: Moisture testing environmental chamber

environmental conditions. Also, sample weights before and after moisture exposure test were recorded to investigate SMPC's moisture absorption.

f) Temperature effect test

Tensile properties of the optimized SMPC in elevated temperatures 45 ^{o}C and 60 ^{o}C were studied as polymer matrices usually tend to degrade when heated. 60 ^{o}C was selected as it's the programming temperature T_S of the SMPC. Three samples were tested for each test and material type. Tests were carried out in MTS 100 kN along with its thermal chamber to maintain required temperature during the test. Tabs were attached to the SMPC tensile samples to avoid sample slip and undesirable damage within fixtures, as the matrix gets soft when heated. A reinforced polymer composite with a higher T_g was used as the tab material. A laser extensometer with two reflective tapes positioned 25 mm apart (as shown in Figure 5.6) were used to measure axial strains during tensile testing. The three point bending tool was used according to ASTM D7264/D7265M-15 standard to study flexural behaviour [19].
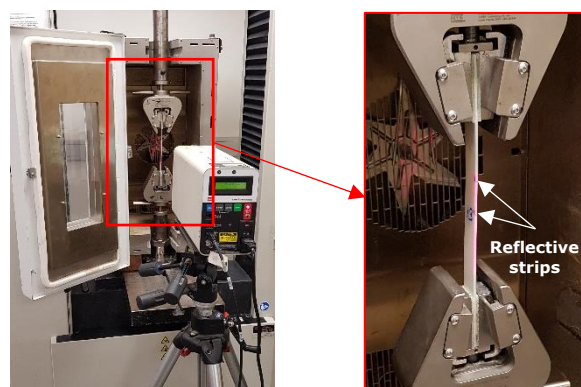
Figure 5.6: Elevated temperature tensile experimental
setup with the laser extensometer and reflective

5.4 UV-VIS light absorption

Materials used in constructions or structural applications are often exposed to sunlight. Such building materials should have the capability to

119

withstand heat and UV effects imposed by daylight maintaining its structural integrity, strength and shape etc. Failure to endure such weather conditions can put safety of people and assets at high risk. As a result of that, UV-VIS light absorption analysis was carried out in order to understand its durability and the extent to which prepared SMPCs absorb or transmit UV radiation.

Figure 5.7 illustrates light transmittance results of neat SMP and fibre reinforced samples for different wavelengths (λ). This provides facts on the extent to which the SMPCs absorb or transmit different wavelengths of light or sun rays. It can be seen with the addition of fibre reinforcement, transmittance of light through the samples have decreased throughout the spectrum for the range UV ($\lambda < 400$ nm), visible (400 nm $< \lambda < 750$ nm) and IR ($\lambda > 750$ nm) regions. Basalt and carbon fibre SMPCs show the least transmittance values due to their opaque characteristics. It is important to understand that high transmittance denote low absorption of light and vice versa. Comparatively, neat SMP shows a low cut off point at 305 nm while glass, basalt and carbon fibre reinforced SMPCs demonstrate cut offs at 320 nm, 520 nm and 1070 nm respectively. However, UV effects will be very high for exposures below 305 nm regardless of the type and fibre composition of the samples. Moreover, glass fibre reinforced SMPCs will have a lower impact from UV radiation in the range 305 nm $< \lambda < 400$ nm in comparison to other tested SMPCs. Recently, Wessam et al have investigated the UV effects on a styrene based SMP and its glass SMPC. The tests were carried out in the range 325 – 400 nm for 1000 hrs and have investigated UV effects on SME, thermal stability and chemical structure of the polymer. Further, it was revealed that due to long term UV radiation exposure, chemical structure has undergone changes resulting in a decreased T_g and shape recovery rate. However, UV exposure have improved thermal stability and shape fixity ratio of the material [103].

Moreover, light activation technique is an emerging new technology in the field of SMPs. SMPCs have been developed which can be activated with near infrared radiation (NIR) of wavelength 808 nm [33]. It is evident

(in Figure 5.7) that SMPC with glass fibre has a near IR transmittance of 45% while basalt and carbon SMPCs show minimal transmittance (less than 5%). Hence it can be argued that, glass SMPC has a lower capacity to absorb NIR radiation comparative to other fibre types. Therefore, basalt and carbon SMPCs can also be used as a photothermal filler in terms of light activation. However, basalt fibre is a better reinforcement relative to expensive carbon fibre in SMPC light triggered applications with its high IR light absorption.
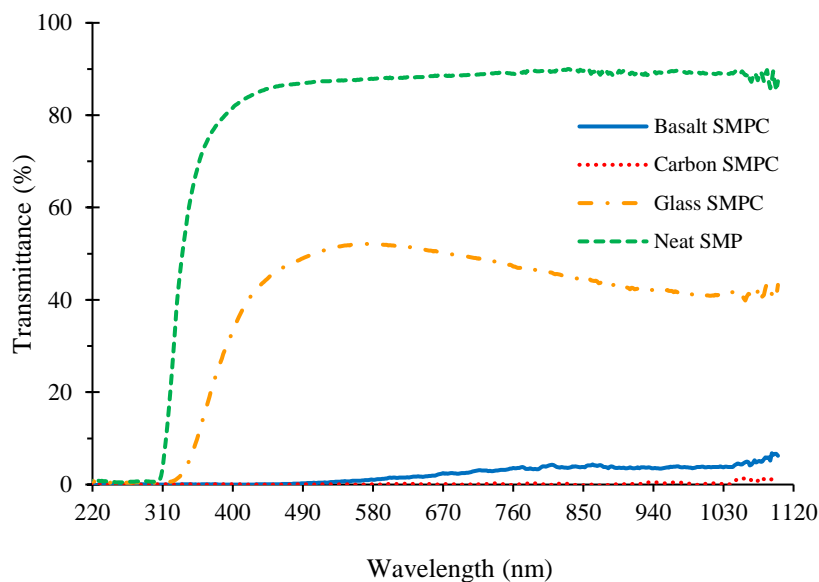
Figure 5.7: Light transmittance of neat and SMPC samples

5.5 Smoke generation under fire

5.5.1 Light transmittance through smoke

Fire safety is a significant concern in all types of civil engineering applications and constructions. Tough design requirements and material performance expected in building codes for construction materials reflect the high level of concern for fire safety. Fire safety consists of prevention, containment, detection and evacuation [195]. During a fire emergency situation, the competency, suitability and applicability of a material in construction are measured mainly by ignition, flame spread, heat release

and smoke generation. Among these critical factors, smoke generation can cause fatalities during a fire with loss of visibility and difficulty in breathing due to toxic materials present in smoke which eventually hinders evacuation [193]. Hence, smoke generation must be analysed when a new material is introduced as a construction or structural material.

Figure 5.10 illustrates the average light transmittance plots for the tested composite samples. During a smoke density test, the specimen will get heated up to a high temperature due to the heat flux applied. As a result of that, the polymer matrix decomposes releasing fumes which consist of low molecular weight volatile constituents. Eventually, the pilot flame ignites released flammable gases initiating a fire on the top surface of the sample. Consequently, the produced smoke resulted in a sudden drop in transmittance which diminishes with continuous generation of smoke. Figure 5.8 shows a burning SMPC sample during a smoke density test. Thermal oxidative decomposition mechanisms of epoxy resins have been reported in 3 ways. Attack of oxygen on the methylene group, oxidation of the tertiary carbons in the aliphatic portion of the chain and oxygen attack on the nitrogen in epoxies cured with amine based hardeners [196].

Figure 5.8: SMPC sample burning during
a smoke density test

Accordingly, both glass and basalt SMPCs resisted ignition for 68 s while carbon fibre composite resisted for 70 s. However, carbon reinforced

SMPC continued to burn for 221 s while glass and basalt composites burnt for 202 s and 193 s respectively (in Figure 5.9). According to Equation 3, at the highest level of smoke generation (T_{MIN}), $D_{S, MAX}$ can be evaluated. Glass and basalt composites produced the highest level of smoke with $D_{S, MAX}$ = 540 while carbon showed 512. Table 5.3 shows the mass losses of SMPCs due to fire.

	Glass SMPC	Basalt SMPC	Carbon SMPC
⊠ Time for ignition	68	68	70
☐ Duration of fire	202	193	221
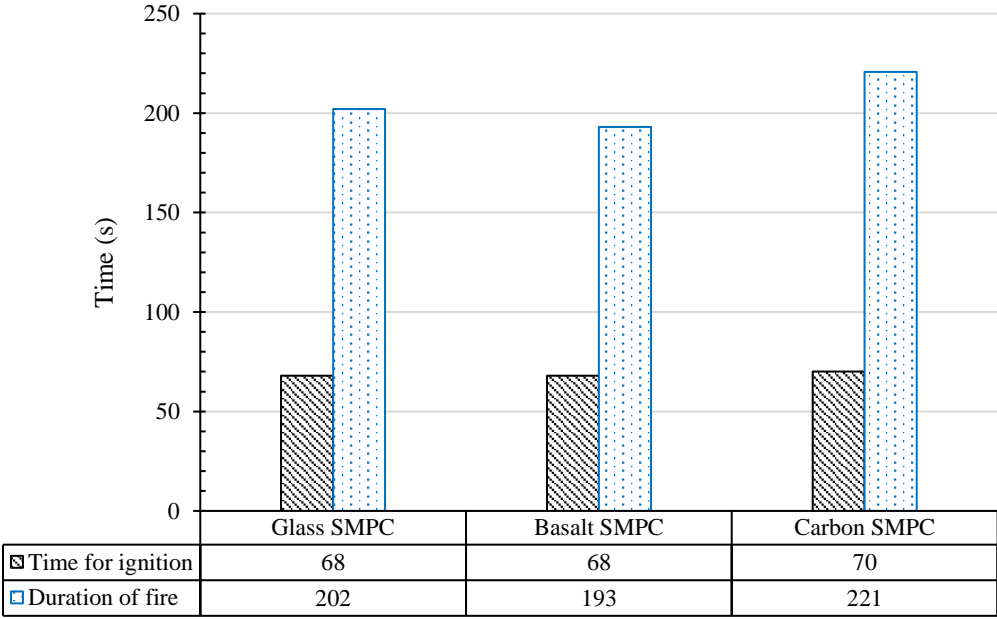
Figure 5.9: Times taken by SMPCs to start and completely terminate fire during testing

Table 5.3: Mass loss of SMPCs after fire tests

Reinforcement	Thickness	Initial mass	Mass loss
	mm	g	%
Basalt	1.46	10.96	44.0
Carbon	1.64	11.43	41.8
Glass	1.93	15.70	34.8

5.5.2 Visibility through smoke

Fire is a critical and disastrous emergency situation for any type of application. Especially in buildings, lot of attention has been taken place mainly to avoid such cases. Also, equipment like fire extinguishers, water lines with automatic sprays and hoses have been installed in buildings in line with emergency exits. More than the heat released in a fire, the generating smoke can put lives of its occupants at high risk. Burnt volatile residues will contain poisonous gases which can make breathing hard and eventually make unconscious. Moreover, high levels of smoke can obstruct visibility and result in an evacuation delay. Consequently, for building materials analysing how the visibility can drop in a fire is crucial.

Optical density D(T) which is a function of the light transmittance (T), given in Equation 5.2 [197] can be used to evaluate the relationship between D and time (t). Curve fitting the plots in Figure 5.10 give T as a function of t (i.e T = T (t)). Therefore, visibility (V) can be related to t as given in Equation 5.3 [198], where L = optical path length = 0.915 m for the test chamber used. According to Rabash et al [198] for fire safety and safe evacuation, occupants require at least 10 m of visibility through smoke. Figure 5.11 shows how visibility degrades when SMPCs burn with time. Basalt, carbon and glass fibre reinforced SMPCs were able to maintain a visibility level over the 10 m margin for approximately 69 s, 72 s and 74 s respectively.

$$D(T) = log_{10} \left[\frac{100}{T} \right] \qquad\qquad 5.2$$

$$V = \frac{L}{D(T)} = \frac{L}{D(t)} \qquad\qquad 5.3$$
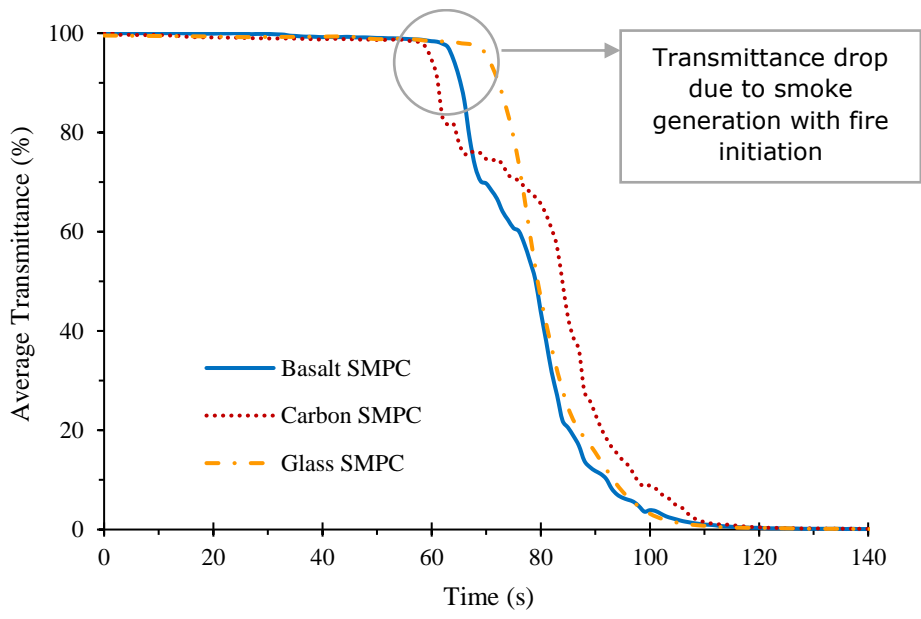
Figure 5.10: Variation of average light transmittance inside the test chamber
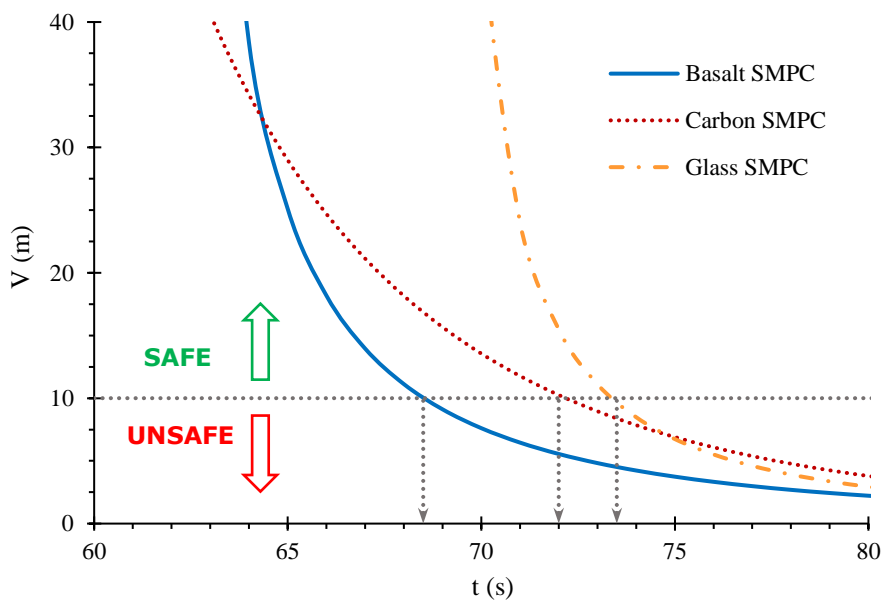
Figure 5.11: Level of visibility when SMPCs are subjected to a fire

5.6 Thermal decomposition

5.6.1 Thermogravimetric analysis (TGA)

As discussed, investigation of the behaviour of construction materials in a fire hazard is vital. Moreover, materials that are exposed to excessive heat generated during a fire will heat up to high temperatures resulting in thermal decomposition. Hence, to understand how selected composites can thermally decompose in a fire hazard, Thermogravimetric tests were performed in the present study.

Figure 5.12 illustrates how SMPCs decomposed at elevated temperatures. The temperature at a 5 % weight loss was considered as the thermal decomposition temperature of the material [199]. All three SMPCs showed similar behaviour up to 380 ^{o}C so that all materials have initiated their thermal decomposition at an identical temperature of 345 ^{o}C. This clearly indicates that the type of reinforcement material is not a governing factor for the thermal decomposition temperature of the selected SMPCs. However, at temperatures higher than 380 ^{o}C, highly thermally stable basalt and glass fibre reinforced composites showed quite an identical behaviour. In contrast, less thermally stable carbon fibre SMPC has shown a higher decline in weight. This can be attributed to the low decomposition temperature of carbon fibre. Therefore, when carbon fibre gets exposed to heat or flame at higher temperatures, there is high potential to get burnt with atmospheric oxygen while leading to a further weight loss.
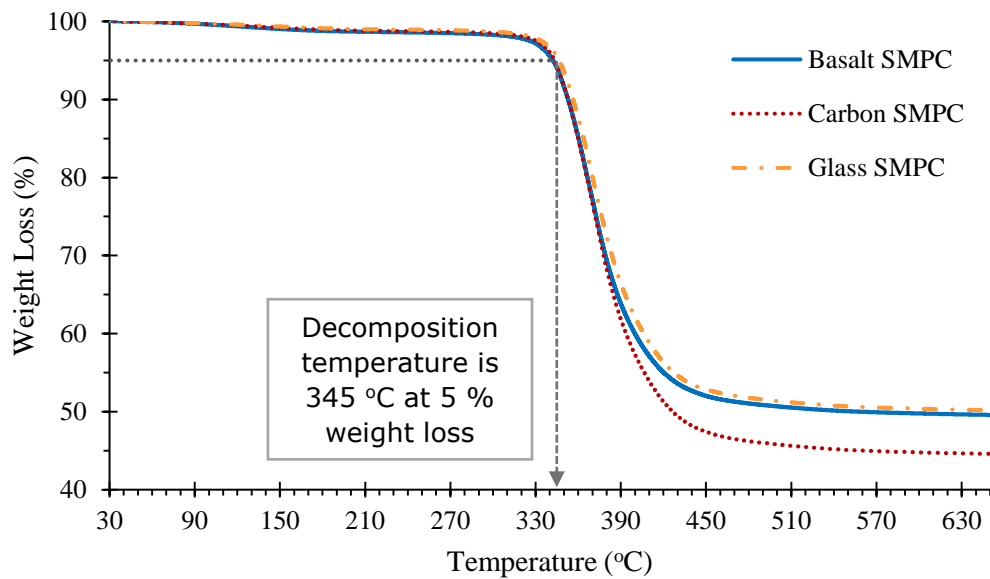
Figure 5.12: Weight loss of SMPCs due to thermal decomposition

5.6.2 TGA-IR analysis of volatile products

The SMPCs undergo a weight loss due to the decomposition at elevated temperatures. Loss of material weight is typically accompanied by gases evolved during the decomposition process. These evolving gases or fumes could be extremely harmful for people if breathed. Hence, the volatile gaseous components of decomposed SMPCs were characterised using FTIR. All three SMPCs have shown similar absorbance spectra for the evolved gases until 380 °C. However, carbon fibre SMPC has shown higher traces of CO_2 beyond 380 °C due to reinforcement oxidisation as discussed earlier. For clarity, only the results of basalt SMPC are provided.
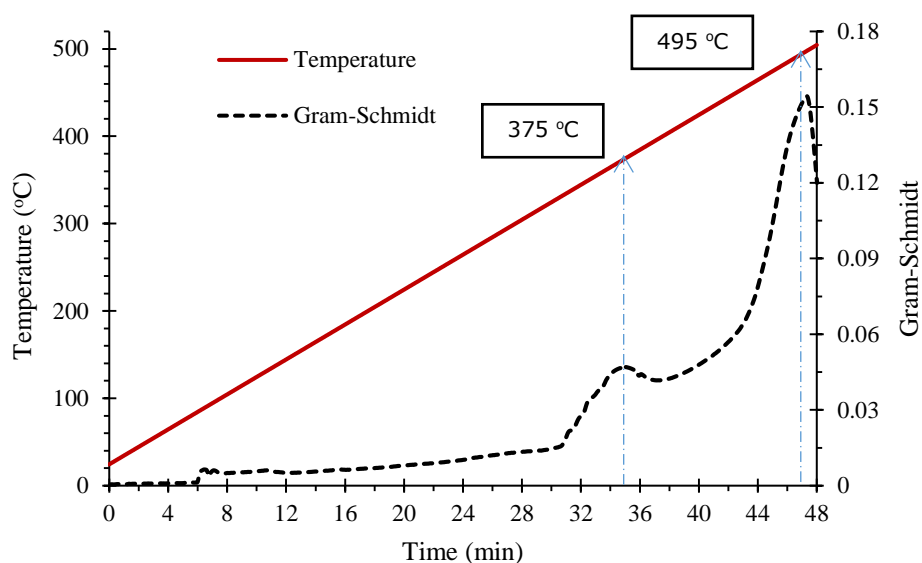
Figure 5.13: TGA-IR Gram-Schmidt intensity variation with time

The Gram-Schmidt profile given in Figure 5.13 shows how overall spectral intensity changed during the TGA-IR test. It can be clearly seen that as the SMPC decomposed two turning points or peaks have appeared at 375 °C (at ~35 min) and 495 °C (at ~ 47 min). Peaks in the Gram-Schmidt plot denote when different compounds in the specimen vaporised and passed through the flow cell absorbing IR energy. The thermal decomposition has initiated after 32 min of test start which corresponds to a temperature of 345 °C. Figure 5.15 illustrates absorbance spectra of volatile components at four selected instances. Plots shown for 20, 32, 36 and 47 min corresponds to spectra considered prior to thermal decomposition, start of decomposition, first peak and second peak in Gram-Schmidt (Figure 5.13) respectively.

For the selected four cases in Figure 5.15, ten clear spikes can be identified. These peaks numbered from 1-10 are given in Figure 5.14. The variation of the intensity at these peaks have shown irregular behaviour for the selected time frames. The identified variations can be categorised as (1) almost constant, (2) gradually increasing and (3) gradual rise followed by a drop.

128

Category 1: Peaks 1 and 2 have not shown significant changes with test time. Fairly appeared peak 1 at 3620-3680 cm^{-1} can be attributed to the OH group that suggests the existence of water vapour [199, 200]. Similarly, peak 2 at 2960 cm^{-1} is due to C-CH stretching of light alkanes, such as ethane or propane [200, 201]. Therefore, it can be predicted that continuous degradation of SMPC may result in a steady formation of water vapour and flammable alkanes. The phenomenon of flammable alkane release can be attributed to the initiation of fire when exposed to the flame in smoke density tests (Figure 5.8).

Category 2: Peaks numbered as 3, 8, 9 and 10 have shown a gradual increase in its absorption. Peak 3 has shown the most significant change throughout the test. Rapid formation of CO_2 is in evidence with the prominent peak of C=O stretching at 2200-2400 cm^{-1} [199, 200]. Peaks 8 (1076 cm^{-1}), 9 (820-890 cm^{-1}) and 10 (640-700 cm^{-1}) have shown the existence of Ether (C-O-C) [201, 202], Alkane (C-C) and Amine (NH_2 and N-H) functional groups [202].

Category 3: Absorption peaks given by 4, 5, 6 and 7 have shown a rapid growth with the start of decomposition at 32 min. These peaks have continued to increase until 36 min followed by a noticeable drop in intensity at 47 min. Wavenumbers 1600 cm^{-1}, 1510 cm^{-1}, 1255 cm^{-1} and 1175 cm^{-1} have shown the existence of an Aromatic double bond (peak 4) [199, 201], Aromatic C=C or N-H stretching (peak 5) and Ester C-O stretching (peak 6 and 7) respectively [202]. According to the identified pattern, it can be concluded that, these volatile traces will increase but gradually drop with continuous SMPC degradation. A summary of the suspected gaseous traces evolved based on the functional groups is given in Table 5.4.
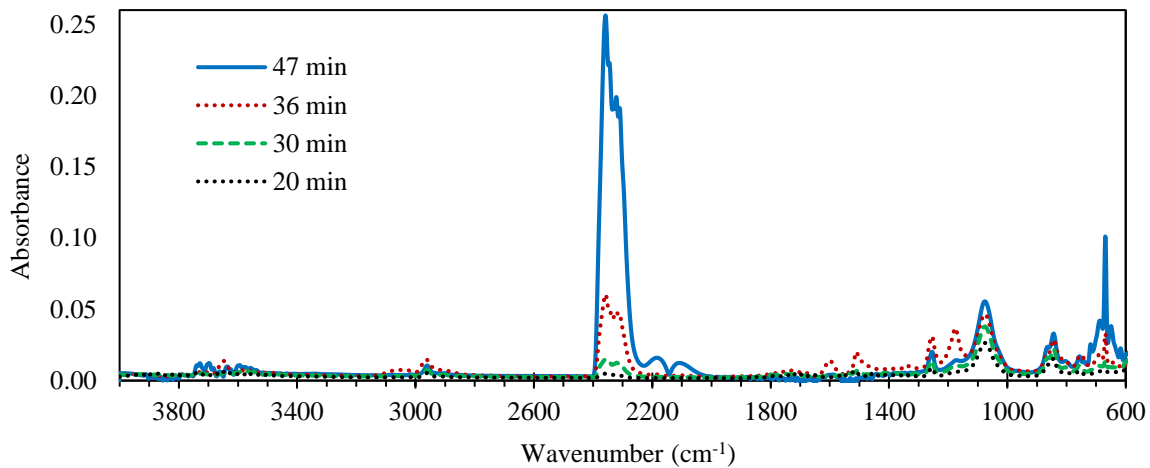
Figure 5.15: Absorbance spectra of evolved gases after 20, 30, 36 and 47 minutes
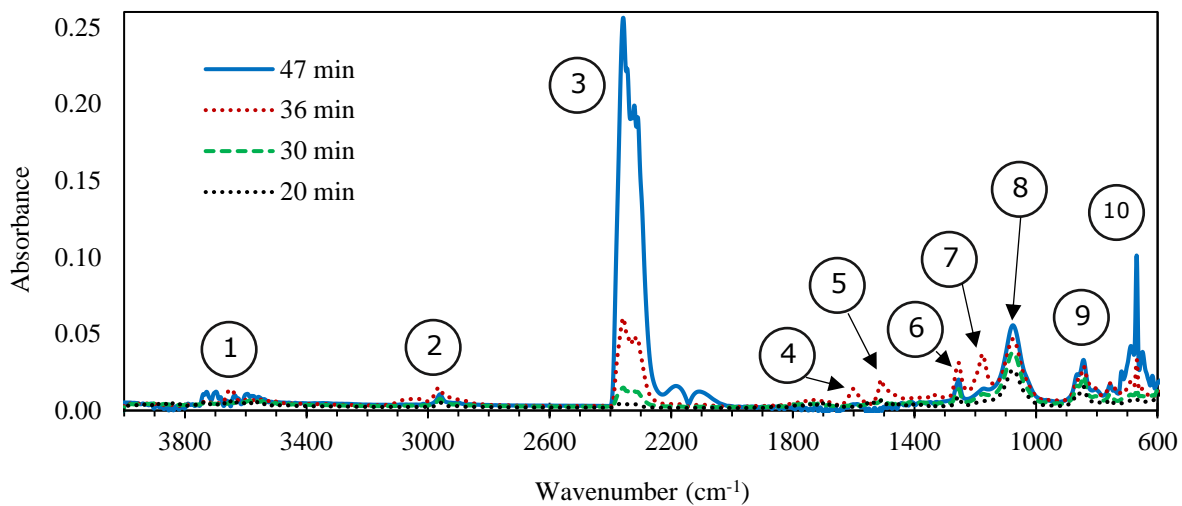
Figure 5.14: Identified peaks in spectra

Table 5.4: Functional groups or materials identified from peak wavenumbers

Peak Number	Wavenumber (cm^{-1})	Functional groups	Suspected materials (or class) produced
1	3620-3680	-OH	Water vapour
2	2960	C-CH	Light alkanes such as ethane or propane
3	2200-2400	C=O	Carbon dioxide (CO_2)
4	1600	Aromatic double bond	Compound containing an aromatic ring
5	1510	Aromatic C=C or N-H	Aromatic (C=C) or amides (N-H)
6	1255	C-O	Ester
7	1175		
8	1076	C-O-C	Ether
9	820-890	C-C	Alkane
10	640-700	NH_2 and N-H	Amines

5.7 Fatigue testing

5.7.1 Fatigue behaviour

Due to different environmental conditions, structural components used in constructions can experience cyclic loading and could lead to a catastrophic destruction with time [203]. Fatigue failure is induced due to critical loading patterns which are lower than UTS of materials. Fatigue behaviour of any material has found to be very complex and challenging to predict. However, it is vital to have an understanding on how the SMPCs behave under fatigue loading to analyse and investigate the applicability in proposed applications. Thus, constant amplitude axial tension- tension fatigue tests were performed for the optimized glass and basalt SMPCs for L values ranging from 40 % to 80 % of UTS. These experimental results allows identification of the fatigue strength (S_n) of the SMPC, which is the safe stress margin for a $2x10^6$ lifetime under cyclic loading.

Figure 5.16 illustrates fatigue lifetimes of glass and basalt SMPCs under tested load percentages. The S-N curves of these SMPCs have shown a similar trend compared to fatigue behaviour of other common materials [204, 205]. During fatigue testing, complete separation of SMPC samples was used as the criterion for failure. At a given load percentage, average value of the number of cycles to failure of each sample type was used to plot the S-N curve. Subsequently, power law equations were fitted to test results and fatigue endurance limits of the SMPCs at $2x10^6$ cycles were evaluated. A fatigue life of $2x10^6$ cycles was selected as per similar fatigue studies performed for fibre reinforced plastic (FRP) [206-208] and lightweight concrete [209] for civil applications.

Interestingly, basalt fibre reinforced SMPCs have shown slightly better performance under high tensile fatigue loading, in contrast glass SMPCs exhibited marginally better resistance against lower fatigue loads. Accordingly, the endurance limit of glass and basalt SMPCs were evaluated as 60.5 MPa and 55.7 MPa respectively (given in Table 5.5). Moreover, the samples have shown similar failure modes in comparison to previous studies on general polymer composites. Thus, tested SMPCs have shown a progressive damage failure behaviour by means of matrix cracking, fibre-matrix debonding, delamination and fibre breakage [204, 205, 210, 211]. In addition, it was clearly seen that the fatigue failure modes of SMPCs were identical to that of static tensile load failure mode which was also presented by Wang et al [211].
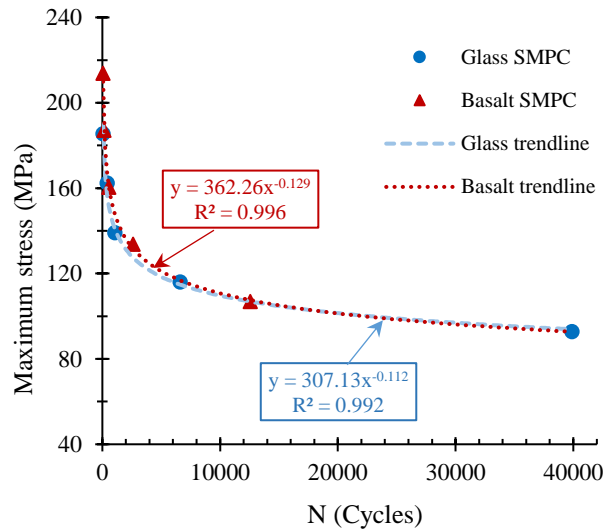
Figure 5.16: S-N fatigue life characteristics for the SMPCs

Table 5.5: Fatigue lives of the SMPCs

Material	Fatigue life (million cycles)	Fatigue/Endurance limit	
		L (%)	S (MPa)
Glass SMPC	2	26	60.5
Basalt SMPC	2	21	55.7

5.7.2 Fatigue predictions

As mentioned previously, fatigue tests were performed at R = 0.1 and 1 Hz frequency. However, in real life situations R and f can have different values. Interestingly, using the empirical model proposed by Epaarachchi et al [212], S-N fatigue characteristics for variable R and f values can be predicted by evaluating two material specific model parameters α and β. In addition, it is possible to avoid repeated testing for different load cases and frequencies saving both time and effort by adhering to this method. Thus, only a few straightforward fatigue tests are required at one R value for a number of load levels to calculate α and β [212].

In the proposed method, deterministic equations were used to derive mathematical relationships between residual strength (σ_R), number of

133

cycles (N) and time (t). Subsequently, considering all other influencing factors, a first order differential equation given in Equation 5.4, was developed to model σ_R in time domain. The terms A, σ_{max} and m_2 represent a constant, fatigue failure load and a material constant respectively. Integrating Equation 5.4 from starting time (= 0) to the time failure occurs, and substituting N for final time, Equation 5.5 yields. By further solving of equations, the unique material parameters α and β were interpreted using a linear function (given in Equation 5.6), where D_F is a function of UTS, σ_{max}, fibre angle, f and β. The complex equation and derivation steps for D_F, are not presented here for clarity. Importantly, in the developed linear function, material parameter α and (N^β-1) represent the gradient and independent x variable, respectively. Using iterative solving techniques, a linear trendline should be fitted to the experimental data points, in order to evaluate material specific unique parameters α and β.

$$\frac{d\sigma_R}{dt} = -A.F(R, \sigma_{max}, UTS).t^{-m_2} \qquad 5.4$$

$$UTS - \sigma_{max} = \alpha.F(R, \sigma_{max}, UTS).\frac{1}{f^\beta}.(N^\beta - 1) \qquad 5.5$$

$$D_F = \alpha.(N^\beta - 1) \qquad 5.6$$

Hence following the proposed technique, respective material specific parameters were evaluated and are illustrated in Figure 5.17 and Table 5.6. Subsequently using evaluated α and β values, fatigue S-N characteristic curves were generated for R values ranging from 0.1 to 0.6 (in Figure 5.18). Interestingly, the model has shown excellent correlation with experimental results for R = 0.1, evidently showcasing its effectiveness. Importantly, based on these results, SMPC fatigue behaviour under different real life applications can be easily studied and predicted. Hence, these results will be vital for future SMPC structural component design to make sure they are safe and can withstand fatigue loads with infinite life.
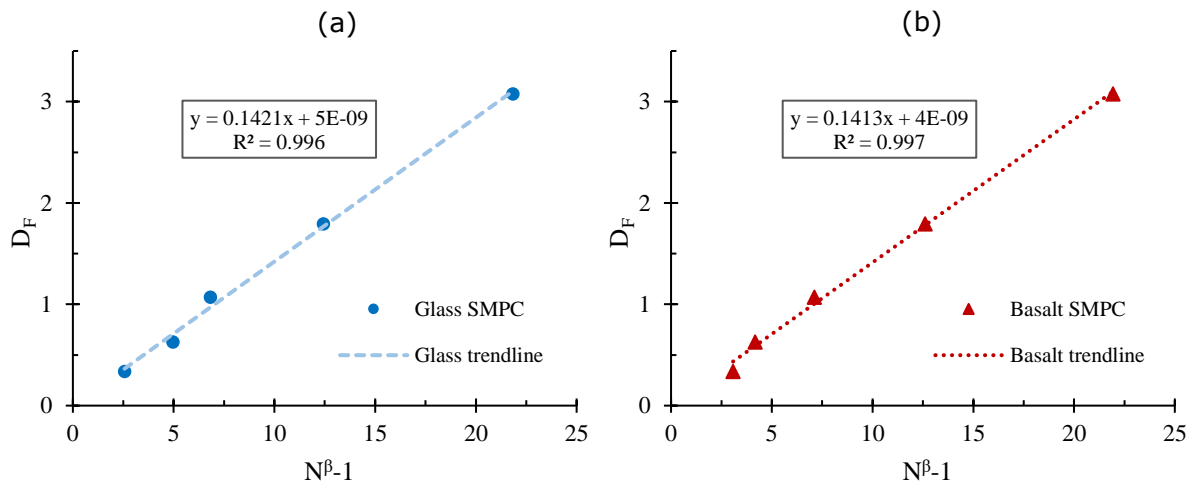
Figure 5.17: Evaluation of fatigue characteristic empirical model parameters for; (a) glass SMPC and (b) basalt SMPC

Table 5.6: Material specific fatigue parameters

Specimen	α	β
Glass SMPC	0.1421	0.2953
Basalt SMPC	0.1413	0.3319
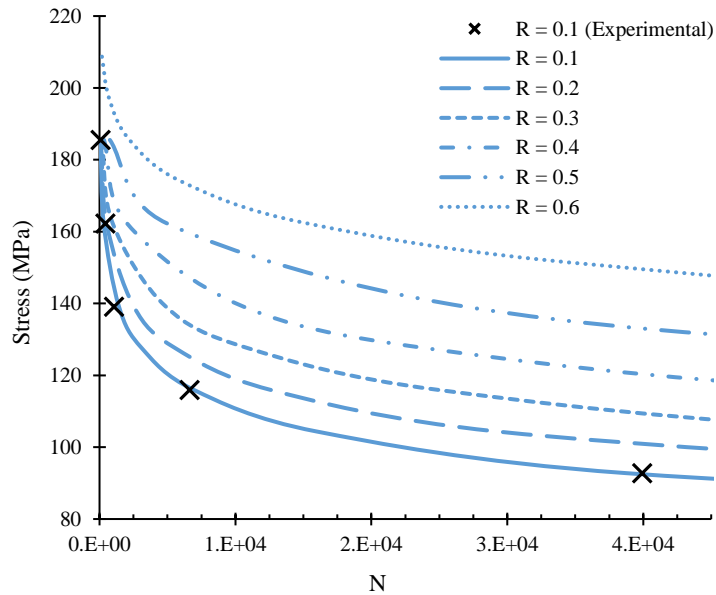
Figure 5.18: Predicted S-N fatigue curves of glass SMPC for different stress ratios

5.8 Moisture exposure

Materials used in constructions often experience a variety of environmental conditions throughout a year. Regardless of the location, moisture is a common constituent of air. However, the level of moisture content in the environment measured by relative humidity (RH %), change with geographical location. To investigate the suitability and performance of the proposed material as a building material in moist conditions, SMPC specimens were conditioned in an environmental chamber at 98 RH % and 60 ^{o}C for 1000 hrs. These extreme environmental conditions were selected as moisture environmental effect exposure cannot be accelerated.

Figure 5.19 shows the average change in sample weights before and after moisture exposure. Weights of specimens slightly increased due to absorption and penetration of water. Interestingly, neat SMP showed the maximum weight increase of 1.95 % while glass and basalt fibre reinforced SMPCs resulted in relatively low values, 1.19 % and 1.31 % respectively. Hence, it can be concluded that pristine SMPs are more vulnerable to moisture effects compared to their fibre composites. With moisture exposure, hydrogen bonding between N-H and C=O groups in chemical structure of the SMP matrix will get weakened with time [106]. Consequently, colour and mechanical properties of the polymer will change. Figure 5.20 presents the colour change of the neat SMP before and after moisture exposure for 1000 hrs.
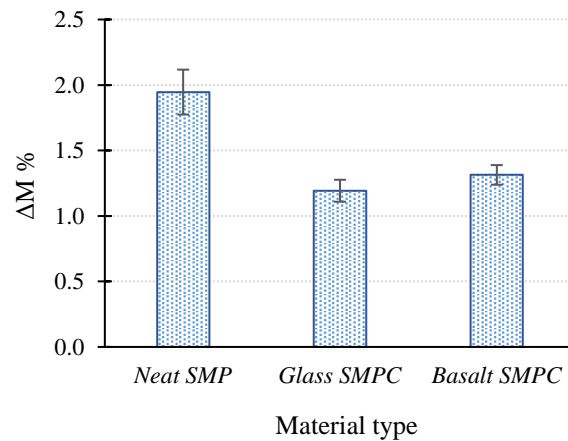
Figure 5.19: Average change in sample weights
after moisture exposure for 1000 hrs

Subsequently with the weakening of the matrix, SMP and SMPC samples resulted in material's mechanical property drops. Undesirable moisture effects on SMPC performance were investigated in terms of tensile, compressive and flexural properties. A summary of the test results are presented in Table 5.7. Importantly, neat SMPs have shown almost identical property change percentages in all three tests. However, glass SMPCs have shown the highest property variation in both tensile and flexural tests, but exhibited better performance under compression (shown in Figure 5.21). Conversely, basalt fibre reinforced SMPCs have performed relatively well under tension and flexure. Thus, it is evident that the reinforcement will also plays a role in terms of SMPC performance in moist environments.

Figure 5.20: Colour of the neat SMP; (a) before
and (b) after moisture exposure

Table 5.7: Summary of material properties before and after moisture exposure

Property	Material	Initial		After exposure		Property change	
		S (MPa)	E (GPa)	S (MPa)	E (GPa)	ΔS %	ΔE %
Tensile	Neat	55.4	2.9	47.2	2.5	14.8	14.3
	GL-SMPC-1	122.9	9.2	57.0	7.8	53.6	15.4
	GL-SMPC-2	231.9	14.1	79.7	11.1	65.6	21.4
	B-SMPC-1	121.3	9.0	121.2	8.0	0.1	11.4
	B-SMPC-2	267.3	12.2	183.0	12.2	31.5	0.3
Compressive	Neat	74.7	0.8	61.1	0.7	18.3	10.1
	GL-SMPC-1	149.6	1.4	146.7	1.2	1.9	17.2
	GL-SMPC-2	184.0	1.8	143.4	1.1	22.1	36.4
	B-SMPC-1	106.2	1.4	69.4	1.4	34.6	3.5
	B-SMPC-2	181.5	1.6	104.7	1.1	42.3	27.5
Flexural	Neat	103.4	3.0	84.9	2.6	17.8	13.2
	GL-SMPC-1	232.0	7.5	75.0	6.9	67.7	8.2
	GL-SMPC-2	307.8	10.8	142.3	10.4	53.8	3.8
	B-SMPC-1	252.1	7.3	187.7	6.8	25.5	6.6
	B-SMPC-2	354.7	9.3	274.1	9.1	22.7	1.6
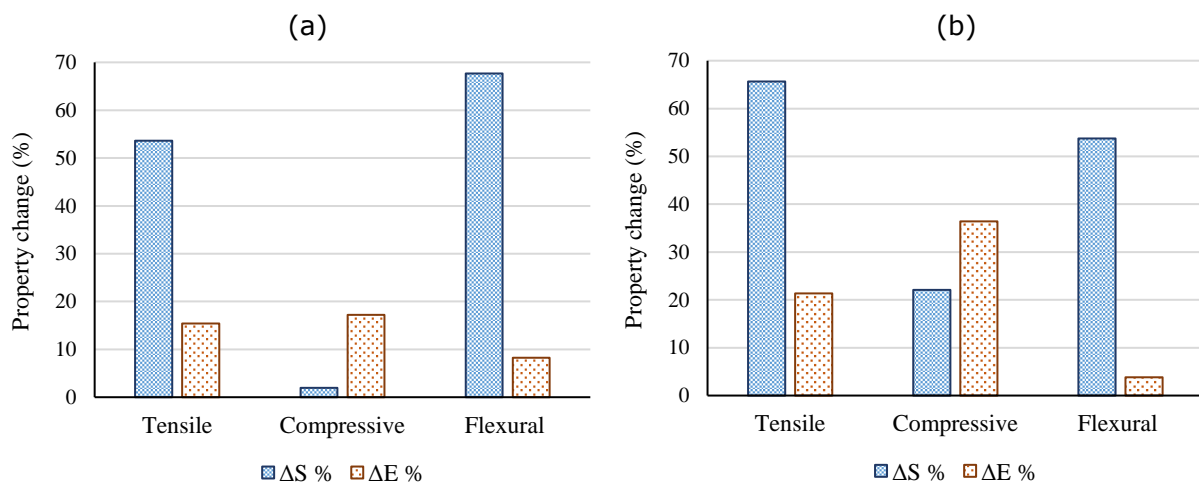
Figure 5.21: Percentage property drop of glass fibre SMPC material due to moisture exposure in (a) transverse, O1 and (b) longitudinal, O2 directions

5.9 Temperature effect test

Changing temperature is a common environmental phenomenon we experience daily. The temperature of the environment can vary due to the

intensity of sunlight, season, weather condition, etc [213]. Consequently, the materials used in civil engineering applications experience continuous temperature changes, throughout their life span. For best performance, safety and durability of constructions, materials should be capable of withstanding adverse effects of temperature fluctuations occurring daily. Typical polymeric materials, are highly responsive to the temperature [214, 215]. Similarly, the developed SMPC which is also derived from a polymer based material, shows high levels of temperature dependency. As can be seen in the storage modulus characterisation properties in Figure 3.16, the storage modulus value of the SMPC declines with increasing temperature. This is a clear indication of the SMPC's material property responsiveness to temperature. Hence, the tensile properties of the developed SMPCs at elevated temperatures, 45 C^o and 60 C^o, were investigated.

A summary of the evaluated tensile strength values of the SMPCs are given in Table 5.8. However, the MTS compatible tensile fixtures used with the thermal chamber had a load capacity of 10 kN. Therefore, the tensile testes were terminated when the load reading reached 10 kN to avoid fixture damage. As a result, some of the samples were not loaded up to their peak strength and are denoted by "x".

Table 5.8: A summary of the tensile strengths of the SMPCs with temperature

	Tensile Strength (MPa)			
	O1		O2	
T (C^o)	Glass	Basalt	Glass	Basalt
25	122.9	121.3	231.9	267.3
45	121.6	x	x	x
60	108.0	120.7	x	x

The elastic moduli of both glass and basalt SMPC types showed a gradual drop with temperature increase (in Figure 5.22). This behaviour was consistent among both directions (O1 and O2) of the SMPCs. The tensile stress-strain curves of the SMPCs, at room temperature (25 C^o) and 60 C^o, are presented in Figure 5.24. Interestingly, both glass and basalt SMPCs displayed a similar behaviour with increased strain at break. This has resulted the gradual drop in elastic moduli and can be attributed to the softening of the SMP matrix due to elevated temperature [176, 178]. Moreover, at 60 C^o the tensile strength of the glass SMPC decreased by 12 %. In contrast, the basalt reinforced SMPCs experienced a minor strength decline of only 0.5 % relative to that of at room temperature. A comparison
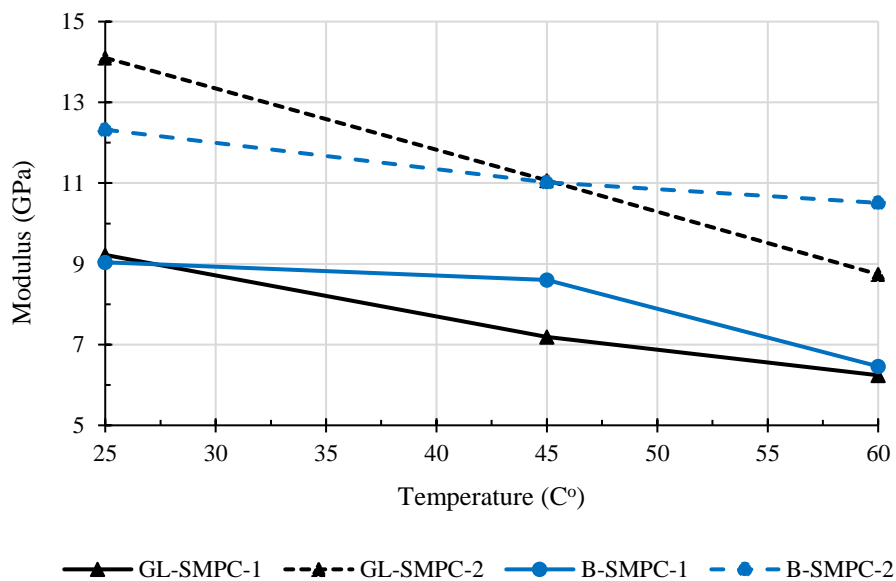
Figure 5.22: Variation of the directional tensile modulus
of the SMPCs with temperature

of the effects of temperature on the SMPC's tensile properties is given in Figure 5.23. Composites used in civil infrastructure, for instance typically have a T$_g$ in the order of 60 ^{o}C to 82 °C and service temperatures that should not exceed T$_g$ − 15 °C [204, 216]. Hence, the SMPCs showcase a very good suitability as a construction material and fit well within the recommended temperature limits.
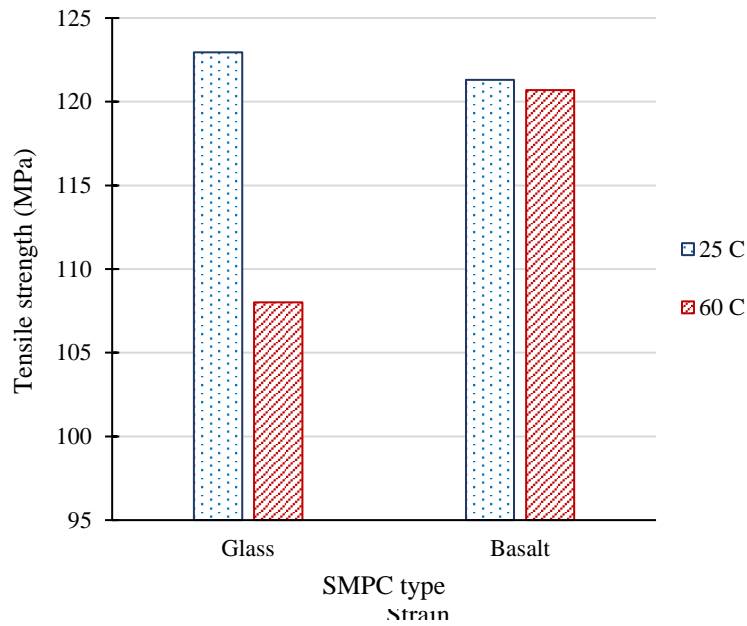
Figure 5.23: A comparison of the effect of temperature
on tensile strength of the SMPCs

5.10 Summary

In this chapter, the durability properties of the SMPC material as a construction material were investigated to evaluate its applicability in the long term. As construction materials often get exposed to a variety of unpredicted circumstances and harsh environmental conditions, investigation of the material behaviour in such situations is vital.

Light absorption studies showed that, due to high opacity of basalt and carbon fibre, they can also act as photothermal fillers in NIR triggered SMPC applications. According to the fire test results, no significant effect from the type of fibre reinforcement to resist and delay ignition was identified. Basalt SMPC has shown the lowest burning time. Hence, it can show better flame retardancy and impose low risk of fire spread. This claim should be validated by means of a Finger Burn Flammability Test to understand how the flame spreads on the SMPC in upcoming research. On the other hand, lowest mass loss during fire was given by the composite with glass fibre. In terms of fire safety, glass reinforced SMPC took the longest (~74 s) to drop visibility less than 10 m, which could provide more

time for occupants to evacuate the danger zone. Moreover, all SMPCs have initiated thermal decomposition at 345 ^{o}C. FTIR results have shown traces of CO_2 and water vapour, and it can be suspected that the evolution of flammable alkanes may result in a fire if exposed to a flame.

According to the tension-tension fatigue characterization, the endurance limits of the glass and basalt SMPCs were 60.5 MPa and 55.7 MPa, respectively. Moreover, the fatigue material specific parameters (α and β) were evaluated, and S-N predictions for non-tested r values are presented. Importantly, a long term exposure of moisture showed adverse effects on the SMPC's material properties and the SMP matrix has undergone a colour change due to moisture absorption. Both SMPCs demonstrated consistent tensile strengths up to an elevated temperature of 60 C^o. On the hand, the elastic moduli experienced a gradual drop as a result of increased ductile properties with polymer matrix softening.

The next chapter presents the conclusions of the current research and suggestions for future work.

CHAPTER 6: CONCLUSIONS AND FUTURE RESEARCH

This thesis intended to investigate the use of SME in CHS and SHS structural sections manufactured from SMPCs that can be used in the civil construction field. The four research objectives defined in Section 1.3 were successfully addressed with a well-planned research methodology. Chapters 3 to 5 comprehensively investigated, discussed and elaborated on the methodology, observations, results and achievements gained through this study. This chapter points out the innovative findings and contributions made by the author of this thesis towards the progress of engineering, material science and technology.

The breakthrough research findings of this study contributed to three Q1 research journal articles and two conference proceedings which are listed in Section 1.5.

6.1 Conclusions

To date, the majority of SMP research has been focused on biomedical applications. The key application interests for the reinforced SMPCs were related to outer space explorations. As a consequence, researchers have not given any attention to developing SMPCs for structural and large scale civil engineering applications.

In this study, a structurally sound, functional and smart SMPC was developed, laying out the design framework and background in order to efficiently implement the unique properties of SMPCs in construction technologies. An epoxy based resin was initially selected for this study due to its availability, low cost and suitability for structural applications compared to other base resin types. To generate the SME out of the epoxy resin, two amine based hardeners, Triethylenetetramine (TETA) and Jeffamine D230, were selected for the study.

Each hardener consists consisted of active amine ($-NH_2$) groups that contribute to the formation of crosslinks/net points/fixed phase and soft segments/reversible phase with the resin when mixed. The T_g, R_f, R_r and long term shape retention properties were tested for neat SMP specimens with different mix ratios. The selections were made to ensure the material performs best for and is well suited to civil applications. Thus, the SMP matrix mass ratio was determined as DGEBA: TETA: D230 = 13.0: 1.0: 1.6. The synthesisation process can be articulated to create different SMPs to suit the requirements of other applications which is an excellent achievement of this project.

Glass, carbon and natural fibre basalt were used in the study as reinforcements. The fibre inclusion significantly enhanced the mechanical properties of the inherently poor mechanical properties of SMP. The structural testing findings proved that the SMPCs are equally compatible with the performances of general fibre reinforced structural composites. Due to their high thickness and fibre content, the SMPCs exhibited a tendency to damage during the shape training process. Such material flaws negatively affected the mechanical properties of the SMPCs, hindering their performance as construction materials. Hence, a L9 Taguchi array was created to identify the optimum SMPC parameters.

The damage quantifier, ADP%, was used to evaluate the damage levels of SMPCs during programming. Glass fibre, 3 mm thickness and 6 layers of fibres, were found to be the best combination to minimize ADP%. The study showed that T_S ($\sim$ 60 ^{o}C) was the ideal temperature to perform the shape training cycle and a higher deformation rate of 1 mm/s resulted in lower damage levels. By analysing the modes of damage, three types of programming damage were identified during the study. They were: Type 1 - internal fibre micro buckling and debonding, Type 2 - delamination and Type 3 – through thickness cracking. However, damage Types 1 and 2 were commonly identified and the central region of the compression side was the most critical for damage. To fully terminate the occurrence of visible

damage, interfacial debonding and tensile strength decline, the reinforcement architecture (5 plain weave + 1 unidirectional) and deformation radius were altered.

To create a SMPC design framework, the experimental damage observations and explanations were validated with a FEA based numerical method via ABAQUS software. The viscoelastic behaviour of the SMPC was used to simulate the SME and programming stage of the material. Further, the methodology to identify the σ_o and CSM of the SMPC was established by incorporating the SMPC's material properties at the programming temperature T_S. During programming, a compressive stress of 70 MPa was found to be the σ_o or interfacial bond strength of the optimized SMPC. The CSM for damage was identified as 70 MPa to 100 MPa.

Importantly, the proposed FEA approach allowed the prompt prediction of any damage, detection of critical locations prone to high stresses, determination of fibre orientation, evaluation of required external forces and optimization of shape training process parameters which can save both cost and time in SMPC designing. Furthermore, being able to provide firsthand knowledge of the concept of programming damage, damage minimizing techniques and FEA design procedures, is a great accomplishment of the study as these can be applied effectively by other SMPC researchers to optimize the material parameters required for other types of SMPCs and applications.

To demonstrate the applicability of SME in structural components used for civil constructions, CHS and SHS sections were selected. The SMPC CHS and SHS structural members were fabricated with a customized mould and tested to evaluate their shape memory performance. The reinforcement architecture defined from the Taguchi damage analysis was implemented in the fabrication of SMPC sections. 60 mm long SMPC sections were initially programmed radially until damaged, and the results were compared with the established FEA technique. The developed numerical technique

demonstrated good consistency with the experimental results and observations, with respect to the deformed shapes, damage initiation, shape fixity and recovery. The FEA results showed error percentages of less than 5.6 % and 3.5 % for R_f and R_r, respectively; further validating the FEA model.

Due to the practical circumstances associated with manufacturing long beams, the model was adopted to investigate the shape memory performance of SMPC long beams and structures. Further, the study recommended that SMPC CHS and SHS long members can be wrapped to a compact temporary shape with bend radii of 420 mm and 650 mm, respectively. The application of SMPC members in deployable structures was also successfully demonstrated considering the SME of the four columns of a 5x5x5 m^3 sized simplified frame structure. The SMPC columns were deformed until the critical compressive stress reached approximately 70 MPa.

Remarkably, huge volume savings of 70 % and 52 % were achieved by the CHS and SHS SMPC integrated deployable structures, showcasing the effectiveness of SMPCs as construction materials for easy transportation and handling of prefabricated modular constructions, curved beams, space deployable habitats, etc. The axial compressive strengths of the CHS and SHS components were calculated as 124.7 MPa and 69.6 MPa, and were within the range of other common construction materials. This confirmed the structural comparability of the SMPC members with respect to other construction material types, further demonstrating their competency. Excitingly, both studied SMPC profile types displayed higher "specific sectional capacities" for bending and axial compression compared to heavy steel sections.

In order to showcase the suitability of SMPCs as alternative construction materials, further investigations were carried out to broaden the understanding of the SMPC's durability based characteristics. Importantly, past research work related to SMPC's fire and fatigue

properties were very limited, and the SMPC research field has showcased poor interest in such vital aspects. Smoke density based fire properties of the SMPCs reinforced with glass, basalt and carbon fibre were characterised in order to evaluate the fire safety conditions in civil constructions, however no significant effect from the type of fibre reinforcement to resist and delay ignition was identified. Considering fire safety, glass reinforced SMPCs took the longest (74 s) to drop visibility less than 10 m. The thermal decomposition was initiated at 345 ^{o}C.

The FTIR study of evolving gases showed evidence for the existence of flammable alkanes which caused the fire to initiate when exposed to the flame. The tension-tension fatigue endurance limit of glass and basalt SMPCs for 2 million fatigue life were evaluated as 60.5 MPa and 55.7 MPa. Importantly, the identification of the material specific fatigue parameters α and β were also presented for further fatigue predictions. Long term exposure to moisture imposes adverse effects on the material properties due to the weakening of the SMP's chemical structure. As a consequence, the mechanical properties of the tested SMPCs declined. Elevated temperature led to a weakening of the SMPC due to temperature responsive matrix softening. At 60 ^{o}C, glass and basalt fibre SMPCs experienced a slight reduction in transverse tensile strength by 12 % and 0.5 %, respectively. However, the materials did not show any drop in strength at the maximum service temperature T_g – 15 ^{o}C (= 45 ^{o}C) for the SMPC. Hence, it can be stated that the SMPC is applicable for applications with service temperatures not exceeding 45 ^{o}C. Additionally, the durability based study of this research directs other researchers to broaden their scope of analysis and develop future SMPCs to be safe and durable enough in other applications as well.

6.2 Summary

With the successful completion of the current study, innovative scientific knowledge and in-depth understanding of SMPCs have been contributed to the field of smart polymer composites, construction materials and engineering. Overall, the research study addressed major challenges related to the design and development of SMPC structural members applicable to civil constructions for the first time. Specifically, both experimental and numerical strategies were implemented in order to investigate and demonstrate the potential of using SME in civil infrastructure.

The presented well-rounded study addressed base resin selection, SMP matrix synthesisation, SMPC parameter optimization, programming damage concepts, identification of damage onset, FEA study of the SME, fabrication of SMPC structural profiles, SME of SMPC profiles, potential applications and advantages of SMPCs in deployable structures, structural performance, and comprehensive characterisation of the long term durability of SMPC construction materials.

Therefore, it can be concluded that the study has successfully emphasised the potential of SMPCs to be utilized as future construction materials. From this study, the initiative has been taken to exploit the application of SMPCs and their SME for civil constructions with significant knowledge and innovative research findings. Further, the research study is highly successful as the innovative research findings of this study open up windows of opportunity for future researchers and engineers to provide innovative solutions for other types of SMPCs and applications.

6.3 Future work and recommendations

Future work and recommendations are as follows:

I. The shape memory performance and programming damage resistance need to be investigated with hybrid fibre reinforcements. Adhering to multiple of reinforcement types in the same SMPC might result in interesting outcomes. Thus, further optimizing the fibre type, specific location and their architecture can improve current application margins of the developed SMPC

II. There is clearly a practical difficulty in fabricating long SMPC structural members with a customized mould. As pultrusion is the best method of polymer composite structural member fabrication, the curing kinetics of the SMP should be modified so that the SMPC fully cures within the heated die. Implementation of the SMPC production via pultrusion is the best way forward. This will lift the production rate and efficiency of SMPC component manufacturing significantly, and aid in meeting customer demands easily

III. Pull winding of fibre threads facilitate directional strengthening of pultruded GFRP against shear. It is also important to evaluate the effects of pull winding reinforcements on SME of pultruded SMPCs.

IV. In addition, the study of shear induced corner failures of the hollow SMPC profiles should also be performed as confining effects are another important performance criterion for hollow profiles.

V. Further development of SMPC programming damage prediction for different SMPCs and laminates, and different programming shapes should be carried out, as effective prediction of this damage is key to facilitating industrial applications.

VI.   With further investigation, SMPCs can also be integrated into other structural profiles such as rectangular hollow sections (RHS), I beams, parallel flange channels (PFC), unequal flange channels (UFC), etc. The availability of a wide range of deformable and smart profiles will be advantageous in future civil engineering advancements and space explorations

VII.   To enhance the durability of SMPCs, a shape memory coating can be introduced as an external protective layer against moisture, UV rays and any other harmful conditions. Additionally, fire retardants can be mixed into the coating to ensure that the fire safety of the SMPC components and structures is maximized. However, the influence of the external protective coating on the fundamental performance of the SMPC must be negligible

VIII.   As a measure to minimize wastage and environmental pollution, the recyclability of the SMPCs should be studied. As recyclability is a highly discussed topic in the Materials world, being able to recycle will be an added advantage for SMPCs.

IX.   To minimize material costs and economically aid the cost-conscious construction industry, it is important to investigate the applicability of other low cost polymers which exhibit SME.

X.   It is important to evaluate profile's compressive properties independent of edge effects. Therefore, effects of end reinforcements and restrains on the compressive performance of SMPC profiles, can be recommended as a future work.

REFERENCES

[1] D. Safranski, J.C. Griffis, Shape-memory polymer device design, William Andrew 2017.

[2] Y. Liu, H. Du, L. Liu, J. Leng, Shape memory polymers and their composites in aerospace applications: a review, Smart Materials and Structures 23(2) (2014).

[3] M. Behl, A. Lendlein, Shape-memory polymers, Materials today 10(4) (2007) 20-28.

[4] W. Small IV, P. Singhal, T.S. Wilson, D.J. Maitland, Biomedical applications of thermally activated shape memory polymers, Journal of materials chemistry 20(17) (2010) 3356-3366.

[5] Y. Liu, H. Lv, X. Lan, J. Leng, S. Du, Review of electro-active shape-memory polymer composite, Composites Science and Technology 69(13) (2009) 2064-2068.

[6] O. Teall, M. Pilegis, R. Davies, J. Sweeney, T. Jefferson, R. Lark, D. Gardner, A shape memory polymer concrete crack closure system activated by electrical current, Smart Materials and Structures 27(7) (2018) 075016.

[7] H.M.C.M. Herath, J.A. Epaarachchi, M.M. Islam, W. Al-Azzawi, J. Leng, F. Zhang, Structural performance and photothermal recovery of carbon fibre reinforced shape memory polymer, Composites Science and Technology 167 (2018) 206-214.

[8] W. Small IV, T.S. Wilson, W.J. Benett, J.M. Loge, D.J. Maitland, Laser-activated shape memory polymer intravascular thrombectomy device, Optics Express 13(20) (2005) 8204-8213.

[9] R.V. Beblo, L.M. Weiland, Light activated shape memory polymer characterization, Journal of Applied Mechanics 76(1) (2009).

[10] Q. Ze, X. Kuang, S. Wu, J. Wong, S.M. Montgomery, R. Zhang, J.M. Kovitz, F. Yang, H.J. Qi, R. Zhao, Magnetic shape memory polymers with integrated multifunctional shape manipulation, Advanced Materials 32(4) (2020) 1906657.

[11] K. Yu, Y. Liu, J. Leng, Shape memory polymer/CNT composites and their microwave induced shape memory behaviors, Rsc Advances 4(6) (2014) 2961-2968.

[12] X. Gu, P.T. Mather, Water-triggered shape memory of multiblock thermoplastic polyurethanes (TPUs), Rsc Advances 3(36) (2013) 15783-15791.

[13] Q. Meng, J. Hu, A review of shape memory polymer composites and blends, Composites Part A: Applied Science and Manufacturing 40(11) (2009) 1661-1672.

[14] C. Liu, H. Qin, P. Mather, Review of progress in shape-memory polymers, Journal of materials chemistry 17(16) (2007) 1543-1558.

[15] T. Mu, L. Liu, X. Lan, Y. Liu, J. Leng, Shape memory polymers for composites, Composites Science and Technology 160 (2018) 169-198.

[16] M.D. Hager, S. Bode, C. Weber, U.S. Schubert, Shape memory polymers: Past, present and future developments, Progress in Polymer Science 49 (2015) 3-33.

[17] S. Madbouly, A. Lendlein, 'Shape Memory Polymer Composites', Advanced Polymer Science, Springer-Verlag Berlin Heidelberg2009, pp. 1-55.

[18] W. Al Azzawi, M. Herath, J. Epaarachchi, Modeling, analysis, and testing of viscoelastic properties of shape memory polymer composites and a brief review of their space engineering applications, Creep and Fatigue in Polymer Matrix Composites (2019) 465-495.

[19] A. International, Standard test method for flexural properties of polymer matrix composite materials, ASTM International, 2015.

[20] X. Lan, Y. Liu, H. Lv, X. Wang, J. Leng, S. Du, Fiber reinforced shape-memory polymer composite and its application in a deployable hinge, Smart Materials and Structures 18(2) (2009) 024002.

[21] W. Al Azzawi, M. Herath, J. Epaarachchi, Modeling, analysis, and testing of viscoelastic properties of shape memory polymer composites and a brief review of their space engineering applications, Creep and Fatigue in Polymer Matrix Composites2019, pp. 465-495.

[22] T. Ohki, Q.-Q. Ni, N. Ohsako, M. Iwamoto, Mechanical and shape memory behavior of composites with shape memory polymer, Composites Part A: Applied Science and Manufacturing 35(9) (2004) 1065-1073.

[23] S.C. Arzberger, N.A. Munshi, M.S. Lake, R. Barrett, M.L. Tupper, P.N. Keller, W. Francis, D. Campbell, K. Gall, Elastic memory composites for deployable space structures, Lafayette, Colorado: Composite Technology Development Inc (2004).

[24] M. Cabanlit, D. Maitland, T. Wilson, S. Simon, T. Wun, M.E. Gershwin, J. Van de Water, Polyurethane shape-memory polymers demonstrate functional biocompatibility in vitro, Macromol Biosci 7(1) (2007) 48-55.

[25] W. Yin, T. Fu, J. Liu, J. Leng, Structural shape sensing for variable camber wing using FBG sensors, Sensors and Smart Structures Technologies for Civil, Mechanical, and Aerospace Systems 2009, 2009.

[26] J. Leng, X. Lan, Y. Liu, S. Du, Shape-memory polymers and their composites: Stimulus methods and applications, Progress in Materials Science 56(7) (2011) 1077-1135.

[27] H. Du, Z. Song, J. Wang, Z. Liang, Y. Shen, F. You, Microwave-induced shape-memory effect of silicon carbide/poly (vinyl alcohol) composite, Sensors and Actuators A: Physical 228 (2015) 1-8.

[28] K.D.C. Emmanuel, H.M.C.M. Herath, L.H.J. Jeewantha, J.A. Epaarachchi, T. Aravinthan, Thermomechanical and fire performance of DGEBA based shape memory polymer composites for constructions, Construction and Building Materials 303 (2021).

[29] K.D.C. Emmanuel, L.H.J. Jeewantha, H.M.C.M. Herath, J.A. Epaarachchi, T. Aravinthan, Damage onset analysis of optimized shape memory polymer composites during programming into curved shapes, Materialia 26 (2022).

[30] W. Ferdous, Y. Bai, T.D. Ngo, A. Manalo, P. Mendis, New advancements, challenges and opportunities of multi-storey modular buildings – A state-of-the-art review, Engineering Structures 183 (2019) 883-893.

[31] F.E. Boafo, J.-H. Kim, J.-T. Kim, Performance of modular prefabricated architecture: case study-based review and future pathways, Sustainability 8(6) (2016) 558.

[32] H.-T. Thai, T. Ngo, B. Uy, A review on modular construction for high-rise buildings, Structures 28 (2020) 1265-1290.

[33] H.M.C.M. Herath, J.A. Epaarachchi, M.M. Islam, J. Leng, Carbon Fibre Reinforced Shape Memory Polymer Composites for Deployable Space Habitats, Engineer: Journal of the Institution of Engineers, Sri Lanka 52(1) (2019).

[34] C. Chastre, P. Faria, J. Neves, M. Ludovico-Marques, H. Biscaia, L. Nunes, Testing Durability on Construction Materials, Advances on Testing and Experimentation in Civil Engineering: Materials, Structures and Buildings, Springer2023, pp. 29-51.

[35] M. Di Tommaso, I. Bordonzotti, NOx adsorption, fire resistance and CO2 sequestration of high performance, high durability concrete containing activated carbon, Book of abstracts, 2016.

[36] G.R. Halford, Fatigue and durability of structural materials, Asm International2006.

[37] S.N. Shoukry, G.W. William, B. Downie, M.Y. Riad, Effect of moisture and temperature on the mechanical properties of concrete, Construction and Building Materials 25(2) (2011) 688-696.

[38] M. Wakchaure, S. Kute, Effect of moisture content on physical and mechanical properties of bamboo, (2012).

[39] V. Kodur, P. Kumar, M.M. Rafi, Fire hazard in buildings: review, assessment and strategies for improving fire safety, PSU research review 4(1) (2020) 1-23.

[40] A.H. Buchanan, A.K. Abu, Structural design for fire safety, John Wiley & Sons2017.

[41] X. Huang, M. Panahi-Sarmad, K. Dong, R. Li, T. Chen, X. Xiao, Tracing evolutions in electro-activated shape memory polymer composites with 4D printing strategies: a systematic review, Composites Part A: Applied Science and Manufacturing 147 (2021) 106444.

[42] A. Lendlein, O.E. Gould, Reprogrammable recovery and actuation behaviour of shape-memory polymers, Nature Reviews Materials 4(2) (2019) 116-133.

[43] J. Hu, Y. Zhu, H. Huang, J. Lu, Recent advances in shape–memory polymers: Structure, mechanism, functionality, modeling and applications, Progress in polymer science 37(12) (2012) 1720-1763.

[44] H. Tobushi, S. Hayashi, S. Kojima, Mechanical properties of shape memory polymer of polyurethane series: basic characteristics of stress-strain-temperature relationship, JSME international journal. Ser. 1, Solid mechanics, strength of materials 35(3) (1992) 296-302.

[45] H. Tobushi, K. Okumura, S. Hayashi, N. Ito, Thermomechanical constitutive model of shape memory polymer, Mechanics of materials 33(10) (2001) 545-554.

[46] C. Liu, S.B. Chun, P.T. Mather, L. Zheng, E.H. Haley, E.B. Coughlin, Chemically cross-linked polycyclooctene: synthesis, characterization, and shape memory behavior, Macromolecules 35(27) (2002) 9868-9874.

[47] H. Kalita, Shape Memory Polymers : Theory and Application, De Gruyter, Inc., Berlin/Boston, GERMANY, 2018.

[48] G. Li, Self-Healing Composites : Shape Memory Polymer Based Structures, John Wiley & Sons, Incorporated, New York, UNITED KINGDOM, 2014.

[49] M. Baghani, H. Mohammadi, R. Naghdabadi, An analytical solution for shape-memory-polymer Euler–Bernoulli beams under bending, International Journal of Mechanical Sciences 84 (2014) 84-90.

[50] A. Lendlein, S. Kelch, Shape-Memory Polymers, Angewandte Chemie International Edition 41(12) (2002) 2034-2057.

[51] X. Xin, L. Liu, Y. Liu, J. Leng, Mechanical Models, Structures, and Applications of Shape-Memory Polymers and Their Composites, Acta Mechanica Solida Sinica 32(5) (2019) 535-565.

[52] X. Lan, L. Liu, Y. Liu, J. Leng, Thermomechanical and electroactive behavior of a thermosetting styrene-based carbon black shape-memory composite, Journal of Applied Polymer Science 135(13) (2018) 45978.

[53] T. Fang, D.A. Shimp, Polycyanate esters: science and applications, Progress in Polymer Science 20(1) (1995) 61-118.

[54] F. Xie, L. Liu, X. Gong, L. Huang, J. Leng, Y. Liu, Effects of accelerated aging on thermal, mechanical and shape memory properties of cyanate-based shape memory polymer: I vacuum ultraviolet radiation, Polymer Degradation and Stability 138 (2017) 91-97.

[55] F. Xie, X. Gong, L. Huang, L. Liu, J. Leng, Y. Liu, Effects of accelerated aging on thermal, mechanical, and shape memory properties of a cyanate-based shape memory polymer: II atomic oxygen, Polymer Degradation and Stability 186 (2021) 109515.

[56] Z. Ping, F. Xie, X. Gong, L. Liu, J. Leng, Y. Liu, Effects of Accelerated Aging on Thermal, Mechanical and Shape Memory Properties of Cyanate-Based Shape Memory Polymer: III Vacuum Thermal Cycling, Polymers 15(8) (2023) 1893.

[57] H. Jayalath, M. Herath, J. Epaarachchi, Cyanate esters as a high performing shape memory polymer: A review, Materials Today: Proceedings (2022).

[58] G.P. Tandon, K. Goecke, K. Cable, J. Baur, Durability Assessment of Styrene- and Epoxy-based Shape-memory Polymer Resins, Journal of Intelligent Material Systems and Structures 20(17) (2009) 2127-2143.

[59] H. Du, Y. Yao, X. Zhou, Y. Zhao, Two-way shape memory behavior of styrene-based bilayer shape memory polymer plate, Polymers for Advanced Technologies 34(1) (2023) 252-260.

[60] A. Ben Abdallah, F. Gamaoun, A. Kallel, A. Tcharkhtchi, Molecular weight influence on shape memory effect of shape memory polymer blend (poly (caprolactone)/styrene-butadiene-styrene), Journal of Applied Polymer Science 138(5) (2021) 49761.

[61] N. Liu, L. Jiang, Effect of microstructural features on the thermal conducting behavior of carbon nanofiber–reinforced styrene-based shape memory polymer composites, Journal of Intelligent Material Systems and Structures 31(14) (2020) 1716-1730.

[62] S. Hayashi, N. Ishikawa, C. Giordano, High moisture permeability polyurethane for textile applications, Journal of Coated Fabrics 23(1) (1993) 74-83.

[63] W. Sokolowski, A. Metcalfe, S. Hayashi, J. Raymond, Medical applications of shape memory polymers, Biomedical Materials 2(1) (2007) S23.

[64] M. Staszczak, M. Nabavian Kalat, K.M. Golasiński, L. Urbański, K. Takeda, R. Matsui, E.A. Pieczyska, Characterization of Polyurethane Shape Memory Polymer and Determination of Shape Fixity and Shape Recovery in Subsequent Thermomechanical Cycles, Polymers 14(21) (2022) 4775.

[65] K. Patel, R. Purohit, S. Hashmi, Microwave-Triggered Thermo-Responsive Shape Memory Polymer (Polyurethane)/GNPS/MWCNTS Composites, Strength of Materials 53(6) (2021) 998-1010.

[66] B. Vollmert, Polymer Chemistry Springer-Verlag Berlin, Heidelberg, New York (1973).

[67] H. Koerner, G. Price, N.A. Pearce, M. Alexander, R.A. Vaia, Remotely actuated polymer nanocomposites—stress-recovery of carbon-nanotube-filled thermoplastic elastomers, Nature materials 3(2) (2004) 115-120.

[68] D.M. Feldkamp, I.A. Rousseau, Effect of the Deformation Temperature on the Shape-Memory Behavior of Epoxy Networks, Macromolecular Materials and Engineering 295(8) (2010) 726-734.

[69] G.Y. Romero-Zúñiga, D. Navarro-Rodríguez, M.E. Treviño-Martínez, Enhanced mechanical performance of a DGEBA epoxy resin-based shape memory polymer by introducing graphene oxide via covalent linking, Journal of Applied Polymer Science 139(2) (2022) 51467.

[70] M. Unnam, R. Velmurugan, S. Kumar, Mechanical, Thermal and Shape Memory Characterization of a Novel Epoxy Shape Memory Polymer, Materials Science Forum, Trans Tech Publ, 2022, pp. 87-96.

[71] Q. Tan, F. Li, L. Liu, Y. Liu, J. Leng, Effects of vacuum thermal cycling, ultraviolet radiation and atomic oxygen on the mechanical properties of carbon fiber/epoxy shape memory polymer composite, Polymer Testing 118 (2023) 107915.

[72] C. Wischke, A.T. Neffe, S. Steuer, A. Lendlein, Evaluation of a degradable shape-memory polymer network as matrix for controlled drug release, Journal of Controlled Release 138(3) (2009) 243-250.

[73] C.M. Yakacki, K. Gall, Shape-memory polymers for biomedical applications, Shape-memory polymers (2009) 147-175.

[74] J. Chen, J. Hu, A.K. Leung, C. Chen, J. Zhang, Y. Zhang, Y. Zhu, J. Han, Shape memory ankle–foot orthoses, ACS applied materials & interfaces 10(39) (2018) 32935-32941.

[75] A. Lendlein, R. Langer, Biodegradable, elastic shape-memory polymers for potential biomedical applications, Science 296(5573) (2002) 1673-1676.

[76] C. Lin, J. Lv, Y. Li, F. Zhang, J. Li, Y. Liu, L. Liu, J. Leng, 4D-printed biodegradable and remotely controllable shape memory occlusion devices, Advanced Functional Materials 29(51) (2019) 1906569.

[77] H. Meng, G. Li, A review of stimuli-responsive shape memory polymer composites, polymer 54(9) (2013) 2199-2221.

[78] W. Xu, G. Li, Constitutive modeling of shape memory polymer based self-healing syntactic foam, International Journal of Solids and Structures 47(9) (2010) 1306-1316.

[79] G. Li, M. John, A self-healing smart syntactic foam under multiple impacts, Composites Science and Technology 68(15-16) (2008) 3337-3343.

[80] E. Hornbogen, Comparison of shape memory metals and polymers, Advanced engineering materials 8(1-2) (2006) 101-106.

[81] F. Zhang, Y. Xia, Y. Liu, J. Leng, Nano/microstructures of shape memory polymers: From materials to applications, Nanoscale horizons 5(8) (2020) 1155-1173.

[82] A.M. Schmidt, Electromagnetic activation of shape memory polymer networks containing magnetic nanoparticles, Macromolecular rapid communications 27(14) (2006) 1168-1172.

[83] N.H. Khiyon, A.A. Rahman, M.F. Arshad, M.K. Kamarudin, S.T.A. Rahman, Dynamic mechanical properties of Polyurethane Shape Memory Polymer Composites (SMPC) with different volume fractions of chopped strand mat glass fiber, International Journal of Integrated Engineering 10(9) (2018).

[84] F. Li, J. Leng, Y. Liu, C. Remillat, F. Scarpa, Temperature dependence of elastic constants in unidirectional carbon fiber reinforced shape memory polymer composites, Mechanics of Materials 148 (2020) 103518.

[85] J. Gu, Z. Xie, S. Wang, H. Sun, X. Zhang, Thermo-mechanical modeling of woven fabric reinforced shape memory polymer composites, Mechanics of advanced materials and structures 26(12) (2019) 1042-1052.

[86] C.A.G. Rosales, M.F.G. Duarte, H. Kim, L. Chavez, D. Hodges, P. Mandal, Y. Lin, T.-L.B. Tseng, 3D printing of shape memory polymer (SMP)/carbon black (CB) nanocomposites with electro-responsive toughness enhancement, Materials Research Express 5(6) (2018) 065704.

[87] C.M. Yakacki, N.S. Satarkar, K. Gall, R. Likos, J.Z. Hilt, Shape-memory polymer networks with Fe3O4 nanoparticles for remote activation, Journal of Applied Polymer Science 112(5) (2009) 3166-3176.

[88] J. Park, S.Y. Park, D. Lee, Y.S. Song, Shape memory polymer composites embedded with hybrid ceramic microparticles, Smart Materials and Structures 29(5) (2020) 055037.

[89] H. Zhang, H. Xia, Y. Zhao, Optically triggered and spatially controllable shape-memory polymer–gold nanoparticle composite materials, Journal of Materials Chemistry 22(3) (2012) 845-849.

[90] L. Chen, W. Li, Y. Liu, J. Leng, Nanocomposites of epoxy-based shape memory polymer and thermally reduced graphite oxide: Mechanical, thermal and shape memory characterizations, Composites part B: engineering 91 (2016) 75-82.

[91] H. Lu, J. Gou, J. Leng, S. Du, Magnetically aligned carbon nanotube in nanopaper enabled shape-memory nanocomposite for high speed electrical actuation, Applied Physics Letters 98(17) (2011) 174105.

[92] G. Tandon, K. Goecke, K. Cable, J. Baur, Environmental durability of fabric-reinforced shape-memory polymer composites, Journal of Intelligent Material Systems and Structures 21(14) (2010) 1365-1381.

[93] M. Yoonessi, Y. Shi, D.A. Scheiman, M. Lebron-Colon, D.M. Tigelaar, R. Weiss, M.A. Meador, Graphene polyimide nanocomposites; thermal, mechanical, and high-temperature shape memory effects, ACS nano 6(9) (2012) 7644-7655.

[94] M. Fejős, G. Romhány, J. Karger-Kocsis, Shape memory characteristics of woven glass fibre fabric reinforced epoxy composite in flexure, Journal of Reinforced Plastics and Composites 31(22) (2012) 1532-1537.

[95] W. Al Azzawi, M.M. Islam, J. Leng, F. Li, J.A. Epaarachchi, Quantitative and qualitative analyses of mechanical behavior and dimensional stability of styrene-based shape memory composites, Journal of Intelligent Material Systems and Structures 28(20) (2017) 3115-3126.

[96] L. Xu, J. Zhao, M. Shi, J. Liu, Z. Wang, Thermodynamic properties of TPI shape memory polymer composites reinforced by GO/SiO2 modified carbon fiber, Composites Science and Technology 226 (2022) 109551.

[97] A. Asar, M. Irfan, K. Khan, W. Zaki, R. Umer, Self-sensing shape memory polymer composites reinforced with functional textiles, Composites Science and Technology 221 (2022) 109219.

[98] C. Liang, C. Rogers, E. Malafeew, Investigation of shape memory polymers and their hybrid composites, Journal of Intelligent Material Systems and Structures 8(4) (1997) 380-386.

[99] Q. Ni, N. Ohsako, T. Ohki, M. Sakaguchi, W. Wang, M. Iwamoto, Development of smart composites based on shape memory polymer, international symposium on smart structures and microsystems, Hong Kong, 2000.

[100] K. Gall, M. Mikulas, N.A. Munshi, F. Beavers, M. Tupper, Carbon fiber reinforced shape memory polymer composites, Journal of intelligent material systems and structures 11(11) (2000) 877-886.

[101] Z. Wei, R. Sandstrorörm, S. Miyazaki, Shape-memory materials and hybrid composites for smart systems: Part I Shape-memory materials, Journal of materials science 33(15) (1998) 3743-3762.

[102] J. Leng, F. Xie, X. Wu, Y. Liu, Effect of the γ-radiation on the properties of epoxy-based shape memory polymers, Journal of Intelligent Material Systems and Structures 25(10) (2013) 1256-1263.

[103] W. Al Azzawi, J.A. Epaarachchi, J. Leng, Investigation of ultraviolet radiation effects on thermomechanical properties and shape memory behaviour of styrene-based shape memory polymers and its composite, Composites Science and Technology 165 (2018) 266-273.

[104] T.-t. Wong, K.-t. Lau, W.-y. Tam, J. Leng, W. Wang, W. Li, H. Wei, Degradation of nano-ZnO particles filled styrene-based and epoxy-based SMPs under UVA exposure, Composite Structures 132 (2015) 1056-1064.

[105] T. Xu, G. Li, S.-S. Pang, Effects of ultraviolet radiation on morphology and thermo-mechanical properties of shape memory polymer based syntactic foam, Composites Part A: Applied Science and Manufacturing 42(10) (2011) 1525-1533.

[106] B. Yang, W.M. Huang, C. Li, L. Li, Effects of moisture on the thermomechanical properties of a polyurethane shape memory polymer, Polymer 47(4) (2006) 1348-1356.

[107] Y.-J. Yu, K. Hearon, T.S. Wilson, D.J. Maitland, The effect of moisture absorption on the physical properties of polyurethane shape memory polymer foams, Smart Materials and Structures 20(8) (2011) 085010.

[108] M. Di Prima, K. Gall, D. McDowell, R. Guldberg, A. Lin, T. Sanderson, D. Campbell, S. Arzberger, Cyclic compression behavior of epoxy shape memory polymer foam, Mechanics of Materials 42(4) (2010) 405-416.

[109] M.F. Öktem, B. Aydaş, Development of Flame Retardant Shape Memory Polymer (SMP) Flax Fiber Composite by Using Organic Polydopamine (PDA) Coating and Nanoparticles, Arabian Journal for Science and Engineering 47(5) (2022) 6461-6475.

[110] R. Abedin, X. Feng, J. Pojman Jr, S. Ibekwe, P. Mensah, I. Warner, G. Li, A Thermoset Shape Memory Polymer-Based Syntactic Foam with Flame Retardancy and 3D Printability, ACS applied polymer materials 4(2) (2022) 1183-1195.

[111] A. Metcalfe, A.-C. Desfaits, I. Salazkin, W.M. Sokolowski, J. Raymond, Cold hibernated elastic memory foams for endovascular interventions, Biomaterials 24(3) (2003) 491-497.

[112] B. Kim, Shape memory polymers and their future developments, BUDAPEST UNIV TECHNOL & ECON DEPT POLYMER ENG, MUEGYETEM RKP 3, BUDAPEST, H …, 2008, pp. 614-614.

[113] X. Lan, J.S. Leng, S.Y. Du, Design of a deployable antenna actuated by shape memory alloy hinge, Materials science forum, Trans Tech Publ, 2007, pp. 1567-1570.

[114] G. Kleinhans, F. Heidenhain, Actively moving polymers, Kunststoffe 76 (1986) 1069-73.

[115] T.D. Dao, N.S. Ha, N.S. Goo, W.-R. Yu, Design, fabrication, and bending test of shape memory polymer composite hinges for space deployable structures, Journal of Intelligent Material Systems and Structures 29(8) (2017) 1560-1574.

[116] W. Francis, M. Lake, K. Mallick, G. Freebury, A. Maji, Development and testing of a hinge/actuator using elastic memory composites, 44th AIAA/ASME/ASCE/AHS/ASC structures, structural dynamics, and materials conference, 2003, p. 1496.

[117] R. Barrett, W. Francis, E. Abrahamson, M. Lake, M. Scherbarth, Qualification of elastic memory composite hinges for spaceflight applications, 47th AIAA/ASME/ASCE/AHS/ASC structures, structural dynamics, and materials conference 14th AIAA/ASME/AHS adaptive structures conference 7th, 2006, p. 2039.

[118] F. Beavers, N. Munshi, M. Lake, A. Maji, K. Qassim, B. Carpenter, S. Rawal, Design and testing of an elastic memory composite deployment hinge for spacecraft, 43rd AIAA/ASME/ASCE/AHS/ASC Structures, Structural Dynamics, and Materials Conference, 2002, p. 1452.

[119] T. Chen, O.R. Bilal, R. Lang, C. Daraio, K. Shea, Autonomous Deployment of a Solar Panel Using Elastic Origami and Distributed Shape-Memory-Polymer Actuators, Physical Review Applied 11(6) (2019).

[120] P. Keller, M. Lake, D. Codell, R. Barrett, R. Taylor, M. Schultz, Development of elastic memory composite stiffeners for a flexible precision reflector, 47th AIAA/ASME/ASCE/AHS/ASC Structures, Structural Dynamics, and Materials Conference 14th AIAA/ASME/AHS Adaptive Structures Conference 7th, 2006, p. 2179.

[121] M. Love, P. Zink, R. Stroud, D. Bye, S. Rizk, D. White, Demonstration of morphing technology through ground and wind tunnel tests, 48th AIAA/ASME/ASCE/AHS/ASC structures, structural dynamics, and materials conference, 2007, p. 1729.

[122] J. Diani, P. Gilormini, C. Frédy, I. Rousseau, Predicting thermal shape memory of crosslinked polymer networks from linear viscoelasticity, International Journal of Solids and Structures 49(5) (2012) 793-799.

162

[123] J. Diani, Y. Liu, K. Gall, Finite strain 3D thermoviscoelastic constitutive model for shape memory polymers, Polymer Engineering & Science 46(4) (2006) 486-492.

[124] H. Tobushi, K. Okumura, M. Endo, S. Hayashi, Thermomechanical Properties of Polyurethane-Shape Memory Polymer Foam, Journal of Intelligent Material Systems and Structures 12(4) (2001) 283-287.

[125] W.A. Azzawi, J.A. Epaarachchi, M. Islam, J. Leng, Implementation of a finite element analysis procedure for structural analysis of shape memory behaviour of fibre reinforced shape memory polymer composites, Smart Materials and Structures 26(12) (2017).

[126] E. Monaldo, F. Nerilli, G. Vairo, Basalt-based fiber-reinforced materials and structural applications in civil engineering, Composite Structures 214 (2019) 246-263.

[127] A. Elmahdy, P. Verleysen, Tensile behavior of woven basalt fiber reinforced composites at high strain rates, Polymer Testing 76 (2019) 207-221.

[128] G. Yang, M. Park, S.-J. Park, Recent progresses of fabrication and characterization of fibers-reinforced composites: A review, Composites Communications 14 (2019) 34-42.

[129] V. Lopresto, C. Leone, I. De Iorio, Mechanical characterisation of basalt fibre reinforced plastic, Composites Part B: Engineering 42(4) (2011) 717-723.

[130] E. Kessler, R. Gadow, J. Straub, Basalt, glass and carbon fibers and their fiber reinforced polymer composites under thermal and mechanical load, AIMS Materials Science 3(4) (2016) 1561-1576.

[131] J.R. Correia, Y. Bai, T. Keller, A review of the fire behaviour of pultruded GFRP structural profiles for civil engineering applications, Composite Structures 127 (2015) 267-287.

[132] C.E. Bakis, L.C. Bank, V. Brown, E. Cosenza, J. Davalos, J. Lesko, A. Machida, S. Rizkalla, T. Triantafillou, Fiber-reinforced polymer composites for construction-state-of-the-art review, Journal of composites for construction 6(2) (2002) 73-87.

[133] J. Qureshi, A Review of Fibre Reinforced Polymer Structures, Fibers 10(3) (2022) 27.

[134] A.K. Gand, T.-M. Chan, J.T. Mottram, Civil and structural engineering applications, recent trends, research and developments on pultruded fiber reinforced polymer closed sections: a review, Frontiers of Structural and Civil Engineering 7(3) (2013) 227-244.

[135] A. Zhou, T. Keller, Joining techniques for fiber reinforced polymer composite bridge deck systems, Composite Structures 69(3) (2005) 336-345.

[136] L. Cheng, V.M. Karbhari, New bridge systems using FRP composites and concrete: a state-of-the-art review, Progress in Structural Engineering and Materials 8(4) (2006) 143-154.

[137] L.C. Bank, Composites for construction: structural design with FRP materials, John Wiley & Sons2006.

[138] T. Keller, N.A. Theodorou, A.P. Vassilopoulos, J. De Castro, Effect of natural weathering on durability of pultruded glass fiber–reinforced bridge and building structures, Journal of Composites for Construction 20(1) (2016) 04015025.

[139] L. Hollaway, A review of the present and future utilisation of FRP composites in the civil infrastructure with reference to their important in-service properties, Construction and building materials 24(12) (2010) 2419-2445.

[140] Wagners-Composite Fibre Technologies (CFT), Wagner nd https://www. wagner. com. au/main/what-we-do/composite-fibre-technologies/cft-home/(accessed March 8, 2020).

[141] N. Boyd, M.M. Khalfan, T. Maqsood, Off-site construction of apartment buildings, Journal of architectural engineering 19(1) (2013) 51-57.

[142] Y.F. Badir, M.A. Kadir, A.H. Hashim, Industrialized building systems construction in Malaysia, Journal of architectural engineering 8(1) (2002) 19-23.

[143] C. Kasperzyk, M.-K. Kim, I. Brilakis, Automated re-prefabrication system for buildings using robotics, Automation in Construction 83 (2017) 184-195.

[144] C. Goodier, A. Gibb, Future opportunities for offsite in the UK, Construction management and economics 25(6) (2007) 585-595.

[145] D.A. Steinhardt, K. Manley, Adoption of prefabricated housing–the role of country context, Sustainable cities and society 22 (2016) 126-135.

[146] S. Kale, D. Arditi, Diffusion of ISO 9000 certification in the precast concrete industry, Construction Management and Economics 24(5) (2006) 485-495.

[147] W. Pan, A.G. Gibb, A.R. Dainty, Leading UK housebuilders' utilization of offsite construction methods, Building research & information 36(1) (2008) 56-67.

[148] H. Jonsson, M. Rudberg, Classification of production systems for industrialized building: a production strategy perspective, Construction management and economics 32(1-2) (2014) 53-69.

[149] N. Bertram, S. Fuchs, J. Mischke, R. Palter, G. Strube, J. Woetzel, Modular construction: From projects to products, McKinsey & Company: Capital Projects & Infrastructure (2019) 1-34.

[150] A.G. Gibb, Off-site fabrication: prefabrication, pre-assembly and modularisation, John Wiley & Sons1999.

[151] Z. Li, G.Q. Shen, X. Xue, Critical review of the research on the management of prefabricated construction, Habitat international 43 (2014) 240-249.

[152] R.M. Lawson, R.G. Ogden, R. Bergin, Application of modular construction in high-rise buildings, Journal of architectural engineering 18(2) (2012) 148-154.

[153] P. Wellman04, Record-breaking Croydon tower gets the go-ahead, (2017).

[154] R. Hausammann, S. Franke, A modular timber construction system made with hollow-box elements, (2014).

[155] T. Gunawardena, Behaviour of prefabricated modular buildings subjected to lateral loads, Department of Infrastructure Engineering (2016).

[156] W. Ferdous, A. Manalo, T. Aravinthan, Bond behaviour of composite sandwich panel and epoxy polymer matrix: Taguchi design of experiments and theoretical predictions, Construction and Building Materials 145 (2017) 76-87.

[157] C. Wu, Z. Zhang, Y. Bai, Connections of tubular GFRP wall studs to steel beams for building construction, Composites Part B: Engineering 95 (2016) 64-75.

[158] S. Satasivam, Y. Bai, Y. Yang, L. Zhu, X.-L. Zhao, Mechanical performance of two-way modular FRP sandwich slabs, Composite Structures 184 (2018) 904-916.

[159] H. Tobushi, S. Hayashi, K. Hoshio, Y. Ejiri, Shape recovery and irrecoverable strain control in polyurethane shape-memory polymer, Sci Technol Adv Mater 9(1) (2008) 015009.

[160] K.H. Boller, Fatigue tests of glass-fabric-base laminates subjected to axial loading, (1958).

[161] A.P. Vassilopoulos, The history of fiber-reinforced polymer composite laminate fatigue, International Journal of Fatigue 134 (2020).

[162] T. Xie, I.A. Rousseau, Facile tailoring of thermal transition temperatures of epoxy shape memory polymers, Polymer 50(8) (2009) 1852-1856.

[163] K.S. Santhosh Kumar, R. Biju, C.P. Reghunadhan Nair, Progress in shape memory epoxy resins, Reactive and Functional Polymers 73(2) (2013) 421-430.

[164] A.L. Bernassau, D. Hutson, C.E. Demore, S. Cochran, Characterization of an epoxy filler for piezocomposites compatible with microfabrication processes [Correspondence], IEEE transactions on ultrasonics, ferroelectrics, and frequency control 58(12) (2011) 2743-2748.

[165] S. Pruksawan, G. Lambard, S. Samitsu, K. Sodeyama, M. Naito, Prediction and optimization of epoxy adhesive strength from a small dataset through active learning, Sci Technol Adv Mater 20(1) (2019) 1010-1021.

[166] S.N.S. Al-Humairi, H.S. Majdi, A.N.S. Al-Humairi, M. Al-Maamori, Future Prospects: Shape Memory Features in Shape Memory Polymers and Their Corresponding Composites, Smart and Functional Soft Materials, IntechOpen2019.

[167] Y. Liu, C. Han, H. Tan, X. Du, Thermal, mechanical and shape memory properties of shape memory epoxy resin, Materials Science and Engineering: A 527(10-11) (2010) 2510-2514.

[168] J. Jeewantha, C. Emmanuel, M. Herath, M. Islam, J. Epaarachchi, Development and characterization of shape memory polymers for non-invasive biomedical applications, Smart

Materials, Adaptive Structures and Intelligent Systems, American Society of Mechanical Engineers, 2021, p. V001T02A001.

[169] G. Li, A. Wang, Cold, warm, and hot programming of shape memory polymers, Journal of Polymer Science Part B: Polymer Physics 54(14) (2016) 1319-1339.

[170] K. Shahi, R. Boomurugan, R. Velmurugan, Cold programming of epoxy-based shape memory polymer, Structures 29 (2021) 2082-2093.

[171] Y.C. Wang, V. Kodur, Variation of strength and stiffness of fibre reinforced polymer reinforcing bars with temperature, Cement and Concrete Composites 27(9-10) (2005) 864-874.

[172] P. Amuthakkannan, V. Manikandan, J.W. Jappes, M. Uthayakumar, Effect of fibre length and fibre content on mechanical properties of short basalt fibre reinforced polymer matrix composites, Materials physics and mechanics 16(2) (2013) 107-117.

[173] H. Ku, H. Wang, N. Pattarachaiyakoop, M. Trada, A review on the tensile properties of natural fiber reinforced polymer composites, Composites Part B: Engineering 42(4) (2011) 856-873.

[174] R. Rahman, S. Zhafer Firdaus Syed Putra, Tensile properties of natural and synthetic fiber-reinforced polymer composites, Mechanical and Physical Testing of Biocomposites, Fibre-Reinforced Composites and Hybrid Composites2019, pp. 81-102.

[175] J. Liu, L. Xiang, T. Kan, The effect of temperature on the bending properties and failure mechanism of composite truss core sandwich structures, Composites Part A: Applied Science and Manufacturing 79 (2015) 146-154.

[176] H. Aglan, Z. Qian, D. Mitra-Majumdar, The effect of temperature on the critical failure properties of advanced polymer composites, Polymer testing 11(3) (1992) 169-184.

[177] D. Li, D. Fang, G. Zhang, H. Hu, Effect of temperature on bending properties and failure mechanism of three-dimensional braided composite, Materials & Design 41 (2012) 167-170.

[178] C. Shenghu, W. Xin, W. Zhishen, Evaluation and prediction of temperature-dependent tensile strength of unidirectional carbon fiber-reinforced polymer composites, Journal of Reinforced Plastics and Composites 30(9) (2011) 799-807.

[179] Z. Jia, T. Li, F.-p. Chiang, L. Wang, An experimental investigation of the temperature effect on the mechanics of carbon fiber reinforced polymer composites, Composites Science and Technology 154 (2018) 53-63.

[180] M.Y. Khalid, Z.U. Arif, R. Noroozi, A. Zolfagharian, M. Bodaghi, 4D printing of shape memory polymer composites: A review on fabrication techniques, applications, and future perspectives, Journal of Manufacturing Processes 81 (2022) 759-797.

[181] D.H. Hall, M.A. Grubb, C.H. Yoo, Improved design specifications for horizontally curved steel girder highway bridges, Transportation Research Board1999.

[182] P.R. Budarapu, S. Kumar, B.G. Prusty, M. Paggi, Stress transfer through the interphase in curved-fiber pullout tests of nanocomposites, Composites Part B: Engineering 165 (2019) 417-434.

[183] S.P.H. Skovsgaard, S. Heide-Jørgensen, Three-dimensional mechanical behavior of composite with fibre-matrix delamination through homogenization of micro-structure, Composite Structures 275 (2021).

[184] P.G. Furth, D.M. Dulaski, M. Buessing, P. Tavakolian, Parking lane width and bicycle operating space, Transportation research record 2190(1) (2010) 45-50.

[185] P. Srinivasa Rao, T. SeshadriSekhar, P. Sravana, Strength properties of glass fibre concrete, ARPN Journal of Engineering and Applied Sciences 5(4) (2010) 1-6.

[186] P.N. Shakor, S. Pimplikar, Glass fibre reinforced concrete use in construction, Int. J. Technol. Eng. Syst 2(2) (2011).

[187] G.B. Maranan, A.C. Manalo, B. Benmokrane, W. Karunasena, P. Mendis, Evaluation of the flexural strength and serviceability of geopolymer concrete beams reinforced with glass-fibre-reinforced polymer (GFRP) bars, Engineering Structures 101 (2015) 529-541.

[188] J.G. Teng, T. Yu, Y.L. Wong, S.L. Dong, Hybrid FRP–concrete–steel tubular columns: Concept and behavior, Construction and Building Materials 21(4) (2007) 846-854.

[189] M.R. Bambach, H.H. Jama, M. Elchalakani, Axial capacity and design of thin-walled steel SHS strengthened with CFRP, Thin-Walled Structures 47(10) (2009) 1112-1121.

[190] B. Gorenc, B.E. Gorenc, R. Tinyou, A. Syam, Steel designers' handbook, UNSW Press2005.

[191] S. Australia, AS 4100 - Steel Structures, The Council of Standards Australia, 2020.

[192] E. Alhassan, D. Olasehinde, A. Musonda, O. Odeniyi, Tensile and flexural behaviour of steel materials used in the construction of crop processing machines, IOP Conference Series: Earth and Environmental Science, IOP Publishing, 2020, p. 012044.

[193] J.A. Purkiss, L.-Y. Li, Fire safety engineering design of structures, CRC press2013.

[194] A. International, Standard Test Method for Tension-Tension Fatigue of Polymer Matrix Composite Materials, ASTM International West Conshohacken, PA, 2019.

[195] R.H. White, M.A. Dietenberger, Fire safety, Wood handbook: wood as an engineering material. Madison, WI: USDA Forest Service, Forest Products Laboratory, 1999. General technical report FPL; GTR-113: Pages 17.1-17.16 113 (1999).

[196] S.V. Levchik, E.D. Weil, Thermal decomposition, combustion and flame-retardancy of epoxy resins?a review of the recent literature, Polymer International 53(12) (2004) 1901-1929.

[197] T. Jin, Visibility through fire smoke (I), Bulletin of Japan Association for Fire Science and Engineering 19(2) (1970) 1-8.

[198] D. Rasbash, Relevance of fire point theory to the assessment of fire behaviour of combustible materials, University of Edinburgh report.(Edinburgh, UK) (1975).

[199] X. Chen, L. Huo, C. Jiao, S. Li, TG–FTIR characterization of volatile compounds from flame retardant polyurethane foams materials, Journal of Analytical and Applied Pyrolysis 100 (2013) 186-191.

[200] L. Tao, G.B. Zhao, J. Qian, Y.K. Qin, TG-FTIR characterization of pyrolysis of waste mixtures of paint and tar slag, J Hazard Mater 175(1-3) (2010) 754-61.

[201] H. Jellinek, K. Takada, Toxic gas evolution from polymers: Evolution of hydrogen cyanide from linear polyurethane, Journal of Polymer Science: Polymer Chemistry Edition 13(12) (1975) 2709-2723.

[202] A.E. Segneanu, I. Gozescu, A. Dabici, P. Sfirloaga, Z. Szabadai, Organic compounds FT-IR spectroscopy, InTech Romania2012.

[203] A. Katunin, A. Wronkowicz, Characterization of failure mechanisms of composite structures subjected to fatigue dominated by the self-heating effect, Composite Structures 180 (2017) 1-8.

[204] P.R. Vieira, E.M.L. Carvalho, J.D. Vieira, R.D. Toledo Filho, Experimental fatigue behavior of pultruded glass fibre reinforced polymer composite materials, Composites Part B: Engineering 146 (2018) 69-75.

[205] S.N. Kukureka, C.Y. Wei, Damage development in pultruded composites for optical telecommunications cables under tensile and flexural fatigue, Composites Science and Technology 63(12) (2003) 1795-1804.

[206] L. Van Den Einde, L. Zhao, F. Seible, Use of FRP composites in civil structural applications, Construction and Building Materials 17(6-7) (2003) 389-403.

[207] P. Kumar, K. Chandrashekhara, A. Nanni, Structural performance of a FRP bridge deck, Construction and Building Materials 18(1) (2004) 35-47.

[208] Z. Wu, X. Wang, K. Iwashita, T. Sasaki, Y. Hamaguchi, Tensile fatigue behaviour of FRP and hybrid FRP sheets, Composites Part B: Engineering 41(5) (2010) 396-402.

[209] M. Saito, Tensile fatigue strength of lightweight concrete, International Journal of Cement Composites and Lightweight Concrete 6(3) (1984) 143-149.

[210] C. Colombo, L. Vergani, Multi-axial fatigue life estimation of unidirectional GFRP composite, International Journal of Fatigue 33(8) (2011) 1032-1039.

[211] Z. Wang, L. Xu, X. Sun, M. Shi, J. Liu, Fatigue behavior of glass-fiber-reinforced epoxy composites embedded with shape memory alloy wires, Composite Structures 178 (2017) 311-319.

[212] J.A. Epaarachchi, P.D. Clausen, An empirical model for fatigue behavior prediction of glass fibre-reinforced plastic composites for various stress ratios and test frequencies, Composites Part A: Applied Science and Manufacturing 34(4) (2003) 313-326.

[213] R. Leemans, B. Eickhout, Another reason for concern: regional and global impacts on ecosystems for different levels of climate change, Global environmental change 14(3) (2004) 219-228.

[214] C. Li, A. Strachan, Molecular dynamics predictions of thermal and mechanical properties of thermoset polymer EPON862/DETDA, Polymer 52(13) (2011) 2920-2928.

[215] C. Li, E. Coons, A. Strachan, Material property prediction of thermoset polymers by molecular dynamics simulations, Acta Mechanica 225(4) (2014) 1187-1196.

[216] K. Soudki, T. Alkhrdaji, Guide for the design and construction of externally bonded FRP systems for strengthening concrete structures (ACI 440.2 R-02), Structures Congress 2005: Metropolis and Beyond, 2005, pp. 1-8.

APPENDIX A

- **1st Q1 journal:**

K. D. C. Emmanuel, H. M. C. M. Herath, L. H. J. Jeewantha, J. A. Epaarachchi, and T. Aravinthan, "Thermomechanical and fire performance of DGEBA based shape memory polymer composites for constructions," Construction and Building Materials, vol. 303, 2021, doi: 10.1016/j.conbuildmat.2021.124442

APPENDIX B

- **2nd Q1 journal:**

K. D. C. Emmanuel, L. H. J. Jeewantha, H. M. C. M. Herath, J. A. Epaarachchi, and T. Aravinthan, "Damage onset analysis of optimized shape memory polymer composites during programming into curved shapes," Materialia, vol. 26, 2022, doi: 10.1016/j.mtla.2022.101599

APPENDIX C

- **3rd Q1 journal:**

K. Emmanuel, L. Jeewantha, H. Herath, J. Epaarachchi, T. Aravinthan, Shape memory polymer composite circular and square hollow members for deployable structures, Composites Part A: Applied Science and Manufacturing 171 (2023) 107559.

Shape memory polymer composite circular and square hollow members for deployable structures

K.D.C. Emmanuel [a,b], L.H.J. Jeewantha [a,b], H.M.C.M. Herath [c], J.A. Epaarachchi [a,b,*], T. Aravinthan [a,b]

[a] School of Mechanical and Electrical Engineering, Faculty of Health Engineering and Sciences, University of Southern Queensland, Toowoomba, Australia
[b] Centre for Future Materials, University of Southern Queensland, Toowoomba, Australia
[c] Department of Engineering Technology, Faculty of Technological Studies, Uva Wellassa University, Badulla, Sri Lanka

ABSTRACT

The exciting shape memorizing ability of shape memory polymer composites (SMPCs) has attracted the interest of researchers catering to the needs of modern constructions. As well as outer space related applications, SMPCs can be used effectively in civil construction techniques. SMPC integrated structures have the capability to deform into a compact shape for easy transportation to site where they can be recovered to their original shape. This paper details the application of the shape memory effect (SME) in glass SMPC circular and square hollow (CHS and SHS) structural members and SMPC incorporated deployable structures. The SME of SMPC members were analysed numerically via ABAQUS software and validated with experimental results. It was revealed that SMPC SHS and CHS integrated large scale structures can be temporarily deformed to achieve a volume saving of 52 % and 70 %, respectively, for easy handling and transportation. Furthermore, the tension–tension fatigue properties of glass and basalt SMPCs were characterized, and the fatigue study provides significant knowledge to an untouched branch of SMPC performance. We believe that these findings will transform current construction strategies into a new approach, making modern day constructions smarter, quicker and cheaper.

1. Introduction

With advancements in construction technology, engineers look for opportunities to develop new construction methods and adopt novel building materials. Such improvements can enhance construction speed, minimize labour requirements, produce less carbon dioxide (CO_2) emissions, and allow people to live in safe and affordable homes. So far, cement, steel, and wood have been used extensively as building materials [1,2]. In addition, traditional construction methods offer very slow construction speeds and are labour intensive. Consequently, the need for new building materials and efficient technologies are increasing day by day. Interestingly, polymer composites have become a successful substitute construction material and are used in a wide variety of structural applications [3]. Importantly, compared to other materials, smart materials such as shape memory polymer composites (SMPCs), have also shown an impressive and unique performance in engineering applications [4,5].

Shape memory polymers (SMP) is a smart branch of polymers,

comprising a unique shape memorizing ability [6]. Unlike traditional polymer materials, SMPs can undergo substantial deformation and retain their temporary compact shape when exposed to an external stimulus [7,8]. SMPs have the ability to recover their initial shape when triggered with the same external stimulus. Researchers have developed different types of shape memory materials that are responsive to external stimuli such as heat, electricity, a magnetic field, microwaves, moisture and light. Heat activation is the most typical stimulus of SMPs and has been extensively studied [9]. To mitigate the poor mechanical properties of SMPs, fibre reinforcements have been incorporated to improve their structural performance [9–13]. Hence, SMPCs with both good structural and shape memory properties can be used effectively in a wide variety of strength demanding applications.

To date, fibre reinforced SMPCs have mainly been developed for outer space exploration applications. The major challenges of conventional structures made of common materials, such as heaviness, high cost and high volume consumed, can be prevented by using lightweight smart SMPC components [14]. SMPCs have also been proposed for use in

deployable lunar habitats to revolutionize rapidly developing space exploration technologies [15]. Moreover, the same concept of incorporating SMPCs can be used in challenging civil applications to enhance construction efficiency. Prefabricated modular construction is a rapidly developing building technology ideal for congested cities where space and time are critical considerations [16]. Despite their remarkable benefits, the handling and transporting of heavy and oversized prefabricated modules have become prominent drawbacks [17]. Also, constructing footbridges in remote areas and challenging terrain requires a lot of labour, time and can become costly. Similarly, the manufacturing and transportation costs of curved and heavy steel beams are very high [18].

However, less attention has been given to integrating SMPCs into structural members such as circular and square hollow (CHS and SHS) sectioned components. Importantly, SMPC CHS and SHS structural components are lightweight, strong and deformable. In addition, to date, most of the research on SMPCs has been limited to low thicknesses (less than 2 mm) and small scaled prototypes. As a result, in our recent work, we studied the adverse effects of increasing the thickness and fibre content of SMPCs on shape programming efficiency. A technique to identify the damage onset stress of SMPCs during programming has also been presented based on finite element analysis (FEA). Interestingly, it was found that programming damage initiates at a compressive stress of 70 MPa and cracks form on the tensioned side beyond 100 MPa [19]. Moreover, research on the durability of SMPCs under fatigue conditions is lacking, as SMPCs have not been proposed for civil constructions.

This article presents the next phase of our recent studies on the development of shape deformable and recoverable SMPC structural members. The structures made from SMPCs are lightweight and can be deformed into a temporary compact shape, allowing easy transportation and handling. Then, the SMPC components can be recovered on the construction site and can be used easily in constructions. They can also be used in the construction of outer space habitats. Consequently, real scale SMPC CHS and SHS components were fabricated, deformed and tested as a proof of concept. The characterization of SMPC fatigue properties which is vital for a construction material is also presented. Importantly, the proposed experimental and FEA framework address some of the exciting and modern SMPC related research aspects which have not been studied adequately. Further, the validated FEA modelling introduces a combination of the material's strength and viscoelastic properties which enables the study of developing stress during programming. The outcomes of this research provide firsthand knowledge of SMPC application in structural components that can be used to remedy current construction challenges. Further, the proposed concepts can be developed to transform traditional, time consuming and costly building procedures into fast paced smart constructions.

2. Materials and methods

2.1. Materials

An epoxy based SMP was synthesized by mixing Bisphenol A epoxy resin Araldite GY 191 with the hardeners Triethylenetetramine (TETA) and Jeffamine D230 to a weight ratio of 13.03: 1: 1.63, respectively. The resin and hardeners were purchased from Huntsman and Sigma-Aldrich, respectively. During fabrication, all SMPCs were initially cured for 24 hrs at room temperature and post cured at 100 °C for 1.5 hrs and at 130 °C for 1 hr.

The SMPC material parameters such as the thickness, reinforcement layers and their orientations were based on the Taguchi optimization presented in our previous study to prevent programming damage. The study showed that excessive compression stress (>70 MPa) can cause three types of visible damage during the programming stage of SMPCs. Also, the storage onset programming temperature (T_S) and rubbery onset temperature of the optimized SMPC were 60 °C and 90 °C, respectively [19].

2.2. Fatigue testing

The fatigue behavior of the optimized SMPCs under tension–tension cyclic loading was investigated in MTS 810–100 kN according to ASTM D3479/D3479M-19 [20]. The specimens were cycled between their minimum and maximum tensile load (stress) under a load control mode at 1 Hz frequency (f). A low frequency was selected to avoid a temperature increase in the sample. The fatigue lives of the SMPC samples were studied for a stress ratio (r = ratio of minimum and maximum stress) of 0.1 and for five selected load levels (L) of 40, 50, 60, 70 and 80 % of ultimate tensile stress (S_{UTS}). The SMPC samples were tabbed to avoid premature failure within the grips along with a 10 Hz data acquisition rate. The tabs were manufactured according to the test standard guidelines from a general purpose polymer reinforced with glass fibre. The load mean (L_M) and amplitude (L_A) were used to define the 'Sine' wave form in the test setup, and the respective values for the glass SMPCs are given in Table 1.

2.3. Temperature effect testing

The SMPC is programmed at the storage onset temperature (T_S = 60 °C). For the material setup of the ABAQUS software, the experimentally measured tensile properties were used to define the SMPC's elastic properties at the programming temperature. Hence, the tensile properties of the optimized SMPCs were only evaluated at the programming temperature of 60 °C. Tests were carried out in MTS 100 kN along with its thermal chamber to maintain the required temperature during the test. As the matrix becomes soft when heated, tabs were attached to the SMPC tensile samples to avoid sample slip and undesirable damage within the fixtures. A reinforced polymer composite with a higher glass transition temperature (T_g) was used as the tab material. A laser extensometer with two reflective tapes positioned 25 mm apart (as shown in Fig. 1) were used to measure the axial strains during tensile testing.

2.4. Fabrication of CHS and SHS members

Two specially designed molds (shown in Fig. 2) were used to fabricate the glass fibre reinforced SMPC CHS and SHS structural members of length 250 mm. The mandrels and outer fixtures were precisely machined to maintain a 3 mm constant thickness in all SMPC components. Additionally, 3 mm spacers were used to position the inner mandrel and restrict its movements inside the mold.

To avoid air bubbles becoming trapped in creating dry patches and to monitor the resin level inside the mold, a resin infusion tube connected to the bottom of the mold was used for pouring the polymer. The pressure differential in the resin infusion tube facilitated an effective and trouble free resin flow when casting the SMPC structural components. Once the molds were filled with SMP, the curing cycle mentioned in Section 2.1 was utilized to fully cure the SMPC components. The key components of the developed mold are listed in Table 2. Subsequently, the fabricated CHS and SHS components were demolded and cut into the lengths required for shape memory testing. Fig. 3 presents manufactured the SMPC CHS and SHS specimens along with their cross sectional dimensions.

Table 1
Load values for glass SMPC fatigue test setup.

SMPC	S_{UTS} (MPa)	r	L %	L_M (kN)	L_A (kN)
Glass	231.9	0.1	80	7.7	6.3
			70	6.7	5.5
			60	6.0	4.9
			50	5.0	4.1
			40	4.0	3.3
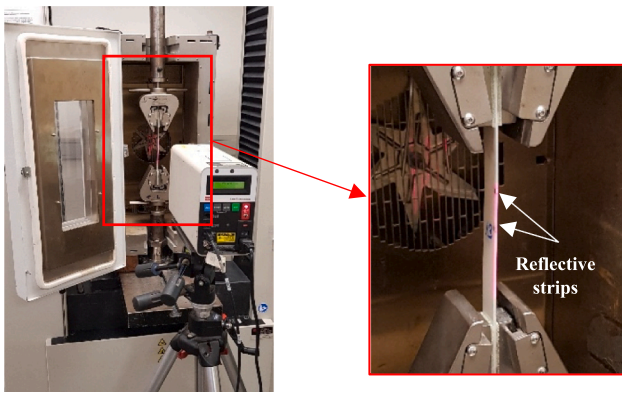
Fig. 1. Elevated temperature tensile experimental setup with laser extensometer and reflective tapes.

Fig. 2. Solid model and actual manufacturing technique of SHS SMPC members; (a) side view (b) inside view of the mold (c) actual fabrication setup.

Table 2
Components of the customized mold.

Part no	Description
1	Funnel
2	Mandrel with mold release
3	Fibre reinforcements
4	8 mm tube
5	Silicone seal
6	3 mm steel spacers

2.5. Axial compression of SMPC components

The compressive strength and failure method of the glass SMPC CHS and SHS components were evaluated in the MTS 100 kN. The length to diameter ratio (L/D) of the SMPC components was approximately 2. A displacement rate of 1.3 mm/min was used to apply a compressive load. All compressive tests were performed at room temperature.

2.6. Relaxation testing

Stress relaxation tests were carried out in a DMA Q800 for neat and reinforced SMPs. A dual cantilever fixture was used to evaluate the stress relaxing behaviour of materials within the temperature range 50 °C to 80 °C with 5 °C increment steps. Once the chamber temperature was set to a specific value, a 10 min isothermal step was used to achieve thermal equilibrium. Then, a constant strain of 0.2 % was applied and relaxation data were recorded for 15 min. The time–temperature superposition (TTS) principle was applied to characterize the viscoelastic properties of materials over an extended time period [21]. The relaxation data were analyzed with the Advantage Software (v5.5.22) rheology module, and Prony relaxation master curves were generated using Williams-Landel-Ferry (WLF) curve shifting technique [22]. The master curve was fitted with the Prony series formula described by the Generalized Maxwell Model given in Equation (1), and was used to evaluate Prony coefficients (E(t)). The shear (G(t)) and bulk moduli (K(t)) required to fully define the viscoelastic properties in ABAQUS were evaluated using Equations (2) and (3). The terms t, τ and υ represent time, relaxation time and Poisson's ratio, respectively.

$$E(t) = E_\infty + \sum_{i=1}^{n} E_i e^{-\frac{t}{\tau_i}} \tag{1}$$

$$G(t) = \frac{E(t)}{2(1+\upsilon)} \tag{2}$$

$$K(t) = \frac{E(t)}{3(1-2\upsilon)} \tag{3}$$

2.7. Shape memory effect testing

To demonstrate the shape memory behaviour of the fully cured SMPC structural components, 60 mm long components were cut and programmed by a radial distributed force along their lengths. As the deformation occurs radially, a similar shape programming behaviour can be expected even in longer specimens. Programming was carried out at a storage modulus onset ($T_S = 60$ °C) which was concluded from previous studies [19]. The experimental setup including the thermal chamber, fixtures and specimen positioning are illustrated in Fig. 4. Prior to the application of programming force, the SMPC structural
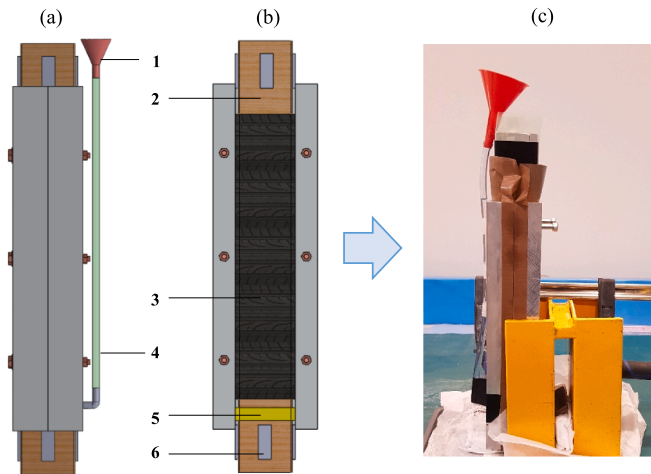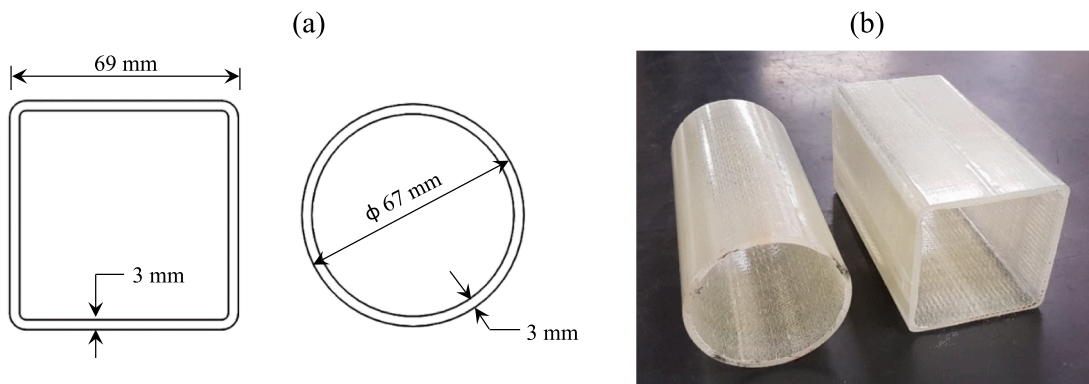

Fig. 3. Fabricated CHS and SHS components; (a) cross sectional dimensions (b) 60 mm long components tested for SME.
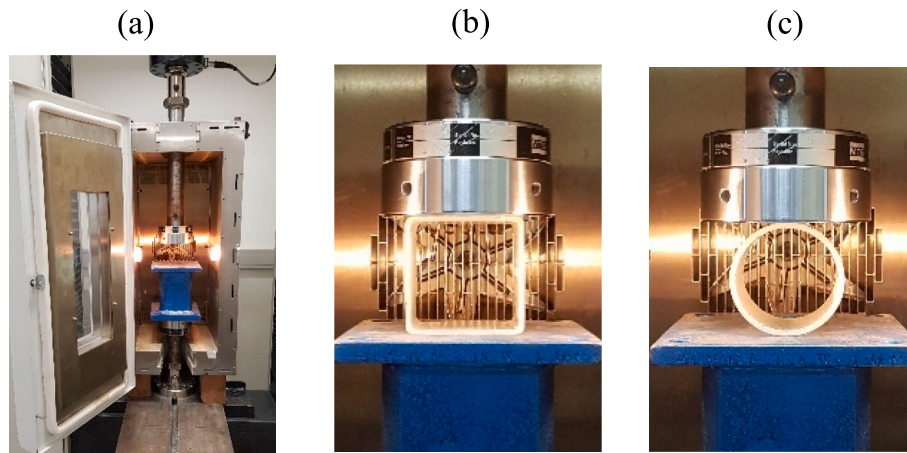
(a) (b) (c)

Fig. 4. SME testing of SMPC components; (a) experimental setup (b) SHS and (c) CHS components prior to programming.

components were held inside the thermal chamber of the MTS 100 kN for 30 min to achieve thermal equilibrium. Next, force was applied with a crosshead movement of 1 mm/s. During the programming stage, the time taken to initiate damage and specific locations were monitored and used to validate the FEA predictions based on the critical stress margins (CSMs) proposed in our recent studies [19]. The programming stage was terminated when the load reading on the MTS began dropping rapidly due material failure such as cracks. Then, the chamber was opened for natural cooling allowing the specimen to cool gradually from 60 °C to room temperature. Next, the applied force was removed allowing the component to spring back and fix its shape. Finally, the specimen was placed in an oven heated to 90 °C, allowing it to recover the initial shape. Photographs of the initial, fixed and recovered shapes of the components were taken to evaluate the SME properties of fixity (R_f) and recovery ratios (R_r). Moreover, Equations (4) and (5) were used to evaluate R_f and R_r [23]. The notations D1, D2, L1 and L2 denote initial height, final height, deformation and fixed deformation, respectively, and are illustrated in Fig. 5.

$$R_f = \frac{L_2}{L_1} \times 100\% \tag{4}$$

$$R_r = \frac{D_2}{D_1} \times 100\% \tag{5}$$

3. Results and discussion

3.1. Fatigue behaviour

Due to different environmental conditions, the structural components used in constructions can experience cyclic loading that can lead to a catastrophic destruction with time. Fatigue failure is induced via critical loading patterns which are lower than the ultimate strength (S_{UTS}) of materials. The fatigue behaviour of any material is very complex and challenging to predict. However, it is vital to have an understanding of how SMPCs behave under fatigue loading to analyze and

investigate their applicability to proposed applications. Thus, constant amplitude axial tension–tension fatigue tests were performed for the optimized glass and basalt SMPCs for r ranging from 40 % to 80 % of S_{UTS}. These experimental results allow the identification of the fatigue strength (S_n) of the SMPC which is the safe stress margin under cyclic loading.

Fig. 6 illustrates the fatigue lifetimes of the glass and basalt SMPCs under tested load percentages. The S-N curves of these SMPCs show a similar trend compared to the fatigue behaviour of other common materials [24 25]. During fatigue testing, as per ASTM D3479/D3479M-19, the complete separation of SMPC samples was used as the criterion for
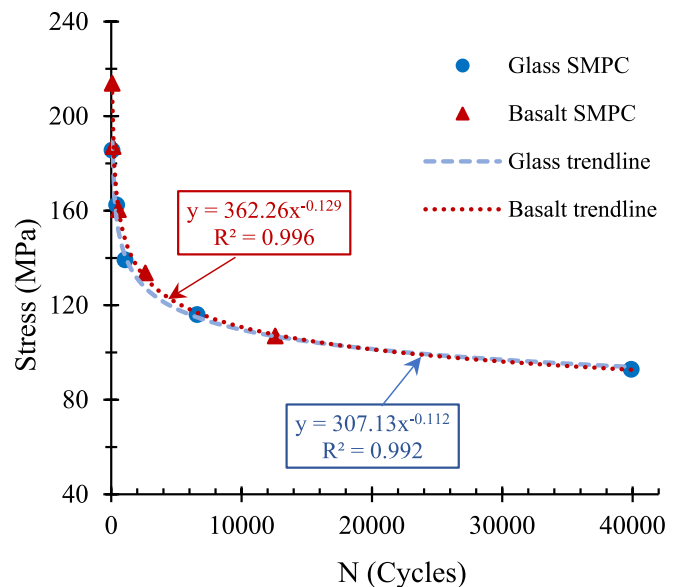
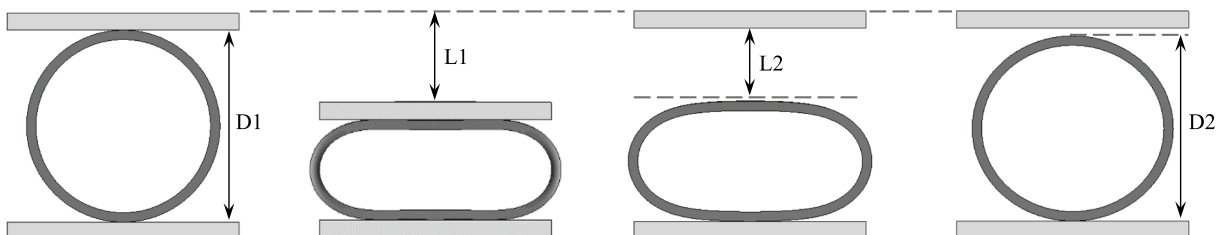

Fig. 6. S-N fatigue life characteristics for SMPCs.

Fig. 5. Parameters used for evaluation of R_f % and R_r %.

failure. At a given load percentage, the average value of the number of cycles to failure of each sample type was used to plot the S-N curve. Subsequently, power law equations were fitted to test results and the fatigue endurance limits of the SMPCs at 2x10^6 cycles were evaluated. The divergences between the experimental and predicted results of glass and basalt SMPCs were calculated using the correlation index (R^2), and the obtained results were 99.2 % and 99.6 %, respectively [26,27]. A fatigue life of 2x10^6 cycles was selected as per similar fatigue studies performed for fibre reinforced plastic (FRP) [28–30] and lightweight concrete [31] for civil applications. Interestingly, basalt fibre reinforced SMPCs showed a slightly better performance under high tensile fatigue loading. In contrast, glass SMPCs exhibited marginally better resistance against lower fatigue loads. Accordingly, the endurance limit for 2 million cycles of glass and basalt SMPCs were evaluated as 60.5 MPa and 55.7 MPa, respectively (given in Table 3). Moreover, the samples have shown similar failure modes in comparison to previous studies on general polymer composites. Thus, tested SMPCs showed progressive damage failure behaviour by means of matrix cracking, fiber–matrix debonding, delamination and fiber breakage [24,25,32,33]. In addition, it was clearly seen that the fatigue failure modes of SMPCs were identical to that of the static tensile load failure mode which was also presented by Wang et al., for glass fibre reinforced epoxy composite embedded with shape memory alloy wires [33].

As mentioned previously, fatigue tests were performed at r = 0.1 with a 1 Hz frequency. However, in real life situations r and f can have different values. Using the empirical model proposed by Epaarachchi et al. [34], S-N fatigue characteristics for variable r and f values can be predicted by evaluating two material specific model parameters α and β. In addition, it is possible to avoid repeated testing for different load cases and frequencies, saving both time and effort by adhering to this method. Thus, only a few straightforward fatigue tests are required at one r value for a number of load levels to calculate α and β [34]. Therefore, following the proposed technique, respective material specific parameters were evaluated, and are illustrated in Fig. 7 and Table 4. Using the evaluated α and β values, fatigue S-N characteristic curves were generated for r values ranging from 0.1 to 0.6 (in Fig. 8). The model has shown excellent correlation with the experimental results for r = 0.1, thus showcasing its effectiveness. Importantly, based on these results, SMPC fatigue behaviour under different real life applications can be studied and predicted with ease. Hence, these results will be vital for future SMPC structural component design, ensuring they are safe and can withstand fatigue loads under operating conditions.

3.2. Axial compressive properties

Depending on their application, structural components often experience compressive loads. Thus, buckling is an important phenomenon that needs to be investigated when components are exposed to compressive stresses. Consequently, the behaviour and damage mode of the SMPC CHS and SHS components was investigated for components with L/D = 2, and are shown in Fig. 9. The CHS SMPC components showed a compressive strength of 124.7 MPa when the edges began to experience damage due to crushing. However, the SHS SMPC components experienced local buckling due to compression, and initiated damage at 69.6 MPa. This can be attributed to the stress concentration at the corners of SHS SMPC specimens, resulting a lower compressive strength compared to CHS SMPCs. Importantly, recent studies of glass

fibre reinforced geopolymer concrete beams used as construction materials showed similar compressive strengths in the range 40 MPa − 85 MPa [35–37]. The comparability of the experimentally evaluated compressive strengths of the SMPC components can be further validated with respect to the results presented for FRP, concrete and steel integrated, tubular and SHS components [38,39]. Thus, the results of the compressive behaviour analysis indicate that the comparative loading capacity of the SMPC components is suitable for construction applications.

3.3. Viscoelastic properties

When the SMP is heated to its T_g, the material transforms its state from solid to rubbery through a transition phase. Hence, in order to simulate the behaviour of the SMP within the phase transition region, characterization of the viscoelastic properties is essential. The generated Prony series curves for all tested specimens are presented in Fig. 10. The relaxation values taken from the Prony series of a certain material at different time values were used to define viscoelastic properties of the SMPCs in ABAQUS software. Importantly, it can be seen that both the glass and basalt fibre SMPCs showed higher relaxation moduli compared to the neat SMP. This can be attributed to the high stiffness attained with improved mechanical performance by reinforcement inclusion and low matrix content. The viscoelastic FEA modelling enables simulation of the complete thermomechanical cycle of SMPCs, and was inspired by a study conducted by Azzawi et al. [22]. In our recent studies [19], modelling of the general shape memory cycle was modified by the inclusion of tensile properties at the programming temperature to study the stress variations during programming and identify damage onset.

3.4. Modelling SME of CHS and SHS components

To improve SMPC component design and applicability in a broad spectrum of civil engineering applications, the programming stage modelling of the SMPC members is vital. FEA analysis of the SMPC component's programming stage allows the prompt prediction of any damage through stress build up, detection of critical locations prone to high stresses, determination of fibre orientation (at compressed side), evaluation of required external forces and optimization of programming process parameters, saving both time and cost. FEA and experimental shape comparisons of CHS and SHS SMPC components during programming are presented in Fig. 11 and Fig. 12, respectively. The shapes of the deformed components during the first 12 s of programming are presented. It is evident that the shapes predicted by FEA matches well with experimental deformed shapes of both tested components. In addition, the FEA model was able to demonstrate the spring back effect during shape fixing and recovery of the initial shape once thermal load is reapplied. The spring back effect can be demonstrated in the FEA model with the help of two additional visco steps for sample cooling and external force removal. Fixity and recovery ratios evaluated according to Equations (1) and (2) are given in Table 5. The evaluated ratios show a good match among FEA and experimental results, with an error percentage less than 5.6 % and 3.5 % for fixity and recovery, respectively, further validating the FEA model used. The slight difference between these results can be attributed to the material damage experienced during experimental programming.

3.4.1. Programming stage damage predictions

As per the guidelines proposed in our previous study [19], 70 MPa and 100 MPa were proposed as the critical stress limits for the SMPC during programming. In addition, Type 1 damage which corresponds to matrix-fibre debonding due to interfacial failure dominates in the stress range 70 MPa to 100 MPa. Beyond 100 MPa, the material can experience delamination and also cracks initiating on the tensioned side. Consequently, these CSMs were used to predict whether damage had occurred during the programming stage or not, and to further determine the
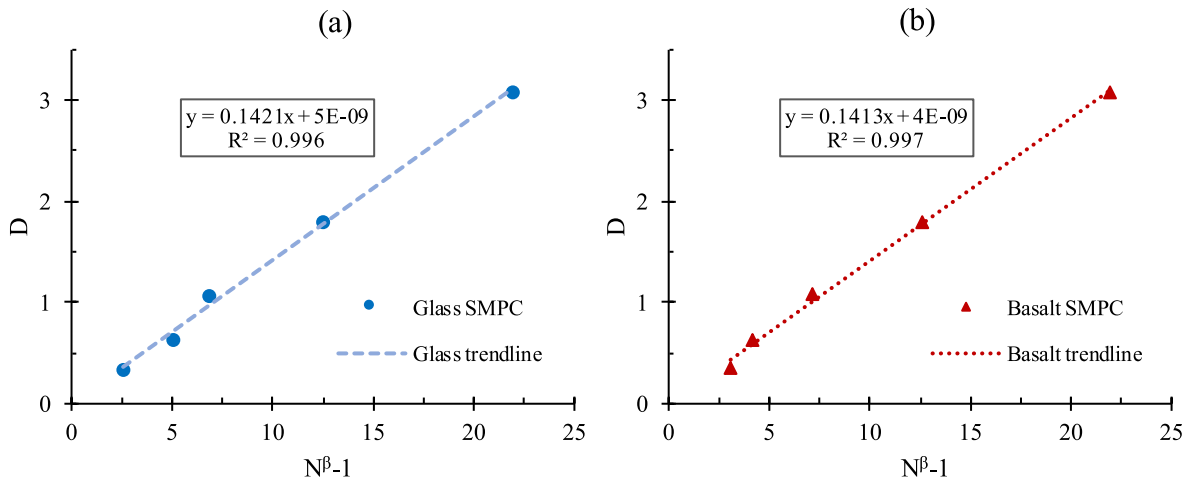
Table 3
Fatigue lives of the SMPCs.

Material	Fatigue life (million cycles)	Fatigue/Endurance limit	
		L (%)	S (MPa)
Glass SMPC	2	26	60.5
Basalt SMPC		21	55.7

(a)

(b)

$$y = 0.1421x + 5E\text{-}09$$
$$R^2 = 0.996$$

$$y = 0.1413x + 4E\text{-}09$$
$$R^2 = 0.997$$

Fig. 7. Evaluation of fatigue characteristic empirical model parameters for (a) glass SMPC and (b) basalt SMPC.

Table 4
Material specific fatigue parameters.

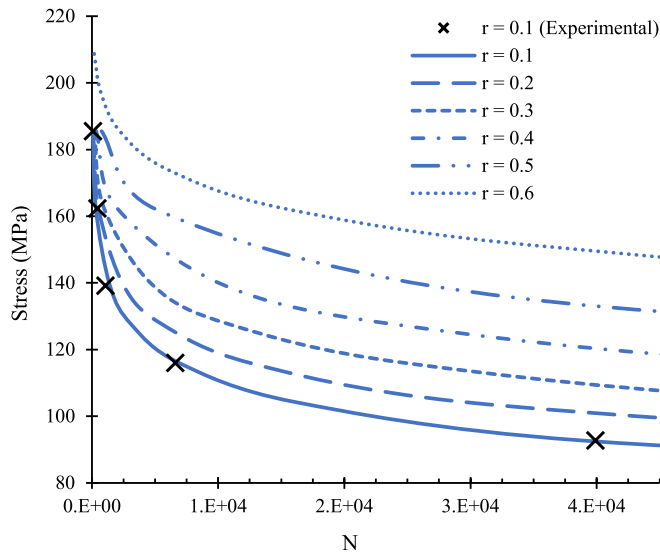| Specimen	α	β
Glass SMPC	0.1421	0.2953
Basalt SMPC	0.1413	0.3319

Fig. 8. Predicted S-N fatigue curves of glass SMPC for different stress ratios.

validity of the model by comparison with the experimental data. For clarity, only the damage prediction of the CHS components are presented.

Fig. 13 illustrates the variation in externally applied load (experimental) during the CHS sample programming and numerical normal stress results at the top (S11) and side (S22) of the specimen. The MTS load reading was utilized in order to recognize the initiation of material damage. As per previous studies, it was suggested that Type 2 delamination and Type 3 cracks could occur beyond a 100 MPa stress level. The material damage Types 2 and 3 refer to delamination and through thickness cracking, respectively. The sudden drop in the experimental load curve in Fig. 13 is a result of the initiation of a crack or considerable material damage. The CHS specimen has experienced material damage during the process of programming when it was deformed by 31.2 mm. The FEA stress level on the side of the CHS sample reached 100 MPa

close to 32 mm. As per developed stresses (Fig. 13) on top and side of the CHS, the top should experience Type 1 and the side should undergo damage Types 2 and 3. Interestingly, these simulation based results showed good consistency with experimentally experienced damage types and are shown in Fig. 14. This proves the effectiveness of the proposed CSMs to numerically investigate and predict the likelihood of material damage during programming. Moreover, most critical locations of the SMPC component prone to damage can also be detected with ease.

In the SHS SMPC samples, a rapid drop in applied test load was seen at a displacement of 11.3 mm, whereas from the FEA results, normal stress on the damaged side achieved 100 MPa at 10.6 mm, demonstrating good consistency with the proposed framework (damage onset at 70 MPa). According to the radial deformability results of the SMPC sections, the SHS showed a quick damage onset at a lower deformation. Hence, the SHS sections can be categorized as more critical compared to CHS which can result in programming damage easily. Consequently, in this paper, SMPC application suggestions are presented considering only SHS SMPC members.

3.5. Application of SMPCs in long beams and deployable structures

a) SMPC long beams.

SMPC SHS and CHS structural components can be used in many challenging civil engineering applications because of their unique intrinsic properties. They can be deformed easily at low cost and with minimal labour to a temporary or confined shape, and then transported to the construction site with ease. Finally, by applying the external stimulus, the deformed SMPC components and structures can be recovered to their initial shapes wherever required. Some suitable engineering applications for these smart SHS and CHS structural components are prefabricated modular constructions, construction of footbridges in remote areas, constructions in challenging terrain, as an alternative to expensive and heavy curved steel beams, for deployable lunar habitats and outer space structures.

The shape memory performance of a large scale 5 m long SHS SMPC member, with the cross section given in Fig. 3 (a), was also investigated via FEA. A displacement boundary condition was applied at the mid span of the SMPC member at 1 mm/s deformation rate. The deformation rate was identified from our recent studies [19]. To demonstrate the shape deformability of the SMPC members, only the FEA analysis for the SHS SMPC is presented here for clarity. The SHS components initiated damage at a lower radial displacement as described in Section 3.4.1. The FEA analysis was performed for different support spans (S) and mid span displacements (D). Subsequently, the developed maximum compressive bending stress and bend radius (R) of the SMPC member was evaluated
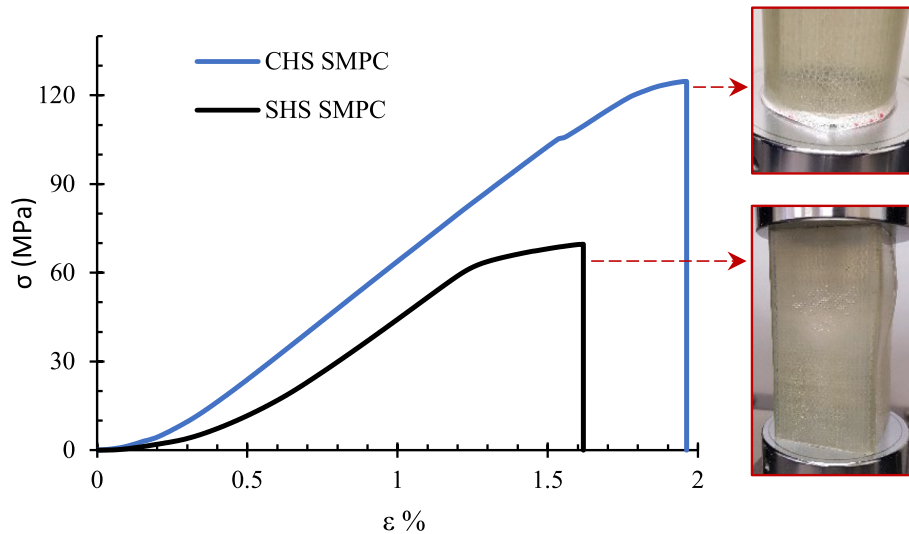
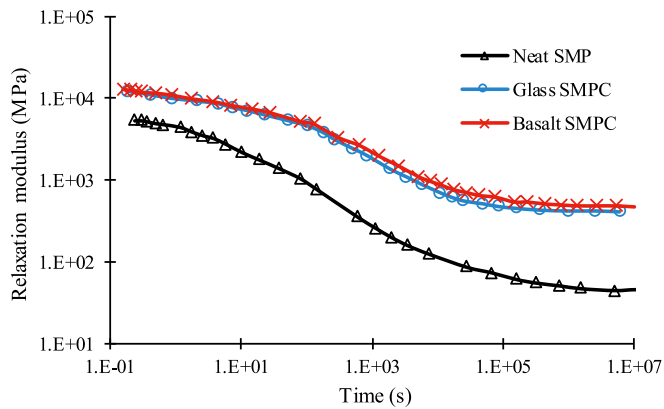**Fig. 9.** Behaviour of CHS and SHS glass SMPCs under axial compression.

Fig. 10. Relaxation Prony series curves for neat SMP and SMPCs.

for analysis. As the compressive side of the SMPC is prone to damage during the programming stage, the compressive stress was used as the tool to predict damage onset.

FEA viscoelastic simulations were performed for five S values and deformed to a maximum of D = 1000 mm. The summary of FEA results is presented in Fig. 15. Interestingly, for S > 1000 mm, the compressive stress was below 70 MPa for all D values. However, the evaluated stress exceeded damage onset stress (σ_o) when S = 1000 mm. Hence, the span of 1000 mm can be identified as the critical span (S_C) value for SHS programming. Moreover, for the configuration with S_C, the R values of the deformed SMPC members were evaluated (in Fig. 16) to determine the limiting bend radius. According to the recognized relationship between R and compressive stress, 650 mm was revealed as the critical bend radius (R_C) for SHS SMPC member programming. Hence, it demonstrates the ability of the fabricated SMPC SHS components to be deformed or wrapped to a compact temporary shape with a bend radius of 650 mm (1.3 m diameter). Similarly, from the FEA study performed for a 5 m long CHS SMPC beam, the R_C was evaluated as 420 mm (0.84 m diameter) for the same S_C. Further, it is clear that CHS SMPC members showed better shape memory performance in comparison to SHS sections, with respect to undamaged shape deformability. These tightly wrapped long SMPC CHS and SHS members can even be stored in a car for transportation as the average width of a passenger car is around 1.75 m [40].

b) Deployable SMPC structures.

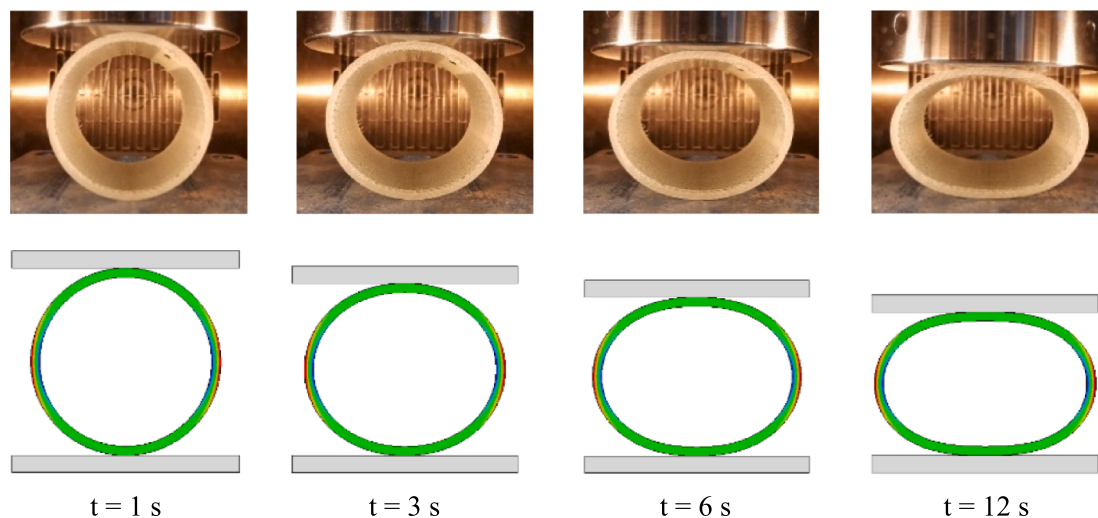To demonstrate the application of large scale SMPC structural

Fig. 11. Shape comparison of CHS SMPC components during first 12 s of programming.
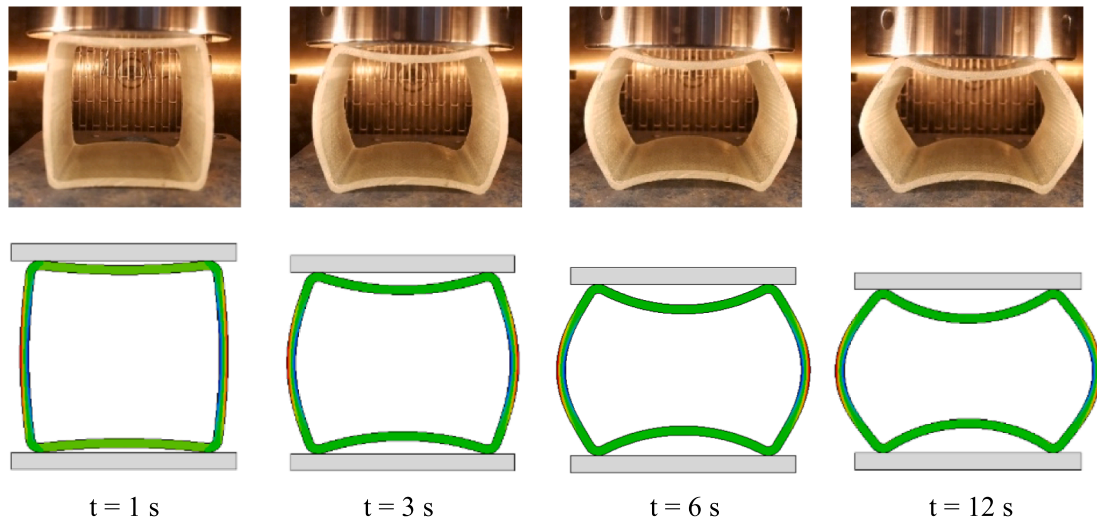
t = 1 s   t = 3 s   t = 6 s   t = 12 s

Fig. 12. Shape comparison of SHS SMPC components during first 12 s of programming.

Table 5
Experimental and FEA fixity and recovery values.

Component	Programming displacement (mm)	Method	R_f %	R_r %
SHS	15	Experimental	72.6	96.5
		FEA	68.5	99.9
CHS	32	Experimental	82.1	98.1
		FEA	78.8	99.8

components in deployable structures, a 5x5x5 m³ frame structure was analyzed numerically with CHS and SHS members, separately. Fig. 17 illustrates the shape programming of a single SHS and CHS vertical strut of the structure, up to a maximum compressive stress (S33) of approximately 70 MPa to ensure no damage occurred. The initial lengths of both members were 5 m. According to the results, the SHS and CHS SMPC members experienced overall length reductions of 2.6 m and 3.5 m, respectively, with no programming damage. Thus, the height of the SMPC structure has reduced to 2.4 m and 1.5 m, respectively for SHS and CHS. The overall compact configuration of the SHS structure with four programmed struts is presented in Fig. 18. A volume reduction of 52 % and 70 % was achieved by the SHS and CHS structures, respectively. Table 6 presents the initial (Vi) and final (Vf) volumes of the two SMPC

structures. Importantly, the results clearly show the space saving advantage that can be achieved by SMPC integration into structural components. In contrast to traditional construction materials and technologies, the use of SMPC structural members can be a game changer for prefabricated modular constructions, heavy curved steel structures, space deployable structures, lunar habitats, foot bridges, etc.

c) Nominal section capacities of SMPC members.

According to the steel designer's handbook [41] and Australian standard AS 4100 [42], the suitability of structural members of a particular material can be assessed by calculating the nominal section capacities. The sectional capacities are categorized according to the subjected loading such as bending (AS 4100–5.2) and axial compression (AS 4100–6.2). To further demonstrate the applicability of SMPCs, the CHS structural capacity to weight ratio (specific strength) was evaluated and compared with steel. Equations (6) and (7) illustrate the nominal section capacity equation for bending and axial compression, respectively. M_S = Nominal section capacity for bending (AS4100-5.2.1), f_y = Yield strength used in design, Z_e = Effective section modulus, N_S = Nominal section capacity for axial compression (AS4100-6.2.1), k_f = Form factor, A_n = Net cross sectional area, d_o = Outer diameter, t = Thickness, ρ = Density). For both loading criteria, the CHS SMPC components demonstrated higher "specific sectional capacities"
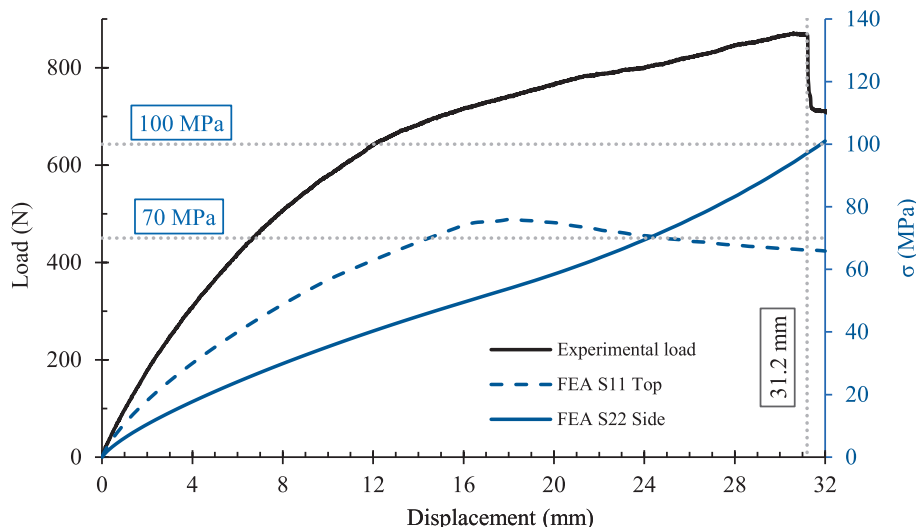

Fig. 13. Comparison of external load applied during experimental programming test and FEA compressive stress results on side and top faces of CHS components.
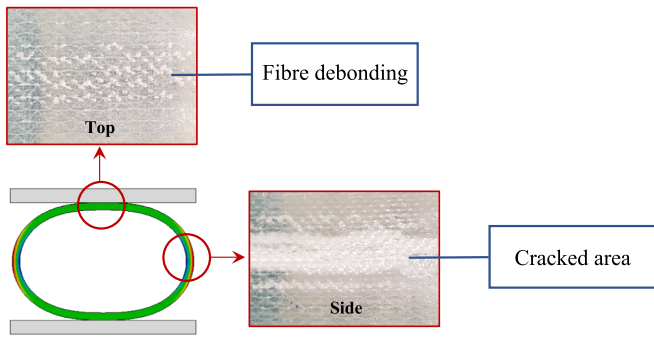
Fig. 14. Damage types on radially deformed CHS components.

showcasing their structural potential as lightweight components in comparison to heavy steel sections. The calculation results for the CHS sections are presented in Table 7.

For bending : $M_S = f_y Z_e$ (6)

For axial compression : $N_S = k_f A_n f_y$ (7)

4. Conclusion

In this paper, we demonstrated the applicability of SMPCs in real scale CHS and SHS structural components. The integration of SMPCs in commonly used members can transform their current capacity, allowing them to be deformed to a compact shape for easy transportation and handling, or incorporate curvy shapes into constructions. Importantly, FEA based damage predictions of the SMPC components were consistent with the experimental results. In addition, it was found that long SHS and CHS SMPC structural members can be wrapped to a minimum radii of 650 mm and 420 mm, respectively, without undergoing any damage during programming. Further, the application of shape deformable SMPC members was presented in a deployable structure which showcased exciting volume savings of 52 % and 70 % for SHS and CHS SMPCs, respectively. According to the tension–tension fatigue characterization, the endurance limits of the glass and basalt SMPCs at 2 million lifetime were 60.5 MPa and 55.7 MPa, respectively. Moreover, the fatigue material specific parameters (α and β) were evaluated, and S-N predictions for non-tested r values are presented. Importantly, the fatigue study contributes significant research knowledge to fill out knowledge gaps related to SMPC performance. Overall, the study

provides a firsthand approach and framework to incorporate the shape memory effect of SMPCs in construction components. This novel application can aid future researchers seeking to revolutionize construction techniques, making them smarter, cheaper and quicker. As future works, it recommended to characterize SMPC properties under complex force situations and durability conditions, as a construction material.

CRediT authorship contribution statement

K.D.C. Emmanuel: Conceptualization, Methodology, Investigation, Writing – original draft. **L.H.J. Jeewantha:** Investigation, Resources. **H. M.C.M. Herath:** Writing – review & editing. **J.A. Epaarachchi:** Conceptualization, Supervision, Writing – review & editing. **T. Aravinthan:** Supervision.

Declaration of Competing Interest

The authors declare that they have no known competing financial interests or personal relationships that could have appeared to influence the work reported in this paper.
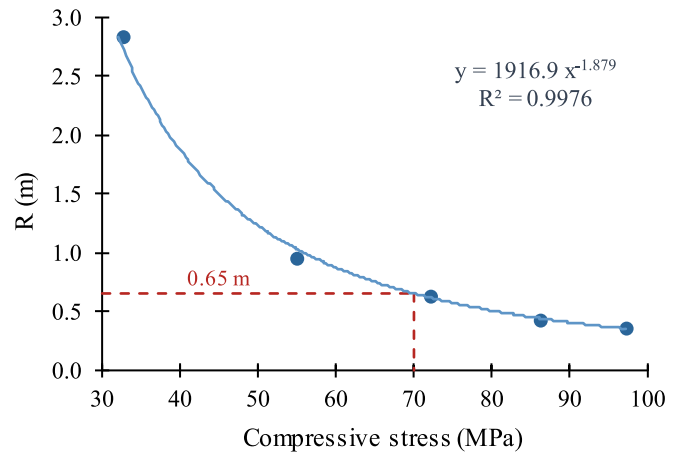

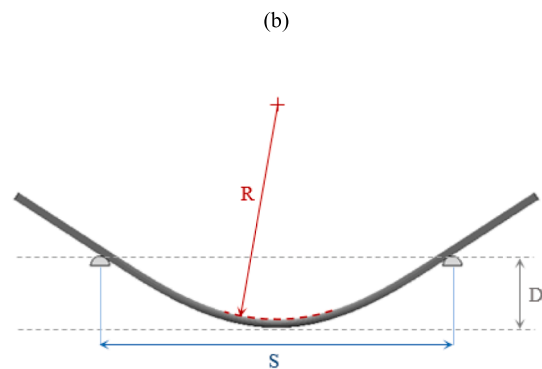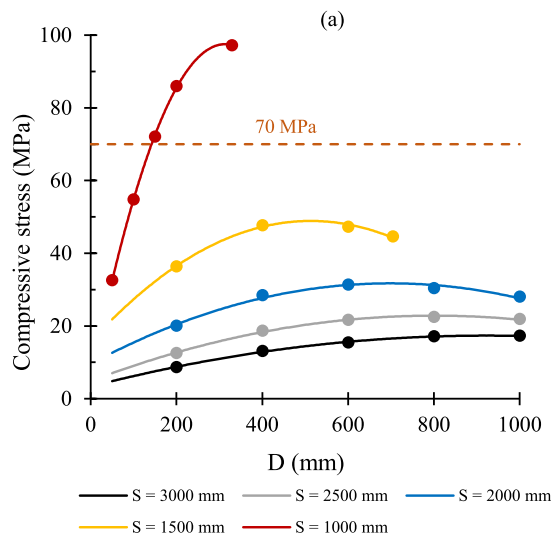**Fig. 16.** Relationship between R and compressive stress for configuration with S_C.

Fig. 15. FEA results summary (a) variation of compressive stress with D and S values (b) test parameters.
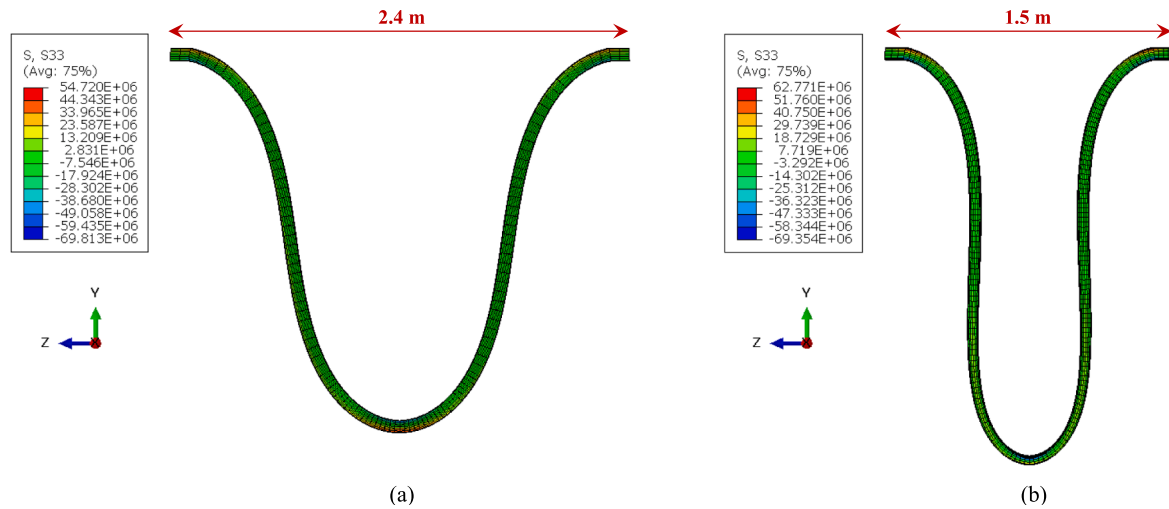
Fig. 17. Shape programming of vertical member in frame structure; (a) SHS and (b) CHS.
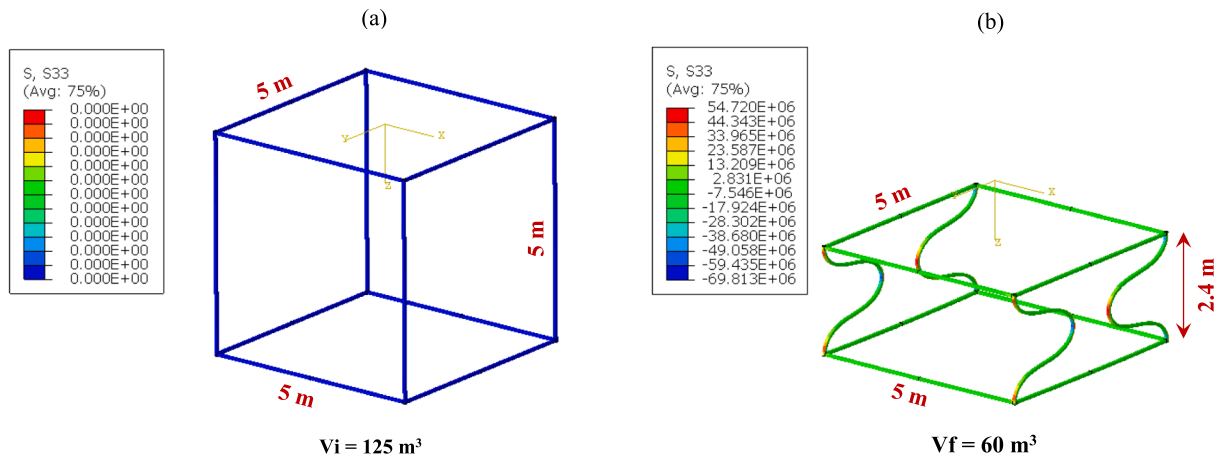

Fig. 18. SHS SMPC structure configurations; (a) initial (b) programmed.

Table 6
Volume savings of (a) SHS and (b) CHS SMPC structures.

SMPC member	Vi (m³)	Vf (m³)	Volume saving (%)
SHS	125	60	52
CHS	125	37	70

Table 7
CHS specific section capacity for mild steel and SMPC.

CHS	d_o (mm)	t (mm)	ρ (kg/m³)	f_y (MPa)	M_S (Nm)	M_S/ρ	N_S/ρ
Mild steel	60.3	2.9	7800	380 [43]	4082	0.5	25.5
SMPC	67	3	1320	232	3215	2.4	57.0

Data availability

Data will be made available on request.

References

[1] Zhang H. Building materials in civil engineering. Elsevier; 2011.

[2] Duggal SK. Building materials. Routledge; 2017.

[3] A. S. Mosallam, A. Bayraktar, M. Elmikawi, S. Pul, and S. Adanur, "Polymer composites in construction: an overview," 2021.

[4] Liu Y, Du H, Liu L, Leng J. Shape memory polymers and their composites in aerospace applications: a review. Smart Mater Struct 2014;23(2):pp. https://doi.org/10.1088/0964-1726/23/2/023001.

[5] Herath HMCM, Epaarachchi JA, Islam MM, Al-Azzawi W, Leng J, Zhang F. Structural performance and photothermal recovery of carbon fibre reinforced shape memory polymer. Compos Sci Technol 2018;167:206–14. https://doi.org/10.1016/j.compscitech.2018.07.042.

[6] Jeewantha J, et al. Shape memory polymer smart plaster for orthopaedic treatments. Smart Mater Struct 2022;31(11):115016.

[7] Lendlein A, Kelch S. Shape-Memory Polymers. Angew Chem Int Ed 2002;41(12):2034–57. https://doi.org/10.1002/1521-3773(20020617)41:12<2034::Aid-anie2034>3.0.Co;2-m.

[8] J. Jeewantha, C. Emmanuel, M. Herath, M. Islam, and J. Epaarachchi, "Development and characterization of shape memory polymers for non-invasive biomedical applications," in *Smart Materials, Adaptive Structures and Intelligent Systems*, 2021, vol. 85499: American Society of Mechanical Engineers, p. V001T02A001.

[9] Meng Q, Hu J. A review of shape memory polymer composites and blends. Compos A Appl Sci Manuf 2009;40(11):1661–72. https://doi.org/10.1016/j.compositesa.2009.08.011.

[10] Li F, Liu Y, Leng J. Progress of shape memory polymers and their composites in aerospace applications. Smart Mater Struct 2019;28(10):pp. https://doi.org/10.1088/1361-665X/ab3d5f.

[11] L. Santo, F. Quadrini, D. Bellisario, and L. Iorio, "Applications of Shape-Memory Polymers, and Their Blends and Composites," in *Shape Memory Polymers, Blends and Composites*, (Advanced Structured Materials, 2020, ch. Chapter 13, pp. 311-329.

[12] Emmanuel KDC, Herath HMCM, Jeewantha LHJ, Epaarachchi JA, Aravinthan T. Thermomechanical and fire performance of DGEBA based shape memory polymer composites for constructions. Constr Build Mater 2021;303. https://doi.org/10.1016/j.conbuildmat.2021.124442.

[13] M. Herath, C. Emmanuel, J. Jeewantha, and J. Epaarachchi, "In-situ performance evaluation of large shape memory polymer components via distributed optical

fibre sensors," in *2021 10th International Conference on Information and Automation for Sustainability (ICIAfS)*, 2021: IEEE, pp. 458-463.

[14] Leng J, Lan X, Liu Y, Du S. Shape-memory polymers and their composites: Stimulus methods and applications. Prog Mater Sci 2011;56(7):1077–135. https://doi.org/10.1016/j.pmatsci.2011.03.001.

[15] Herath HMCM, Epaarachchi JA, Islam MM, Leng J. Carbon Fibre Reinforced Shape Memory Polymer Composites for Deployable Space Habitats. Engineer: Journal of the Institution of Engineers, Sri Lanka 2019;52(1). https://doi.org/10.4038/engineer.v52i1.7323.

[16] Ferdous W, Bai Y, Ngo TD, Manalo A, Mendis P. New advancements, challenges and opportunities of multi-storey modular buildings – A state-of-the-art review. Eng Struct 2019;183:883–93. https://doi.org/10.1016/j.engstruct.2019.01.061.

[17] Thai H-T, Ngo T, Uy B. A review on modular construction for high-rise buildings. Structures 2020;28:1265–90. https://doi.org/10.1016/j.istruc.2020.09.070.

[18] Hall DH, Grubb MA, Yoo CH. Improved design specifications for horizontally curved steel girder highway bridges, no. 424. Transportation Research Board; 1999.

[19] Emmanuel KDC, Jeewantha LHJ, Herath HMCM, Epaarachchi JA, Aravinthan T. Damage onset analysis of optimized shape memory polymer composites during programming into curved shapes. Materialia 2022;26. https://doi.org/10.1016/j.mtla.2022.101599.

[20] *Standard Test Method for Tension-Tension Fatigue of Polymer Matrix Composite Materials*, A. International, 2019.

[21] W. Al Azzawi, M. Herath, and J. Epaarachchi, "Modeling, analysis, and testing of viscoelastic properties of shape memory polymer composites and a brief review of their space engineering applications," *Creep and Fatigue in Polymer Matrix Composites*, pp. 465-495, 2019.

[22] Azzawi WA, Epaarachchi JA, Islam M, Leng J. Implementation of a finite element analysis procedure for structural analysis of shape memory behaviour of fibre reinforced shape memory polymer composites. Smart Mater Struct 2017;26(12): pp. https://doi.org/10.1088/1361-665X/aa928e.

[23] Xie T. Tunable polymer multi-shape memory effect. Nature 2010;464(7286): 267–70.

[24] Vieira PR, Carvalho EML, Vieira JD, Toledo Filho RD. Experimental fatigue behavior of pultruded glass fibre reinforced polymer composite materials. Compos B Eng 2018;146:69–75. https://doi.org/10.1016/j.compositesb.2018.03.040.

[25] Kukureka SN, Wei CY. Damage development in pultruded composites for optical telecommunications cables under tensile and flexural fatigue. Compos Sci Technol 2003;63(12):1795–804. https://doi.org/10.1016/s0266-3538(03)00132-5.

[26] Liu J, Xing Z, Lu H, Fu Y-Q. Interfacial confinement in semi-crystalline shape memory polymer towards sequentially dynamic relaxations. Int J Appl Mech 2021; 13(10):2150117.

[27] Liu J, Gorbacheva G, Lu H, Wang J, Fu Y-Q. A dynamic hysteresis model for customized glass transition in amorphous polymer towards multiple shape memory effects. Smart Mater Struct 2022;31(12):125022.

[28] Van Den Einde L, Zhao L, Seible F. Use of FRP composites in civil structural applications. Constr Build Mater 2003;17(6–7):389–403. https://doi.org/10.1016/s0950-0618(03)00040-0.

[29] Kumar P, Chandrashekhara K, Nanni A. Structural performance of a FRP bridge deck. Constr Build Mater 2004;18(1):35–47. https://doi.org/10.1016/s0950-0618(03)00036-9.

[30] Wu Z, Wang X, Iwashita K, Sasaki T, Hamaguchi Y. Tensile fatigue behaviour of FRP and hybrid FRP sheets. Compos B Eng 2010;41(5):396–402. https://doi.org/10.1016/j.compositesb.2010.02.001.

[31] Saito M. Tensile fatigue strength of lightweight concrete. Int J Cem Compos Light Concr 1984;6(3):143–9.

[32] Colombo C, Vergani L. Multi-axial fatigue life estimation of unidirectional GFRP composite. Int J Fatigue 2011;33(8):1032–9. https://doi.org/10.1016/j.ijfatigue.2011.01.001.

[33] Wang Z, Xu L, Sun X, Shi M, Liu J. Fatigue behavior of glass-fiber-reinforced epoxy composites embedded with shape memory alloy wires. Compos Struct 2017;178: 311–9. https://doi.org/10.1016/j.compstruct.2017.07.027.

[34] Epaarachchi JA, Clausen PD. An empirical model for fatigue behavior prediction of glass fibre-reinforced plastic composites for various stress ratios and test frequencies. Compos A Appl Sci Manuf 2003;34(4):313–26. https://doi.org/10.1016/s1359-835x(03)00052-6.

[35] Srinivasa Rao P, SeshadriSekhar T, Sravana P. Strength properties of glass fibre concrete. ARPN Journal of Engineering and Applied Sciences 2010;5(4):1–6.

[36] Shakor PN, Pimplikar S. Glass fibre reinforced concrete use in construction. Int J Technol Eng Syst 2011;2(2):pp.

[37] Maranan GB, Manalo AC, Benmokrane B, Karunasena W, Mendis P. Evaluation of the flexural strength and serviceability of geopolymer concrete beams reinforced with glass-fibre-reinforced polymer (GFRP) bars. Eng Struct 2015;101:529–41. https://doi.org/10.1016/j.engstruct.2015.08.003.

[38] Teng JG, Yu T, Wong YL, Dong SL. Hybrid FRP–concrete–steel tubular columns: Concept and behavior. Constr Build Mater 2007;21(4):846–54. https://doi.org/10.1016/j.conbuildmat.2006.06.017.

[39] Bambach MR, Jama HH, Elchalakani M. Axial capacity and design of thin-walled steel SHS strengthened with CFRP. Thin-Walled Struct 2009;47(10):1112–21. https://doi.org/10.1016/j.tws.2008.10.006.

[40] Furth PG, Dulaski DM, Buessing M, Tavakolian P. Parking lane width and bicycle operating space. Transp Res Rec 2010;2190(1):45–50.

[41] Gorenc B, Gorenc BE, Tinyou R, Syam A. Steel designers' handbook. UNSW Press; 2005.

[42] *AS 4100 - Steel Structures*, S. Australia, 2020.

[43] Alhassan E, Olasehinde D, Musonda A, Odeniyi O. Tensile and flexural behaviour of steel materials used in the construction of crop processing machines. In: IOP Conference Series: Earth and Environmental Science, vol. 445, no. 1. IOP Publishing; 2020. p. 012044.